NASA CONTRACTOR REPORT

NASA CR-904

NASA CR-904

FACILITY FORM 602

N67-4○○○○
(ACCESSION NUMBER)   (THRU)

(PAGES)   /
                                      (CODE)

(NASA CR OR TMX OR AD NUMBER)   (CATEGORY)

EXTENSION OF GAGE CALIBRATION STUDY IN EXTREME HIGH VACUUM

(Orbitron and Magnetron Studies)

by F. Feakes, E. C. Muly, and F. J. Brock

Prepared by
NATIONAL RESEARCH CORPORATION
Cambridge, Mass.
for

NATIONAL AERONAUTICS AND SPACE ADMINISTRATION • WASHINGTON, D. C. • OCTOBER 1967

EXTENSION OF GAGE CALIBRATION STUDY

IN EXTREME HIGH VACUUM

(Orbitron and Magnetron Studies)

By F. Feakes, E. C. Muly, and F. J. Brock

Distribution of this report is provided in the interest of information exchange. Responsibility for the contents resides in the author or organization that prepared it.

TABLE OF CONTENTS

LIST OF FIGURES

LIST OF TABLES

SUMMARY

During recent years it has become increasingly apparent that the techniques for the production of an extremely low pressure environment have outstripped the methods and techniques of measurement of low pressure. The present work represents part of a continuing effort to develop more reliable and higher sensitivity pressure gauges for pressures below 10^{-10} Torr. The report is divided into two parts. Part I is a consideration of the orbitron gauge. This type of gauge appears to have high potential for the measurement of extremely low pressures. In addition it appears to have high potential for aerospace pressure measurements because it does not require magnets of relatively high mass.

The major fraction of the present work on the orbitron is concerned with a theoretical analysis of the orbitron principle. In this part of the program a method has been developed for obtaining a self-consistent solution for the electron motion, charge density distribution, and space charge dependent potential distribution in an orbitron. The solution may have any prescribed accuracy, since the final accuracy of the solution is a function only of the number of iterations performed. The assumptions used are equivalent to asserting that the space charge is all electronic and is only a function of r (these are later shown to be valid for practicable configurations and modes of operation). The interelectrode space is divided into 3 concentric cylindrical regions such that all the space charge is contained in the middle region. The Poisson Equation is solved in the middle region for an arbitrary charge distribution and matched at its boundaries with solutions of the Laplace Equation in the adjacent regions. The force equations are solved for the radial component of the electron velocity for an arbitrary potential distribution. The continuity equation is solved for the charge distribution for an arbitrary electron

radial velocity. The 1st approximation to the charge distri-
bution is obtained by using the space charge free electron
radial velocity. This charge distribution is substituted into
the potential distribution and integrated numerically to given
the first approximation to the space charge dependent distri-
bution. This result is substituted into the radial velocity
equation to obtain the 2nd approximation to the electron radial
velocity which is substituted back into the continuity equation
to obtain the 2nd approximation to the charge distribution and
begin the 2nd iteration. A comparison of the 1st and 2nd
approximations of the charge distribution indicates that the
iteration process converges rapidly and that the result of
the 1st iteration is a useful approximation to the self-
consistent solution.

The 1st iteration has been worked out for a particular
subset of self-consistent solutions. Using these results as
a 1st approximation to the final self-consistent solution,
conditions are derived which optimize the total space charge
stored in the rotating electron cloud such that the electron
trajectories are stable and the space charge distribution is
uniform in θ-space and the electron mean kinetic energy has
a prescribed value. Under these conditions, it turns out
that the total space charge stored in the rotating electron
cloud approximates that stored on one plate of a cylindrical
capacitor which has the same dimensions and anode potential.
It is found that the ion current generated per centimeter of
length of the lectron cloud (along the z-axis) is of the
order of 1 to 15 amp/Torr (Argon) for anode potentials in
the range 0.4 to 10KV. This corresponds to ionic pumping speeds
(for Argon) of the order of 0.2 to 3 liters/sec (for each
centimeter of pump length) and to ion gage sensitivities of
the order of 10^4 to 10^5 Torr^{-1} (Argon) for a conventional
size device (l=10 cm). Further it is found, in ion gage

applications, that modes of operation are possible which are substantially free of x-ray induced residual current.

An experimental orbitron gage for extremely low pressure measurement was designed and constructed but performance characteristics were not measured during the present program.

Part II of the present report outlines work carried out on the normal magnetron type of gage. The major emphasis of this part of the program was on the measurement of the sensivities of a normal magnetron gage over wide ranges of anode voltages, magnetron field strengths and pressures. Sensitivities were measured at the following pressures: 5.2×10^{-8} Torr, 5.2×10^{-10} Torr, 2.7×10^{-11} Torr, and 1.2×10^{-11} Torr. Anode voltages were varied from 1000 to 8000 volts and magnetic field strengths from 1100 to 2000 gauss. The study confirmed earlier work and showed that considerable changes in gage sensitivity may occur as the operating parameters are varied. However, broad general patterns exist in the performance characteristics and gage sensitivities may be more than doubled from the 4.5 amp/Torr obtained at about 5000 volts and 1000 gauss if considerably higher anode voltages and magnetic field strengths are used. Some evidence was developed which suggested that the linear operation of the normal magnetron could be extended to lower pressures by operating the gage at different combinations of anode voltage and magnetic field strength -- e.g., 3000 volts and 1100 gauss, also 4800 volts and 1250 gauss. However, it appeared that a lower pressure limit was obtained for the range where the gauge was linear or close to linear for these conditions also. For instance, with an anode voltage of 4800 volts and a filled strength of 1250 gauss the gage had a response curve with a slope of approximately 0.9 down to 1.2×10^{-11} Torr. But the results indicated that the gage again turns to non-linear operation at lower pressures.

A short study was made of the r.f. oscillatory behavior of the normal magnetron gage. The results obtained confirmed previous measurements. The generation of stable r.f. frequencies could not be detected below 2×10^{-10} Torr-the pressure below which the gage is non-linear.

Experimental work on the effects of ultra-violet radiation and electron injection were inconclusive because of possible effects of photo-desorption and thermal desorption.

Work was initiated on the theoretical and practical aspects of some of the possible sources of anomolous currents at the cathode of the magnetron gage.

A large number of photographs of the discharge inside the experimental magnetron gage were taken. From these it was possible to estimate the shape of the discharge and its intensity. The effects of pressure, anode voltage and magnetic field strength on the discharge were broadly examined. It was not possible to obtain photographs of the discharge below 2×10^{-10} Torr.

GENERAL INTRODUCTION

As a part of a previous program (NASw-625), the operating characteristics of four UHV ionization gages were examined at pressures below 10^{-10} Torr. The gages chosen for study were those which appeared to have the highest potential for the measurement of extremely low pressures. They were a nude modulated Nottingham gage, a suppressor-grid gage, an inverted magnetron gage, and a normal magnetron gage. The work indicated that the normal magnetron gage should continue to be included in the further investigations of the measurement of extremely low pressure mainly because of its high sensitivity and the fact that hot filaments were not required to supply the ionizing electron flux. The work clearly indicated that a considerable improvement would result if the linear region of the normal magnetron gage were extended below 2×10^{-10} Torr. It therefore became the aim of the present program to investigate the possibilities of "linearizing" the normal magnetron and to improve its low pressure operating characteristics. One of the aspects considered under the latter heading was the possibility of reducing the noise level of the gage at low pressures. This was to include the reduction of spurious currents arising from microphonics, dielectric polarization, and leakage.

In addition, it had become apparent in the period of performance of the first program that another gage, not investigated in that program also held considerable promise for low pressure measurement. This was the orbitron gage.[1] Consequently, theoretical and experimental investigations of the orbitron gage were initially included in the present program.

The work carried out under the present program is divided up into two parts. Part I is a report of work carried out in the present program on the orbitron gage. The major fraction

is connected with a theoretical analysis of the orbitron principle. The second section of Part I describes work on the design and construction of an experimental orbitron gage. This work predated the theoretical analysis and in consequence it was not feasible to incorporate the results of the theoretical analysis in the design of the experimental orbitron gage. Part II is a report of the various aspects of work carried out on the normal magnetron gage.

Part 1 ORBITRON GAGE
1.1 INTRODUCTION

The orbitron principle has been applied to ion gages and ion pumps by the group at the University of Wisconsin under the direction of Professor R.G. Herb.[1] The activity of this group has been principally applied to the experimental development of practical pumps and gages with a secondary emphasis on the theory and analysis of the orbitron principle. The theory of the orbitron principle appears to have been studied first by W.E. Waters[2] and then independently by R.H. Hooverman,[3] stimulated by Herb's work. However, in both of these studies only the space charge free potential distribution was considered. While the results of these studies may correctly describe the electron trajectories for a very low electron density stored in the rotating electron cloud, the results are not applicable to practical orbitrons since existing experimental data indicate that the electron density in the space charge cloud is not negligible, in fact it may even approach saturation. The space charge free analysis yields little, if any, insight into the dynamics of the orbitron since all the questions of substance involve the space charge dependent potential distribution. For example, questions concerning electrode geometry for optimum charge storage in the rotating space charge cloud, launcher location for optimum charge storage, anode potential for optimum charge storage, self-consistent orbit injection parameters, mean orbiting life-time of the electrons, orbit stability criteria, dependence of average kinetic energy of the electron on stored charge, and injection (emission) current necessary to maintain optimum charge storage can not be answered without knowledge of the space charge dependent potential distribution.

The orbitron principle appears to contain a natural feedback mechanism which, for a given electrode geometry and potential, and a self-consistent set of prescribed injection parameters, launcher location and injection current, limits the number of electrons stored in the space charge cloud. However, it appears possible to over-ride this feedback mechanism and over-populate the electron cloud if all geometrical, electrical and dynamic parameters are not self-consistent. The over-population of the electron cloud substantially modifies the potential distribution

3

such that the injection parameters now violate the orbit stability criteria and the electron mean life-time is reduced to transit time between the launcher and anode.

From the above discussion it is clearly essential that the analysis of the orbitron be self-consistent if it is to be applicable to real orbitrons, provide insight into the principle, and provide answers to the practical questions implied above. That is, the analysis must be self-consistent in the sense that the differential equations which describe the electron motion must contain a potential distribution which is in part a function of the electron motion and thus take proper account of the average electron distribution within the space charge cloud. This appears to be a formidable task, since the self-consistent set of differential equations describing the electron motion (Force Equations, Poisson Equation , and Continuity Equation) reduce to an essentially nonlinear integral equation of a type for which no general solution is known (except, perhaps, in a few special, restricted cases). However, a solution to the self-consistent set of equations is possible using iterative, numerical methods. A method of solving these equations such that the solution has a prescribed accuracy is outlined later on and the first approximation is worked out in some detail. Even from this approximate solution, considerable insight into the answers to many of the above questions is developed.

1.2 ORBITRON PRINCIPLE AND APPLICATION

In principle, the orbitron consists of two coaxial cylinders having radii R_i (inner) and R_o (outer), between which is applied a potential difference $V(R_i) > 0$ and $V(R_o) = 0$, yielding a logarithmic electrostatic potential distribution in the interelectrode space and a central force field which is attractive for electrons. It is assumed that the cylinder lengths are large compared to their radii thus minimizing the importance of end effects. Electrons are injected into the central force field with angular momentum and kinetic energy such that they are captured in bound, stable orbits around the inner cylinder (anode). For certain sets of orbit injection parameters the individual electron trajectories resemble open ellipses as viewed from a stationary reference system. While the electrons execute ellipse-like trajectories in a radial plane they drift slowly in the axial direction until they arrive in the neighborhood of the end of the coaxial cylinders, where they are reflected by a weak electron mirror field (produced by auxiliary electrodes). Thus the total trajectory is similar to an elliptical spiral repeatedly folded back on itself.

If the individual electron orbits are not closed, the electrons collectively form a space charge cloud, the charge density of which is uniform in azimuth and the local angular velocity of which is equal to the average angular velocity of the electrons at that radius. Thus, not all parts of the cloud have the same angular velocity; the inner part of the space charge cloud rotates at a much higher angular velocity than the outer part of the cloud.

Although, under the proper conditions, the charge density of the space charge cloud is uniform in θ-space, it is never uniform in r-space. The electron cloud does not occupy the entire interelectrode space but rather has an inner and outer boundary which corresponded respectively to the inner and outer turning points in the electron trajectories. The radial charge density is proportional to the interval of time that the electron occupies an increment of the radius between the inner and outer turning points (inner and outer cloud boundaries). Thus the radial charge density distribution is inversely proportional to the radial component of

5

the electron velocity. The charge density is thus high in the neighborhood of the boundaries and low in the neighborhood of the radial center of the space charge cloud.

The electronic (negative) space charge associated with the rotating electron cloud modifies the interelectrode electrostatic potential distribution. The potential distribution associated with the electron density distribution is always negative, regardless of the particular shape of the density distribution. Thus the total potential distribution, that due to applied potential plus that due to interelectrode electronic space charge, is everywhere lower than the applied potential distribution. Therefore the electric field inside the inner space charge boundary is higher than the applied electric field and the field outside the outer cloud boundary is lower than the applied electric field. Thus, within the cloud the field gradient (total) is much steeper than it would be if the space charge density were negligibly low. These modifications of the potential and field distributions obviously have strong effects on the motion of the electrons which produced them. This is the source of nearly all the difficulties in understanding and in applying the orbitron principle. For very low space charge densities where the actual potential distribution is nearly identical with the applied potential distribution the orbitron principle is simultaneously elegant and simple, and is almost completely understood.[1,2,3] However the principal advantage of real orbitrons is the ability to attain relatively high charge densities.

The value of applying the orbitron principle to ion gages and ion pumps is that large numbers of electrons having long mean life-times may be stored in the space charge cloud and efficiently used to generate ions by impact ionization. This, of course, assumes that the electrons are injected into stable (long life-time) trajectories, a condition which requires a knowledge of the space charge dependent potential distribution. There is another substantial advantage in applying the orbitron principle to ion gages: It appears possible to operate an orbitron ion gage in a mode which produces no soft x-ray induced background current. In conventional ion gages, electrons having kinetic energy in the neighborhood of

100 eV are abruptly decelerated in the surface of the electron collector (grid). A fraction of the soft x-rays produced by the decelerated electron flux are radiated from the electron collector surface to the ion collector surface, and produce free electrons by the phoeoelectric process. (The electrons which have final momentum vectors such that they penetrate the surface barrier and escape into the vacuum.) The photoelectric current leaving the ion collector is indistinguishable from an ion current arriving at the collector. Thus there exists a background or residual current which is dependent only on the emission current. In the orbitron, provided the electrons are properly injected into stable orbits, the electrons do not reach the anode except if they have lost sufficient energy in a collision to make it energetically possible. A large fraction of the collisions of this kind are ionizing collisions (for electron energies in the neighborhood of 100 eV). Thus the subsequent emission of a photoelectron at the ion collector (outer cylinder), by a soft x-ray emitted from the anode in the process of collecting the ionizing electron, simply enhances the current associated with the ionizing event. Those electrons which do not encounter a gas atom continue to orbit the anode until they eventually return to the launcher, or exit from the orbitron structure. It appears possible to arrange the potential of the launcher such that returning electrons arrive with a relatively low kinetic energy, under which condition the generation of soft x-rays is an improbable process. Thus, operation of an orbitron ion gage in this mode avoids the usual defect of generating a residual current which is dependent only on the emission current.

The relization of the advantages inherent in the orbitron principle, in applications to practical ion gages and ion pumps, requires optimization of the total ionization rate. The principal parameters involved in this optimization are: orbit stability,the electron kinetic energy, space charge cloud location,

and the number of electrons stored in the space charge cloud (per unit length). There is considerable value in a brief, preliminary observation of how these parameters influence the application of the orbitron principle to a practical device.

The probability of an electron encountering a gas atom, of course, increases as the electron orbiting life-time increases. The probable orbiting life-time is maximum for stable orbits. Thus the electrons must be injected into stable orbits.

The probability that an electron-atom collision yields an ion (in an inelastic collision) is a function of the kinetic energy of the electron. The maximum ionization probability in most gases occurs for an electron kinetic energy in the neighborhood of 100 eV. However, the ionization probability as a function of energy generally falls off much faster for energies less than this value than it does for energies greater than this value. Thus the electrons must be injected into orbit such that their minimum kinetic energy (outer turning point) is not substantially less than the kinetic energy corresponding to the ionization efficiency maximum, even though the kinetic energy is substantially above this value at the inner turning point.

The ionization rate (per unit length), of course increases as the number of orbiting electrons in unit length of the space charge cloud increases. The maximum number of electrons that can be stored in unit length of the cloud is a function of the electron kinetic energy, the orbit stability, the applied potential, and all geometrical parameters. The requirements of the above two paragraphs, in effect, specify the first two of these parameters and also assign a minimum value to the applied potential. Thus the geometrical parameters and the maximum value of the applied potential must be chosen such that the number of electrons in unit length of the cloud is maximized.

Failure to follow the above prescriptions, in one way or another reduces the ionization rate below its optimum value (although the stored charge may actually increase) and increases the residual current (in ion gage applications). The details of the methods of satisfying the above require-

ments are developed later on.

There are several important constraints which should be recognized in any application of the orbitron principle to practical devices. The ratio $\frac{R_o}{R_i}$ should not be too large. Ultimately, the quantity of charge that may be stored in the electron cloud depends on the field-energy density within the interelectrode volume. As $\frac{R_o}{R_i}$ increases the total field-energy decreases. Further, for $\frac{R_o}{R_i}$ large, the field-energy density is high only in the neighborhood of the anode and low elsewhere. Thus as $\frac{R_o}{R_i}$ increases the useful fraction of the volume within the interelectrode space shrinks. For $\frac{R_o}{R_i}$ large, a non-negligible fraction of the total population of the electron cloud may be electrons that have already experienced one or more collisions with gas atoms, since the probability of capturing an electron at the anode immediately following a collision decreases as $\frac{R_o}{R_i}$ increases.

The electron trajectories should be such that regions of low electric field are avoided since in these regions the magnetic forces on the electron (arising from spurious magnetic fields) may be comparable with the electric forces.

1.3 PROCEDURE

It is considered useful to outline here the analytical procedure that is followed in subsequent sections since some of the analyses are rather long, some intricate, and some encounter rather cumbersome analytical expressions. To minimize the possibility of arithmetic inundation some of the demonstrations and computations have been placed in appendices.

The first step in the procedure consists of solving Poisson's Equation for an arbitrary charge density distribution extending over an arbitrary region of the interelectrode space. It is therefore necessary to divide the interelectrode space into three concentric regions and solve the Poisson Equation in each. The solution for each region is then matched at its boundaries with the solutions for the adjacent regions. In the process, electrode boundary conditions are applied. Three expressions are finally obtained for the potential distribution, one for each of the three regions, in terms of the applied potential, geometrical parameters and integrals over the arbitrary charge density distribution.

The differential equations (force equations) for the motion of an electron are solved for an arbitrary potential distribution. Only a solution for the velocity is required since the turning points may be obtained directly from the velocity equation and a detailed knowledge of the orbit shape is unnecessary in nearly all meaningful questions. However, much can be inferred concerning the general orbit shape from various analytical results. In developing an expression for the velocity it is useful to distinguish between stable and unstable trajectories. The results of the stability analysis are incorporated into the velocity equation.

The charge density distribution is then obtained from the continuity equation in terms of the radial component of the electron velocity. The same expression is derived from statistical reasoning.

At this point three equations have been obtained in terms of three unknown functions: the potential distribution, the charge density distribution, and the electron velocity. Solving this system of equations for the potential distribution yields a nonlinear integral equation. This equation has a form for which no general solution is known. However, a particular solution is possible using numerical techniques. By numerical integration and iteration, a solution having any prescribed accuracy may be obtained.

The electron velocity corresponding to the space charge free potential distribution is taken as a first trial solution. The space charge free electron velocity is integrated numerically and the result used to obtain a first approximation to the space charge dependent potential distribution. Inserting this potential into the electron velocity equation yields a second approximation for the charge density distribution.

This procedure, although not done here, may be continued until a solution is obtained having the prescribed accuracy. The additional computation required to obtain a convergent, self-consistent solution involves considerable computer time.

1.4 POTENTIAL DISTRIBUTION

In solving Poisson's Equation for the space charge dependent potential distribution, it is unnecessary to consider all possible charge density distributions. Rather, only those distributions are considered which lead to near optimum electron storage, since the principal function of the electron cloud is to generate ions, which can be done at the maximum rate if the number of electrons stored in the cloud is optimized. It is obvious that those charge density distributions which are most uniform in θ-space, produce the smallest modification of the electrostatic potential distribution for a prescribed total charge. Since the electron orbits must remain stable and the electrons must have a kinetic energy greater than a prescribed minimum, there is a limit to the magnitude of the space charge modification of the electrostatic potential distribution that can be allowed.

A uniform charge density distribution in the radial direction is incompatible with the differential equations which describe the motion of orbiting electrons. Thus the applicable form of Poisson's Equation will always have at least one independent variable, r.

If the electron drift velocity in the z-direction is such that the period of oscillation in the z-direction is a non-integral multiple of the orbit period, the charge density distribution is nearly uniform in the z-direction, except in the neighborhood of the electron mirrors at the ends of the cylinders where the charge density increases slightly since the mirrors introduce z-direction turning points. It therefore is allowed to eliminate z as one of the independent variables in Poisson's Equation, a considerable simplification. Formally stated then, the first assumption in the analysis is: The charge density distribution is sufficiently uniform in the z-direction that its variation may be neglected in the analysis.

Concerning the dependence of the charge density distribution on θ, the situation is not so elementary. Both uniform and strongly θ-dependent charge distributions are possible. This may be seen more clearly by considering first, those trajectories which lead to θ-dependent charge density distributions. If electrons are injected into trajectories which close after the execution of n orbits, the complete trajectory of the electrons resembles n superimposed, open-ellipse-like trajectories such that the angle between successive outer turning points is $\frac{2m\pi}{n}$. (See Appendix C). The electron continues in this trajectory indefinitely, retracing it once for each m circuits around the anode. That is, for a closed trajectory the electron returns again to the point of orbit injection, same r and θ but different z, and passes through this point with the same kinetic energy and angular momentum that it possessed at orbit injection. It necessarily follows that trajectories of this type are stationary since the individual orbits of the anode resemble ellipses having a relatively large counter rotating precession velocity such that the major axis rotates about the anode exactly m times while the electron is orbiting the anode n times. If all electrons are launched from the same point and injected into orbit with the same angular momentum and kinetic energy (which is very probable), then all electrons proceed along the same closed trajectory. Thus the charge density distribution in θ-space is nonuniform, being concentrated principally in the neighborhood of the $2n$ turning points of the n superimposed ellipse-like trajectories, and is stationary. Even if the electrons were all injected at equal intervals in time, at any given instant later they are not equally spaced along their common trajectory. These motions are investigated quantitatively in Appendix C.

It is clear, by comparison with the above results, that open trajectories lead to charge density distributions which are uniform in θ-space. That is the result of the continuing precession of the orbit eventually smears the charge uniformly

through θ-space. This conclusion holds even if all electrons are injected into the same open trajectory. As stated previously, optimum charge storage is associated with the absence of charge clusters, that is with uniform charge density distributions. Thus the second assumption, implicit in the following analysis is: The charge distribution in θ-space is uniform, that is that the range of allowed orbit injection parameters are such that the electron trajectories are open or at least close only after n is very large. This eliminates θ as an independent variable in Poisson's Equation and reduces it and the continuity equation to one dimensional ordinary differential equations in r.

Since the electron trajectories do not occupy the entire interelectrode space but rather only a thick cylindrical region located somewhere within the interelectrode space and with its axis coinciding with the axis of symmetry, it is necessary to divide the interelectrode space into three thick cylindrical regions: Region 1 ≡ the volume between the anode surface and the inner boundary of the electron cloud; Region 2 ≡ the volume occupied by the electron cloud; Region 3 ≡ the volume between the outer boundary of the electron cloud and the surface of the outer cylinder. A radial cut through the interelectrode space is shown in the figure below, which also defines some of the pertinent parameters.
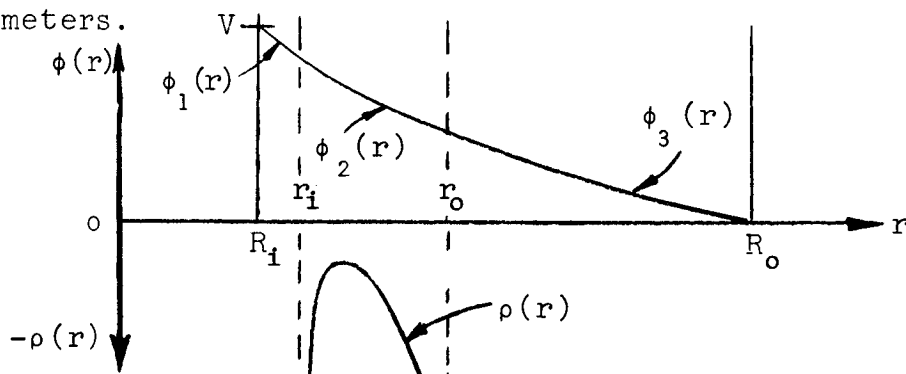
In Region 1, the potential distribution $\phi_1(r)$ is obtained from the homogeneous Poisson Equation (Laplace Eq.)

$$\frac{1}{r}\frac{d}{dr}\left[r\left(\frac{d\phi_1}{dr}\right)\right] = 0, \quad (R_i \leq r \leq r_i). \tag{1}$$

In Region 2, the Poisson Equation applies

$$\frac{1}{r}\frac{d}{dr}\left(r\frac{d\phi_2}{dr}\right) = -\frac{\rho(r)}{\epsilon_0} , (r_i \le r \le r_0).$$ (2)

In Region 3, the Laplace Equation again applies

$$\frac{1}{r}\frac{d}{dr}\left(r\frac{d\phi_3}{dr}\right) = 0 , (r_0 \le r \le R_0).$$ (3)

At the boundary between Regions 1 and 2, the potential distribution and the electric field must be continuous. Therefore the solutions to Eqs.(1) and (2) must satisfy

$$\phi_1(r_i) = \phi_2(r_i) ,$$ (4)

and

$$\frac{d\phi_1}{dr}\Big|_{r=r_i} = \frac{d\phi_2}{dr}\Big|_{r=r_i} .$$ (5)

At the boundary between Regions 2 and 3 again the potential and electric field must be continuous. Therefore the solutions to Eqs.(2) and (3) must satisfy

$$\phi_2(r_0) = \phi_3(r_0),$$ (6)

and

$$\frac{d\phi_2}{dr}\Big|_{r=r_0} = \frac{d\phi_3}{dr}\Big|_{r=r_0}.$$ (7)

At the surface of the anode, the potential must equal the applied voltage V. Therefore

$$\phi_1(R_i) = V .$$ (8)

15

At the surface of the outer cylinder the potential must be zero. Therefore

$$\phi_3(R_o) = 0 \ . \tag{9}$$

The solutions to Eqs.(1), (2) and (3) are (before evaluating the constants of integration)

$$\phi_1(r) = c_{11} \log r + c_{12} \ , \quad (R_i \leq r \leq r_i), \tag{10}$$

$$\phi_2(r) = - \int \frac{dr}{r} \int \frac{\rho(r)}{\varepsilon_o} \ r \ dr \ + c_{21} \log r + c_{22} \ , \ (r_i \leq r \leq r_o), \tag{11}$$

$$\phi_3(r) = c_{31} \log r + c_{32} \ , (r_o \leq r \leq R_o). \tag{12}$$

Using the six conditions expressed in Eqs.(4) through (9) to evaluate the six constants of integration gives

$$\phi_1(r) = V \frac{\log \frac{R_o}{r}}{\log \frac{R_o}{R_i}} + \left\{ I(r_o) - I(r_i) + I'(r_o) \log \frac{R_o}{r_o} - I'(r_i) \log \frac{R_o}{r_i} \right\} \frac{\log \frac{r}{R_i}}{\log \frac{R_o}{R_i}} \ ,$$
$$(R_i \leq r \leq r_i), \tag{13}$$

$$\phi_2(r) = V \frac{\log \frac{R_o}{r}}{\log \frac{R_o}{R_i}} + \left[I(r_o) + I'(r_o) \log \frac{R_o}{r_o} \right] \frac{\log \frac{r}{R_i}}{\log \frac{R_o}{R_i}}$$

$$+ \left[I(r_i) - I'(r_i) \log \frac{r_i}{R_i} \right] \frac{\log \frac{R_o}{r}}{\log \frac{R_o}{R_i}} - I(r), \ (r_i \leq r \leq r_o), \tag{14}$$

$$\phi_3(r) = V \frac{\log \frac{R_o}{r}}{\log \frac{R_o}{R_i}} - \left[I(r_o) - I(r_i) - I'(r_o) \log \frac{r_o}{R_i} + I'(r_i) \log \frac{r_i}{R_i} \right] \frac{\log \frac{R_o}{r}}{\log \frac{R_o}{R_i}} \ ,$$

$$(r_o \leq r \leq R_o), \tag{15}$$

where

$$I'(r_x) = \int \frac{\rho(r)}{\varepsilon_o} \, r \, dr \bigg|_{r=r_x} , \tag{16}$$

and

$$I(r_x) = \int \frac{dr}{r} \int \frac{\rho(r)}{\varepsilon_o} \, r \, dr \bigg|_{r=r_x} . \tag{17}$$

Equations (13) through (15) define the interelectrode potential distribution in terms of geometry, applied potential, and the charge integrals in Eqs.(16) and (17) for an arbitrary charge distribution, the evaluation of which must await specification of the actual charge density distribution from the results of the orbit analysis.

1.5   TRAJECTORIES

The differential equations for the motion of an electron in a cylindrically symmetric attractive, central force field are:

$$m (\ddot{r} - r\dot{\theta}^2) = -eE(r), \text{ (radial force component)}, \tag{18}$$

and

$$\frac{d}{dt}(mr^2\dot{\theta}) = 0, \qquad \text{(azimuthal component)}, \tag{19}$$

where $E(r) \equiv$ electric field due to both the applied potential and the space charge distribution.

Integrating Eq.(19) gives

$$mr^2\dot{\theta} = \ell \tag{20}$$

where

$\ell \equiv$ electron angular momentum (a constant throughout the orbital motion).

Therefore ℓ is one of the orbit injection parameters.   Using Eq.(20) to eliminate $\dot{\theta}$ in Eq.(18) gives the radial force as a function of r alone

$$m\ddot{r} = \frac{\ell^2}{mr^3} - eE(r). \tag{21}$$

The space charge radial distribution must eventually be derived from the solution to this equation.

Before proceeding with the solution of this equation, it will be rewritten to satisfy the orbit stability criteria, that is it must be modified such that it applies only to stable electron trajectories and excludes from consideration all trajectories which are unstable against radial perturbations. The motivation for introducing this modification is simply to concentrate the analytical work on that subset of trajectories which has the longest probable orbiting life time, since in

18

practical devices these trajectories are the most useful. There are many disturbances which may perturb the electron trajectory; for example, variation in electrode potentials due to power supply noise, variation in potential distribution induced by collective space charge oscillations, local magnetic fields, motion of the orbitron in these fields, elastic (nonionizing) collisions with gas atoms, etc. It is obvious that those trajectories which are unaffected by such disturbances have the highest probability of survival. Those trajectories which are least affected are the stable trajectories.

It is shown in Appendix A that the open-ellipse-like trajectories are stable only if the electron angular momentum satisfies the stability criteria

$$\ell^2 = \alpha^2 m e E_2(r_o) r_o{}^3, \tag{22}$$

where α is an independent stability parameter which quantitatively labels the stability of an orbit and has the allowed range

$$\text{(approaching instability)} \quad \frac{1}{3} < \alpha^2 \leq 1 \quad \text{(most stable)} \ . \tag{23}$$

It is shown in Appendix B that α is a function only of $e_c^* \equiv$ the effective eccentricity of the open-ellipse-like electron trajectories in the orbitron. It is shown in Appendix C that there are certain discreet values of α within the range given by Eq.(23), but which must be disallowed since they not only violate one of the analytical assumptions, but lead to stationary nonuniform charge distributions in θ-space and therefore nonoptimum charge density distribution.

Thus, the modification which must be made in the radial force equation, Eq.(21), is simply to introduce the stability criteria into that equation such that the system of equations applies to stable orbits only. Essentially, this constrains the allowed range of one of the orbit injection parameters (angular momentum) to a relatively narrow range.

The actual constraint, which sorts out of all possible electron trajectories those which are stable, is introduced into the system by replacing the angular momentum in Eq.(21) with its constrained value given by Eq.(22). The radial acceleration of the electron, applicable to stable orbits only, then is given by

$$\ddot{r} = \frac{e}{m}\left[\alpha^2 E_2(r_o)\frac{r_o^3}{r^3} - E_2(r)\right].$$ (24)

This introduces a third formal assumption into the analysis: Allowed orbits are members of the orbit subset which satisfy the stability criteria Eq.(22) only, however there is a discreet series of orbits within this subset which are disallowed since they lead to stationary nonuniform charge distributions in θ-space.

Proceeding now with the solution to Eq.(24), the radial component of the electron velocity is obtained by multiplying this equation by dr, recalling that $\ddot{r}dr = \dot{r}d\dot{r}$, that $-E(r)dr = d[\phi(r)]$, and integrating. The result is

$$\dot{r}^2 = \frac{2e}{m}\left[-\frac{\alpha^2 r_o^3 E_2(r_o)}{2\,r^2} + \phi_2(r)\right] + c,$$ (25)

where c is a constant of integration. This constant may be conveniently evaluated at either the inner or outer turning points where the radial component of the electron velocity passes through the value zero. There is, however, some advantage in using the outer turning point. Thus, setting the left side of Eq.(25) equal to zero, evaluating the right side at $r=r_o$, solving for c, and substituting the result back into Eq.(25) gives the radial velocity in terms of physical parameters

$$\dot{r}^2 = \frac{2e}{m}\left[\frac{\alpha^2 r_o E_2(r_o)}{2}\left(1 - \frac{r_o^2}{r^2}\right) + \phi_2(r)-\phi_2(r_o)\right].$$ (26)

This equation has two roots: the larger is of course at r_o, the smaller is at r_i (the inner turning point) which may be obtained by setting $\dot{r}^2 = 0$ giving the transcendental equation

$$\frac{r_o^2}{r_i^2} = 1 + \frac{2}{\alpha^2}\left\{\frac{\phi_2(r_i) - \phi_2(r_o)}{E_2(r_o)r_o}\right\} . \tag{27}$$

The potential distribution in Eq.(26) is that previously obtained for the space charge region, Eq.(14). The electric field at the outer turning point is obtained from Eq.(14) by taking the negative derivative with respect to r and evaluating the result at r_o. Both of these functions depend, in part, on the charge density distribution through the charge integrals, Eqs.(16) and (17), which are yet unspecified. Further progress in developing a self-consistent solution for the electron motion in the orbitron requires the definition of the charge density distributions.

1.6   SPACE CHARGE DISTRIBUTION

Recalling the previous discussion concerning the possible form of
the charge density distribution, it was concluded that it could not be
a function of z since only small gradients existed in the z-direction
resulting in a charge density which is nearly uniform in the z-direction,
and that it could not be a function of θ since only those launch param-
eters corresponding to open orbits (nonstationary) are allowed, which
after sufficient time result in a charge density distribution which is
uniform in the θ-direction. If sufficient time is allowed after the be-
ginning of injection, the charge density at all points in the electron
cloud will have built up to its final, equilibrium value and will thus be
independent of time. This neglects the small time dependent component of
the charge density associated with the collision loss rate and the orbit
injection rate, since the mean orbiting life-time is relatively long
(except at high pressures) in comparison with the injection or loss
transit time. This amounts to introducing into the analysis a 4th formal
assumption: The time-dependent component of the charge density distribu-
tion corresponding to the collision loss rate and the balancing injection
rate is negligible in comparison to the stationary (equilibrium) charge
density distribution.

Under the above conditions the charge density distribution is a
function of r only, and thus the continuity equation

$$\nabla \cdot \vec{j} + \frac{\partial \rho}{\partial t} = 0, \qquad (28)$$

reduces to

$$\frac{d}{dr} (r \, j_r) = 0. \qquad (29)$$

For any equilibrium (stationary) charge density distribution $\frac{\partial \rho}{\partial t} = 0$. It necessarily follows that the quantity of charge flowing into any volume element equals the quantity flowing out of that element. The radial component of the current density at any point within the space charge region must therefore consist of a positive and negative component, such that

$$j_{r+}(r) = \frac{1}{2} \rho(r) \dot{r}_+(r) \tag{30}$$

and

$$j_{r-}(r) = \frac{1}{2} \rho(r) \dot{r}_-(r) \tag{31}$$

and have the property

$$j_r(r) = j_{r+}(r) + j_{r-}(r) = \frac{1}{2} \rho(r)[\dot{r}_+(r) + \dot{r}_-(r)] = 0 , \tag{32}$$

since

$$\dot{r}_+(r) = -\dot{r}_-(r) ; \tag{33}$$

since $\dot{r}(r)$ is a single valued function of r. However, since all the charge is electronic and $\rho(r)$ is a scalar, the charge density is independent of the sign of $j_r(r)$. Thus each component of $j_r(r)$ contributes equally to the local charge density $\rho(r)$. Therefore the function that must be inserted into Eq.(29) for the current density is

$$|j_{r+}(r)| + |j_{r-}(r)| = \frac{1}{2} \rho(r)[|\dot{r}_+(r)| + |\dot{r}_-(r)|] = \rho(r)|\dot{r}(r)| . \tag{34}$$

The contunuity equation thus becomes

$$\frac{d}{dr} \{r \rho(r)|\dot{r}(r)|\} = 0. \tag{35}$$

The solution to this equation is obviously

$$\rho(r) = \frac{c}{r|\dot{r}(r)|} . \tag{36}$$

The constant of integration may be evaluated as follows: Suppose there are N_L electrons in unit length of the electron cloud (unit length along the cylindrical axis). The integral of the charge density distribution over the volume of a unit length of the space charge region must equal the total charge within that region, thus

$$\int_{r_i}^{r_o} \int_{o}^{2\pi} \rho(r)\, r dr d\theta = -eN_L \tag{37}$$

where $(-e) \equiv$ electron charge. Since $\rho(r)$ is independent of θ this equation may be written

$$\int_{r_i}^{r_o} \rho(r) r dr = -\frac{eN_L}{2\pi}. \tag{38}$$

Substituting from Eq.(36) for $\rho(r)$ and solving for the normalization constant c, gives

$$c = -\frac{eN_L}{2\pi} \frac{1}{\int_{r_i}^{r_o} |\dot{r}(r)|^{-1} dr}. \tag{39}$$

Substituting this result back into Eq.(36) gives the charge density distribution within the space charge region

$$\rho(r) = -\frac{eN_L}{2\pi \int_{r_i}^{r_o} |\dot{r}(r)|^{-1} dr} \cdot \frac{1}{r|\dot{r}(r)|}. \tag{40}$$

Although this result (that the charge density is inversly proportional to the radial component of the velocity) is not a common form of charge density distribution, it has been encountered in other situations (see for example Landau and Lifschitz in Ref.5 where a similar result is obtained in another connection concerning the motion of bound electrons).

The charge density distribution may be derived directly from statistical considerations which do not involve (explicitly) the integration of the continuity equation. This derivation also yields a somewhat different insight into the connection between charge density distribution and the electron dynamics. Consider the motion of a single electron along a stable trajectory in an orbitron. The fraction of the orbit period that the electron spends in traversing the infinitesimal interval Δs along its trajectory s is

$$\frac{t(s+\Delta s) - t(s)}{\tau},$$ (41)

where τ is the orbit period and t is considered a function of orbit position s. The probability that the electron is within the interval Δs at s is the probability distribution $\psi(s)$ (probability per unit length of trajectory). Thus $\psi(s)$ is simply the fraction of the orbit period spent in Δs divided by the length of Δs,

$$\psi(s) = \frac{t(s+\Delta s) - t(s)}{\tau \, \Delta s} .$$ (42)

Taking the limit $\Delta s \to 0$ gives

$$\psi(s) = \frac{1}{\tau |v(s)|} ,$$ (43)

since

$$\lim_{\Delta s \to 0} \frac{t(s+\Delta s) - t(s)}{\Delta s} \equiv \frac{dt}{ds} = \frac{1}{v(s)}$$ (44)

where $v(s) \equiv$ orbit velocity as a function of the trajectory coordinate s, and the absolute value of the orbit velocity has been taken to avoid the possibility of a physically meaningless negative probability distribution (especially later, when a transformation is made from the trajectory coordinate s to polar coordinates r, θ). The charge associated with a single electron may be considered as distributed over the electron orbit in exactly the same way that the probable position is distributed. The charge distribution at any point s along the orbit is then given by the product of

the electron charge and the position probability distribution. Thus the increment of charge in the interval ds at s is given by

$$dQ(s) = -e \ \psi(s) \ ds \qquad (45)$$

Referring to the figure below, the increment of charge contained in the volume between two concentric cylindrical surfaces of radii r and r+dr respectively, must be given by the product of the local density $\rho(r)$ and the volume element dV. Thus

$$dQ(r) = \rho(r) \ dV = \rho(r) \ 2\pi \ rdr \qquad (46)$$

where $Q(r) \equiv$ charge per unit length of cylindrical volume (also applies to Eq.(45)),

$\rho(r) \equiv$ charge density at r associated with a single orbiting electron.
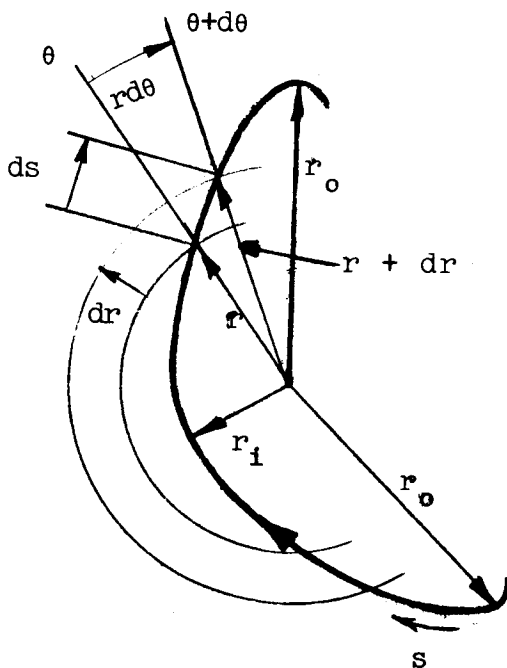
Since the electron trajectory passes twice through the volume element considered, the increment of charge in Eq.(46) is twice the increment in Eq.(45). Therefore

$$\pi\rho(r)\, rdr = -e\ \psi(s)ds = -\frac{e\ ds}{\tau|v(s)|}. \tag{47}$$

The right side of this equation may be transformed to polar coordinates by recalling that

$$ds = \left\{1 + \left(\frac{d\theta}{dr}\right)^2\right\}^{\frac{1}{2}} dr\ , \tag{48}$$

and

$$|v(s)| = +\left\{1 + \left(\frac{d\theta}{dr}\right)^2\right\}^{\frac{1}{2}}|\dot{r}(r)|. \tag{49}$$

Equation (47) then may be written

$$\left\{\pi\rho(r)r + \frac{e}{\tau|\dot{r}(r)|}\right\}dr = 0. \tag{50}$$

Therefore the charge density distribution of a single bound electron executing a stable, open orbit in an orbitron is

$$\rho(r) = -\frac{e}{\pi\tau}\cdot\frac{1}{r|\dot{r}(r)|}\ , \tag{51}$$

and the charge density distribution for N_L electrons per unit length of space charge region is finally

$$\rho(r) = -\frac{e\ N_L}{\pi\tau}\ \frac{1}{r|\dot{r}(r)|}\ . \tag{52}$$

This result agrees with that previously derived, Eq.(40), if

$$\int_{r_i}^{r_o} \frac{dr}{|\dot{r}(r)|}$$

is equal to $\frac{\tau}{2}$. But by definition, the orbit period is given by

$$\tau = \int_o^\tau dt = 2 \int_{r_i}^{r_o} \frac{dr}{|\dot{r}(r)|} . \tag{53}$$

Therefore Eq.(40) and Eq.(52) give identical results for the charge density distribution.

Completely electronic charge density distributions of the form given by Eq.(52) permit some simplification of the potential distribution given by Eqs.(13) through (15), since certain of the charge integrals appearing in these equations are zero. Apart from the negative sign associated with the electronic charge, (-e), the integral of the charge density distribution, see Eq.(16), is a positive, increasing function of r and is zero for $r < r_i$ and $r > r_o$ since $\rho(r)$ is zero outside these limits. Therefore the first charge integral evaluated at the lower limit, the inner boundary of the space charge cloud, is zero. Thus

$$I'(r_i) = 0. \tag{54}$$

A similar arguement applies to the second integral of the charge density distribution, see Eq.(17), since it represents the area under the curve $\frac{Q(r)}{r}$. Therefore

$$I(r_i) = 0. \tag{55}$$

Thus the quantity within the second set of brackets appearing in Eq.(14) is zero.

28

It may be useful to emphasize several observations concerning $\rho(r)$. At both the inner and outer turning points $\rho(r)$ diverges since $\dot{r}(r_i) = \dot{r}(r_o) = 0$. However the integral of $\rho(r)$ remains finite and it is generally an integral function of $\rho(r)$ that is required in the analysis. Perhaps the most important property of $\rho(r)$ (because of its serious consequence) is its form. The form of $\rho(r)$ renders the Poisson Equation nonintegrable analytically. Although this is a serious mathematical handicap implying that a general solution to the problem is not possible, self-consistent particular solutions having any prescribed accuracy can be developed using iterative, numerical integration. These latter difficulties are the consequence of the fundamental nonlinearity of the orbitron.

1.7 SELF-CONSISTENT SOLUTION (1st APPROXIMATION)

The analysis has now yielded all the information necessary to develop a self-consistent solution for the electron motion in an orbitron: Eq. (14) gives the potential distribution for an arbitrary charge density distribution; Eq. (26) gives the electron radial velocity for an arbitrary potential distribution; and Eq. (52) gives the charge density distribution as a function of the radial component of the electron velocity. These equations may be considered a set of consistent, simultaneous integro-differential equations. $\dot{r}(r)$ and $\rho(r)$ may be eliminated by substituting Eq. (26) into Eq. (52) and then substituting the result into Eq. (14) which gives a single nonlinear, integral equation in $\phi(r)$ alone. This equation is not written here since it is nonintegrable analytically; implying that a general solution to the orbitron problem is **not** possible.

However, after having specified all pertinent parameters, a particular solution may be developed (one solution for each set of parameters) by iterative, numerical integration. The continuation of the analysis beyond this point therefore involves a combination of both numerical and analytical techniques.

The starting point for obtaining a particular self-consistent solution using these methods is the radial velocity equation (radial mode kinetic energy equation). The application of numerical methods requires a knowledge of the specific range of integration. Thus it is first necessary to establish the turning points (space charge boundaries). The ratio of the turning points is, in general, given by Eq. (27) but for the present need it is more convenient to write it in the unconstrained form (without the stability constraint which will be reinserted later on) by substituting from Eq. (22) for $E_2(r_o)$ and recalling that the outer turning point kinetic energy $T(r_o)$, is given by

$$T(r_o) = \frac{\ell^2}{2mr_o^2}.$$ (56)

Eq. (27) may then be written

$$\frac{r_o^2}{r_i^2} = 1 + e^{\frac{[\Phi_2(r_i) - \Phi_2(r_o)]}{T(r_o)}}$$ (57)

From Eq.(14) and using Eqs.(54) and (55) the difference in the space charge dependent potential between r_i and r_o is given by

$$\Phi_2(r_i) - \Phi_2(r_o) =$$

$$\left\{ V + I'(r_o) \left[\log\frac{r_o}{R_i} - \frac{I(r_o)}{I'(r_o)} \right] \right\} \frac{\log\frac{r_o}{r_i}}{\log\frac{R_o}{R_i}} - I'(r_o) \left[\log\frac{r_o}{r_i} - \frac{I(r_o)}{I'(r_o)} \right].$$ (58)

It may be observed from Eqs.(16), (17) and (52) that the ratio of charge integrals, $\frac{I(r_o)}{I'(r_o)}$, is not explicitly dependent on the magnitude of the total charge stored in the space charge cloud. The explicit dependence of the potential difference in Eq.(58) on the magnitude of the stored charge may be eliminated by imposing the stability constraint. Taking the negative derivative of Eq.(14) with respect to r and applying Eqs.(54) and (55) gives the space charge dependent electric field distribution

$$E_2(r) = \left\{ V + I'(r_o) \left[\log\frac{r_o}{R_i} - \frac{I(r_o)}{I'(r_o)} \right] \right\} \frac{1}{\log\frac{R_o}{R_i}} \frac{1}{r} - \left[I'(r_o) - I'(r) \right] \frac{1}{r}.$$

(59)

31

Evaluating this equation at r_o and substituting the results into the stability criteria, Eq.(22), and using Eq.(56) to eliminate ℓ^2 in terms of $T(r_o)$ gives

$$T(r_o) = \frac{\alpha^2}{2}eE_2(r_o)r_o$$

$$= \frac{\alpha^2 e}{2}\left\{V + I'(r_o)\left[\log\frac{r_o}{R_i} - \frac{I(r_o)}{I'(r_o)}\right]\right\}\frac{1}{\log\frac{R_o}{R_i}} \qquad (60.)$$

From this equation it follows that

$$-I'(r_o) = V\frac{\left[1 - \frac{2T(r_o)}{\alpha^2 ev}\log\frac{R_o}{R_i}\right]}{\left[\log\frac{r_o}{R_i} - \frac{I(r_o)}{I'(r_o)}\right]}\ . \qquad (61)$$

Using this equation to eliminate $I'(r_o)$ in Eq. (58) gives for the potential difference between r_i and r_o

$$\Phi_2(r_i) - \Phi_2(r_o) =$$

$$\frac{2T(r_o)}{\alpha^2 e}\log\frac{r_o}{r_i} + V\left[1 - \frac{2T(r_o)}{\alpha^2 ev}\log\frac{R_o}{R_i}\right]\frac{\left[\log\frac{r_o}{r_i} - \frac{I(r_o)}{I'(r_o)}\right]}{\left[\log\frac{r_o}{R_i} - \frac{I(r_o)}{I'(r_o)}\right]} \qquad (62)$$

which does not depend explicitly on the magnitude of the stored charge.

It is shown in Appendix E that optimization of the total charge stored in the rotating electron cloud corresponds, in part, to maximizing it with respect to r_i. The maximization

of N_L with respect to r_i requires that $r_i \simeq R_i$. That is that the inner turning point (and the inner boundary of the space charge cloud) is displaced from the surface of the anode only by a very small distance, sufficient to assure that the electrons do not collide with the surface. In practice, this distance may be of the same order of magnitude as the surface roughness and therefore very small compared with R_i. Setting $r_i \simeq R_i$ thus does not involve a substantial approximation and the difference between them may be neglected in the analysis (see Appendix E). Although this condition is very important to the optimization of the stored charge, it has other, equally important, consequences. Setting $r_i \simeq R_i$ reduces the system from a 6 parameter system to a 5 parameter system, but accomplishes the reduction in a way which permits considerable additional analytical progress without specifying all other parameters. Applying $r_i \simeq R_i$ to Eq.(62) reduces that equation to

$$\Phi_2(r_i) - \Phi_2(r_o) = \frac{2T(r_o)}{\alpha^2 e} \log \frac{r_o}{r_i} + V\left[1 - \frac{2T(r_o)}{\alpha^2 \, eV} \log \frac{R_o}{R_i}\right], (r_i \simeq R_i),$$

(63)

and substituting this into Eq.(57) and rearranging gives the following transcendental equation for the ratio of the outer to inner turning points

$$\log \frac{r_o}{r_i} + \frac{\alpha^2}{2}\left(1 - \frac{r_o^2}{r_i^2}\right) + \beta = 0, \quad (r_i \simeq R_i),$$

(64)

where

$$\beta = \frac{\alpha^2 eV}{2T(r_o)} - \log \frac{R_o}{R_i}.$$

(65)

33

β is not an independent parameter, but a specific function of prescribed parameters. Thus the introduction of β does not amount to introducing a new parameter since all the parameters on the right side of Eq.(65) are prescribed parameters and therefore specify β. Alternatively, β may be considered a subset label, specifying not a single particular solution but rather an entire subset of particular solutions in which there remains a considerable range of variation of the parameter on which β depends, subject only to the condition that β remain constant. β is here introduced as a mathematicl convenience, however, in Appendix D its physical interpretation is discussed and it is shown that $\beta > 0$ for all electronic charge distributions and β may be considered a measure of the reduction in electric field at the outer cylinder resulting from the space charge insertions.

Eq.(64) gives the ratio of turning points in terms of prescribed parameters only, which do not explicitly involve the charge density distribution. Actually, since it has been specified that $r_i \simeq R_i$ and R_i is prescribed, Eq.(64) gives the outer turning point in terms of prescribed values of α^2 and β. This substantially reduces the number of self-consistent particular solutions for electron trajectories in the orbitron since all solutions for which $r_i > R_i$ are rejected. However, this is a considerable advantage since only those particular solutions are retained for which the charge stored in the electron cloud is optimized.

It is obvious that the space charge integrals $I'(r_o)$, $I(r_o)$ and $I(r)$ in Eq.(14) must apply to exactly the same region of r-space as that to which $\phi_2(r)$ applied. The first approximation to these integrals is obtained by substituting into $\rho(\dot{r}) = - \frac{eN_L}{\pi\tau} \cdot \frac{1}{r\dot{r}}$, the space charge free $\dot{r}$. Therefore the

ratio of the outer to inner turning points in the space charge free radial velocity equation, $\left(\dfrac{r_o}{r_i}\right)_o$ (where the subscript o indicates that $\beta = 0$), must be the same as the ratio of the outer to inner turning points in the space charge dependent radial velocity equation, $\left(\dfrac{r_o}{r_i}\right)_\beta$ (where the subscript β indicates any value of $\beta > 0$ implying $|\rho| > 0$). Thus

$$\left(\frac{r_o}{r_i}\right)_o = \left(\frac{r_o}{r_i}\right)_\beta \tag{66}$$

$\left(\dfrac{r_o}{r_i}\right)_o$ is a function of α^2 only as may be seen from Eq.(64) for $\beta = 0$ and $\left(\dfrac{r_o}{r_i}\right)_\beta$ is a function of both α^2 and β. If α_o^2 is some value of α^2 applicable to Eq.(64) for $\beta = 0$ and α_β^2 is the value of α^2 applicable to some prescribed value of $\beta > 0$, the only way Eq.(66) can be satisfied is if $\alpha_\beta^2 > \alpha_o^2$. Thus, from Eq.(66), it follows that the set of equations

$$\log \frac{r_o}{r_i} + \frac{\alpha_o^2}{2} \left(1 - \frac{r_o^2}{r_i^2}\right) = 0 \tag{67}$$

and

$$\log \frac{r_o}{r_i} + \frac{\alpha_\beta^2}{2} \left(1 - \frac{r_o^2}{r_i^2}\right) + \beta = 0 \tag{68}$$

must be solved simultaneously for $\dfrac{r_o}{r_i}$ and α_β^2 for some pre-scribed set (α_o^2, β). According to the stability criteria, the minimum value of α_o^2 is $\frac{1}{3}$. This value of α^2 strictly applies only to α_β^2 and not to α_o^2 since the space charge free $\dot{r}$ is used only as an initial generating function known to have an approximately correct shape. However, in this first development of a self-consistent solution, the stability criteria is applied to both α_o^2 and α_β^2. This value of α^2 corresponds to the maximum value of $\left(\dfrac{r_o}{r_i}\right)_o$ and thus yields the highest (allowed) probability that electrons miss the launcher during

the first few orbits after injection. (See Appendix E). From Fig.1,where numerical solutions of Eq.(64) for $\frac{r_o}{r_i}$ as a function of α^2 with β as family parameter are plotted, it may be seen that

$$\left(\frac{r_o}{r_i}\right)_o \bigg|_{max} = 2.59, \; (\alpha_o^2 = \frac{1}{3}). \tag{69}$$

From Eqs.(66) and (69) and Fig.2, where $\left(\frac{r_o}{r_i}\right)_\beta$ is plotted as a function of β for $\alpha_\beta^2 = 1$, it may be seen that the maximum value that may be prescribed for β is about 1.9. In this first development of a self-consistent solution, a mid-range β is arbitrarily chosen such that

$$\beta = 1.0. \tag{70}$$

For this value of β and from Eqs.(66) and (69) and Fig.1, it follows that

$$\alpha_\beta^2 = 0.684. \tag{71}$$

These numerical values are needed for later computations.

The first approximation to the charge density distribution is given by

$$\rho_1(r) = \frac{-eN_L}{\pi\tau_o} \cdot \frac{1}{r\, \dot{r}_o}, \tag{72}$$

where the subscript o indicates that the electrons have been arbitrarily assigned the radial velocity strictly applicable only to electrons in a space charge cloud which has a negligibly low charge density. This does not imply that $\rho_1(r)$ is necessarily small (N_L in Eq.(72) may be large), but only that Eq.(72) is an approximate relation which is to be refined in
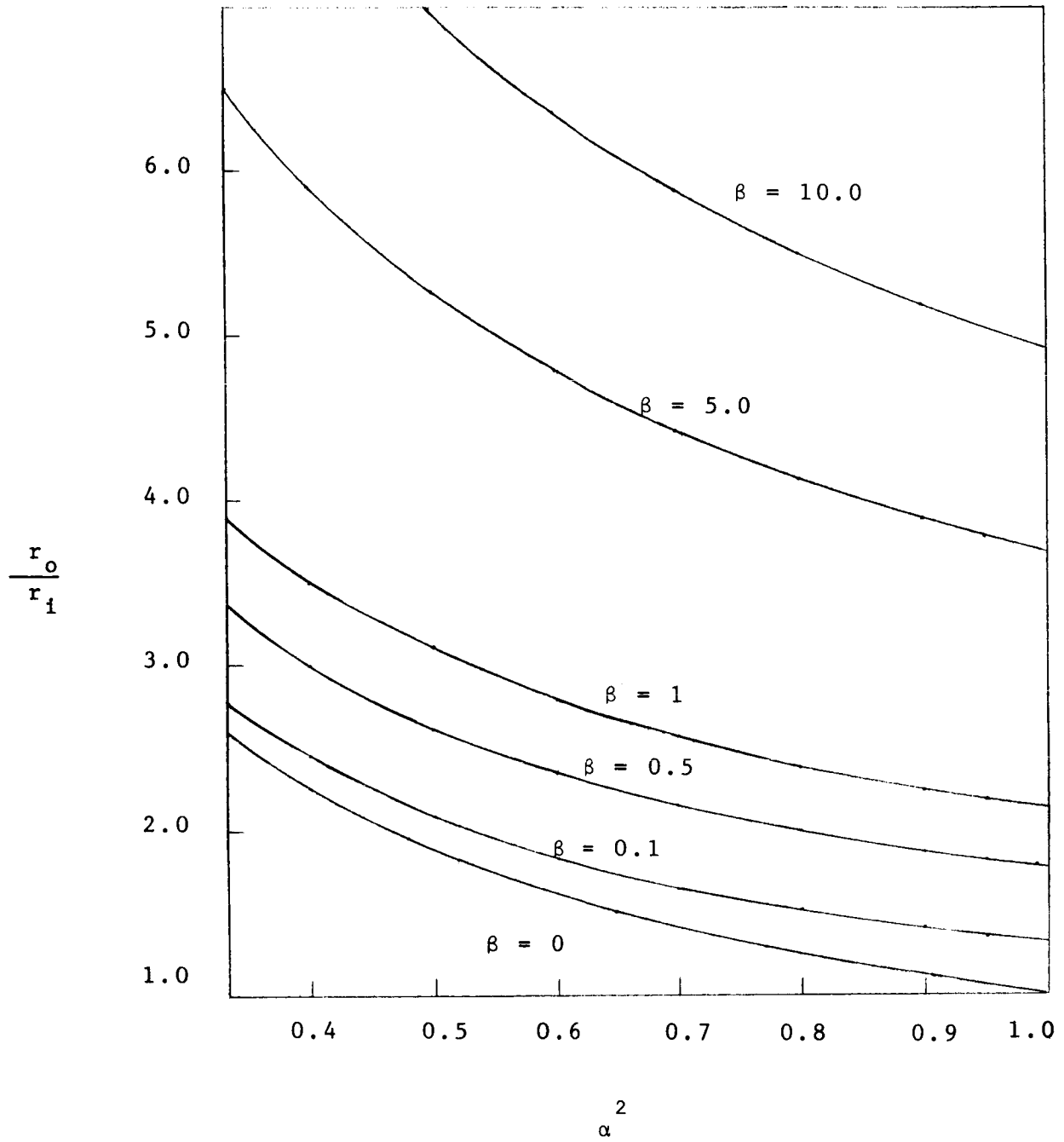
Fig. 1 Numerical Solution of Eq. (64)
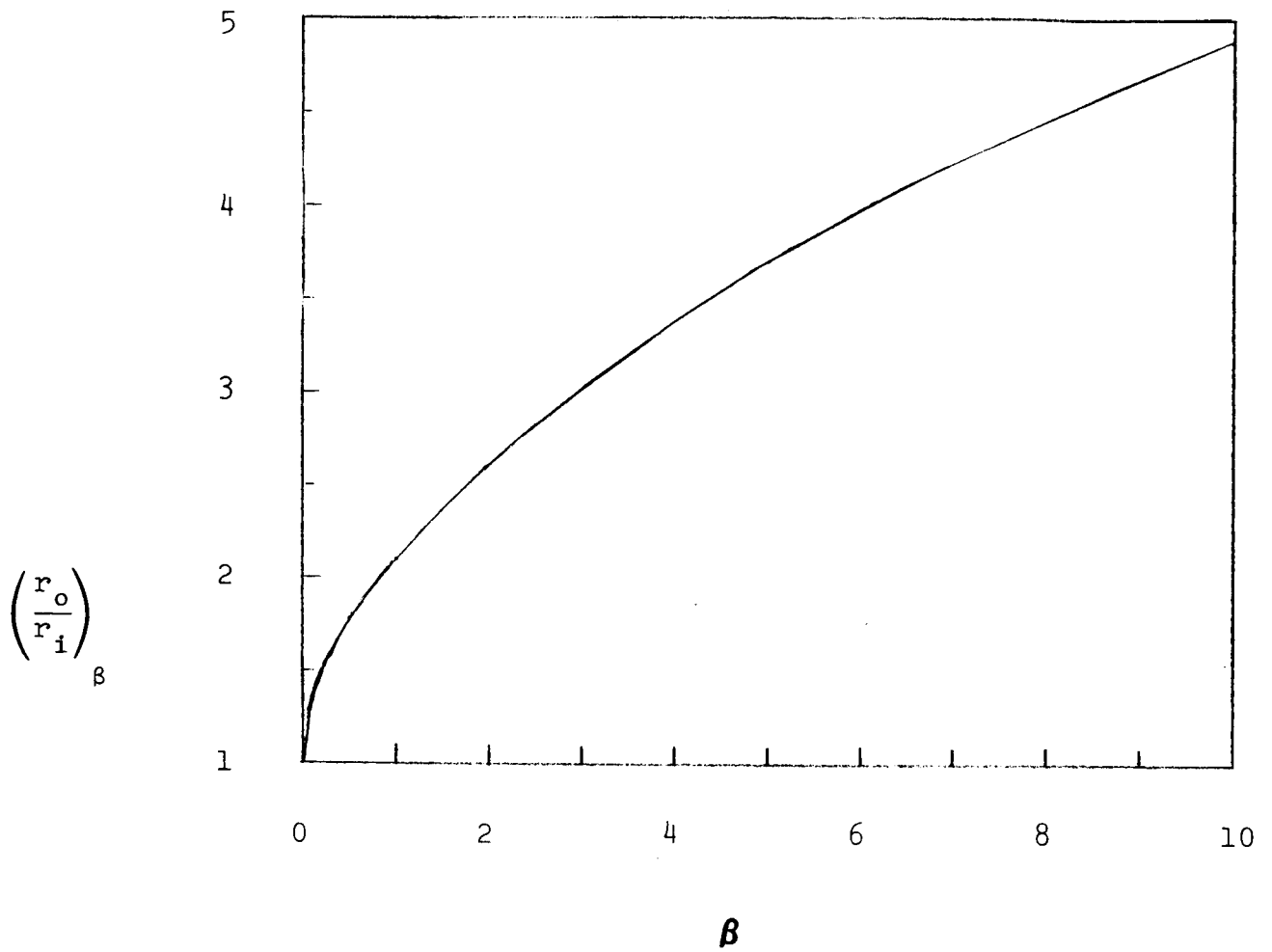
Fig. 2   Numerical Solution of Eq.(68) for the Maximum
          Value of α_β^2 ($\alpha_\beta^2 = 1$).

Note: This value of α_β^2 allows the maximum range of
          β constant with Eq.(66) and thus the maximum
          range of N_L.

subsequent iterations. From Eqs.(14) and (26), Eq.(72) may be written in the following dimensionless form (after setting all charge integrals to zero),

$$\frac{r_o r \rho_1(r)}{\left(\frac{-eN_L}{2\pi}\right)} = \frac{\left\{\log\frac{r_o}{r} + \frac{\alpha_o^2}{2}\left(1-\frac{r_o^2}{r^2}\right)\right\}^{-\frac{1}{2}}}{\int_{r_i}^{r_o}\left\{\log\frac{r_o}{r} + \frac{\alpha_o^2}{2}\left(1-\frac{r_o^2}{r^2}\right)\right\}^{-\frac{1}{2}}\frac{dr}{r_o}} \quad . \tag{73}$$

The denominator of this equation has been integrated numerically and the equation is plotted in Fig.3 as $f_1(\alpha_o, \frac{r}{r_o})$ for $\alpha_o^2 = \frac{1}{3}$, where

$$f_1(\alpha_o, \frac{r}{r_o}) \equiv \frac{r_o r \rho_1(r)}{\left(\frac{-eN_L}{2\pi}\right)} \quad . \tag{74}$$

The first approximation to the first charge integral $I_1'(r)$ is then obtained by substituting Eq.(73) into Eq.(16) and performing a numerical integration, using Eq.(69) to define the lower limit of integration. The result is plotted in Fig.4 as $g_1'(\alpha_o, \frac{r}{r_o})$ (a dimensionless function obtained by dividing Eq.(16) by $-\frac{eN_L}{2\pi\epsilon_o}$),

$$g_1'(\alpha_o, \frac{r}{r_o}) \equiv \frac{I_1'(r)}{-\frac{eN_L}{2\pi\epsilon_o}} \tag{75}$$

The first approximation to the second charge integral $I_1(r)$ is then obtained by substituting the numerical results from Fig.4, Eq.(75), into Eq.(17) and performing the second integration, again numerically. The results are plotted in Fig.5 as $g_1(\alpha_o, \frac{r}{r_o})$ (a dimensionless function obtained

$f_1(\alpha_o, \frac{r}{r_o})$

6

5

4

3

2

1

0.4   0.5   0.6   0.7   0.8   0.9   1.0

$\frac{r}{r_o}$
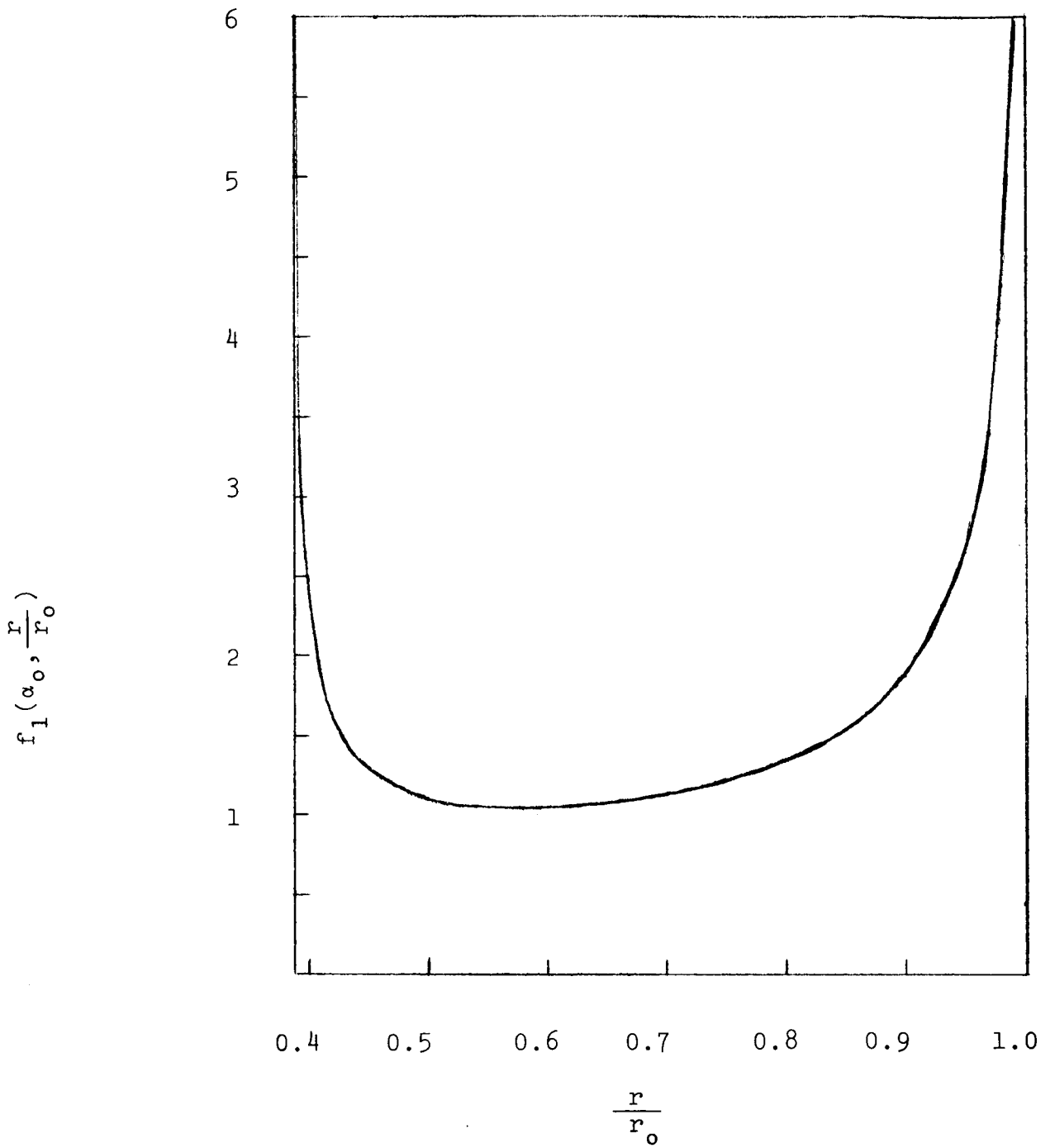
Fig. 3   1st Approximation to the Space Charge
Distribution
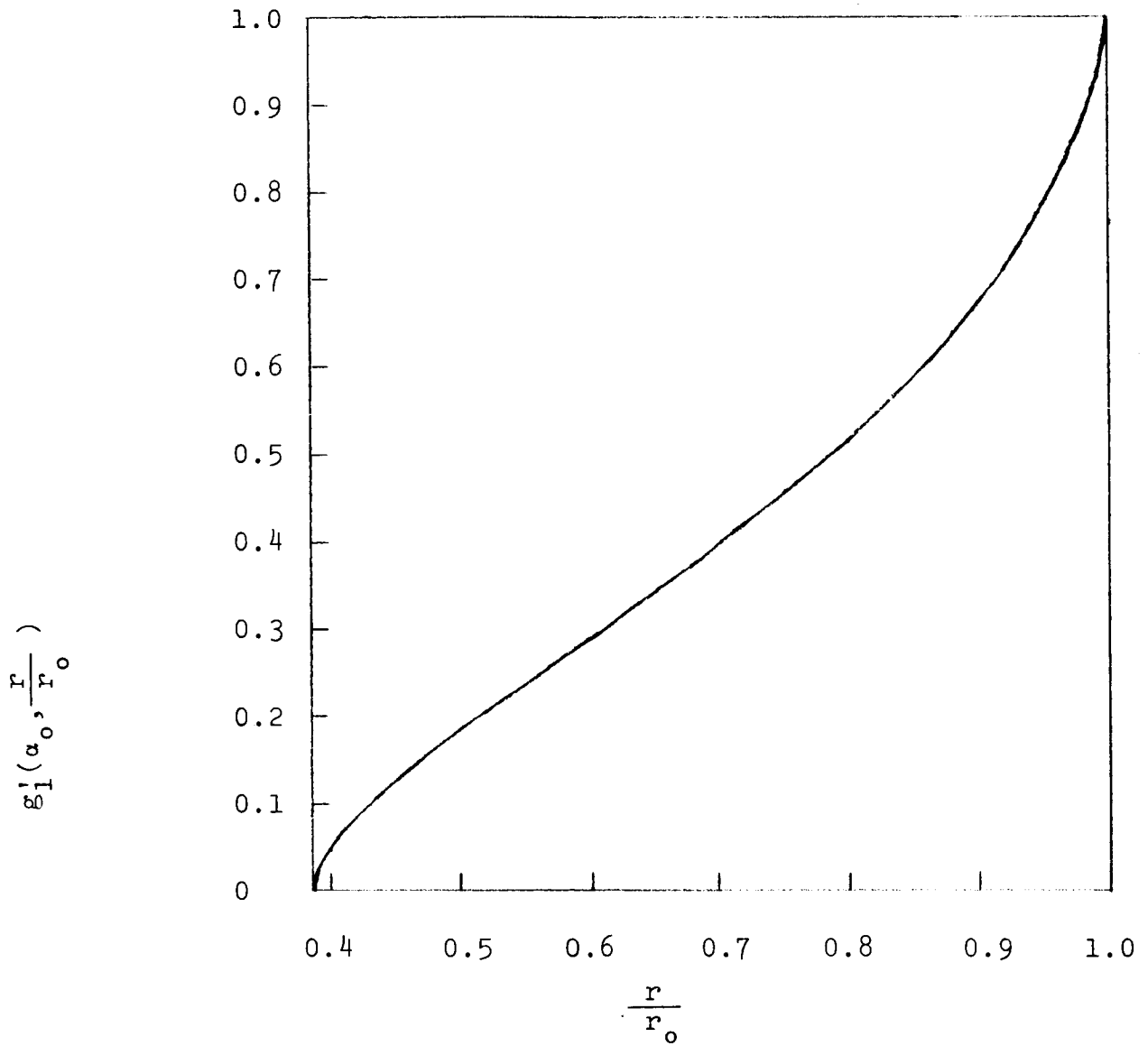
Fig. 4   1st Integral of $f_1(\alpha_o, \frac{r}{r_o})$
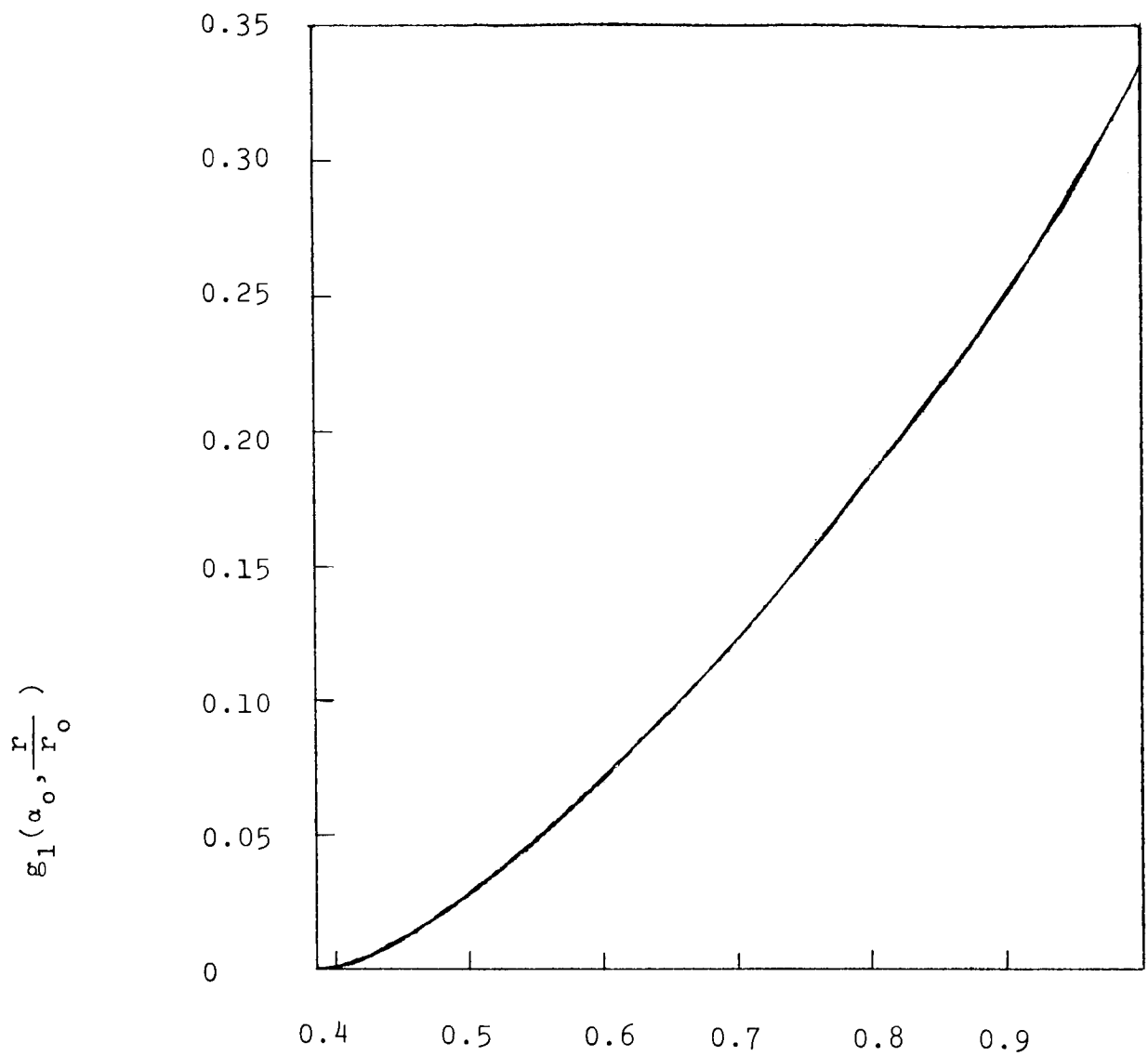
Fig. 5   2nd Integral of $f_1(\alpha_o, \frac{r}{r_o})$

by dividing Eq.(17) by $-\frac{eN_L}{2\pi\epsilon_0}$),

$$g_1(\alpha_0,\frac{r}{r_0}) \equiv \frac{I_1(r)}{-\frac{eN_L}{2\pi\epsilon_0}} \ . \tag{76}$$

g' and g have been introduced as a mathematical convenience. They are the same as I ' and I except that they do not depend explicitly on N_L.

Substituting these numerical results back into Eq.(14) gives

$$\Phi_{21}(r) = \frac{V \log\frac{R_0}{r}}{\log\frac{R_0}{R_i}} - \frac{eN_L}{2\pi\epsilon_0} \left\{ \left[\log\frac{R_0}{r_0} + g_1(\alpha_0,1) \right] \frac{\log\frac{r}{R_i}}{\log\frac{R_0}{R_i}} - g_1(\alpha_0,\frac{r}{r_0}) \right\} \tag{77}$$

where the second subscript on $\Phi_{21}(r)$ indicates that it is the first approximation to the space charge dependent potential distribution. In Eq.(77), Eqs.(54) and (55) have been applied and the result

$$g_1'(\alpha_0,1) = 1 \tag{78}$$

has been used.

The first approximation to the electron radial velocity as a function of the space charge dependent potential distribution is obtained by substituting Eq.(77) into Eq.(26), then using Eq.(61) to eliminate N_L after having substituted the numerical results of Figs.4 and 5, Eqs.(75) and (76), into Eq.(61). The result of these operations is

43

$$\dot{r}_1^2 = \frac{4T(r_0)}{\alpha_\beta^2 \, m} \left\{ \log \frac{r_0}{r} + \frac{\alpha_\beta^2}{2}\left(1-\frac{r_0^2}{r^2}\right) + \beta \left[\frac{\log \frac{r_0}{r} + g_1(\alpha_0,\frac{r}{r_0})-g_1(\alpha_0,1)}{\log \frac{r_0}{r_i} - g_1(\alpha_0,1)} \right] \right\}$$

It may be seen that $\dot{r}_1$ does not depend explicitly on N_L. This completes the development of the first approximation to a self-consistent solution of the electron motion and distribution in an orbitron (except for several detail calculations which are made later).

The second approximation to the charge density is obtained by substituting Eq.(79) into Eqs.(52) and (53) which gives

$$\frac{r_0 r \, \rho_2(r)}{\left(-\frac{eN_L}{2\pi}\right)} = \frac{\left\{ \log \frac{r_0}{r} + \frac{\alpha_\beta^2}{2}\left(1-\frac{r_0^2}{r^2}\right) + \beta\left[\frac{\log \frac{r_0}{r}+g_1(\alpha_0,\frac{r}{r_0})-g_1(\alpha_0,1)}{\log \frac{r_0}{r_i}-g_1(\alpha_0,1)}\right]\right\}^{\frac{1}{2}}}{\int_{r_i}^{r_0}\left\{ \log \frac{r_0}{r} + \frac{\alpha_\beta^2}{2}\left(1-\frac{r_0^2}{r^2}\right)+\beta\left[\frac{\log \frac{r_0}{r}+g_1(\alpha_0,\frac{r}{r_0})-g_1(\alpha_0,1)}{\log \frac{r_0}{r_i}-g_1(\alpha_0,1)}\right]\right\}^{\frac{1}{2}}\frac{dr}{r_0}} \quad (80)$$

The denominator of this equation has been integrated numerically and the equation is plotted in Fig.6 as $f_2(g_1,\alpha_\beta,\beta,\frac{r}{r_0})$ where

$$f_2(g_1,\alpha_\beta,\beta,\frac{r}{r_0}) \equiv \frac{r_0 r \, \rho_2(r)}{\left(-\frac{eN_L}{2\pi}\right)} , \qquad (81)$$

which does not depend explicitly on N_L. The function $\rho_2(r)$, Eq.(80), may now be used in the same way as above to begin the second iteration and thus generate the second approximation to the dimensionless charge integral functions $g_2'(g_1,\alpha_\beta,\beta,\frac{r}{r_0})$ and
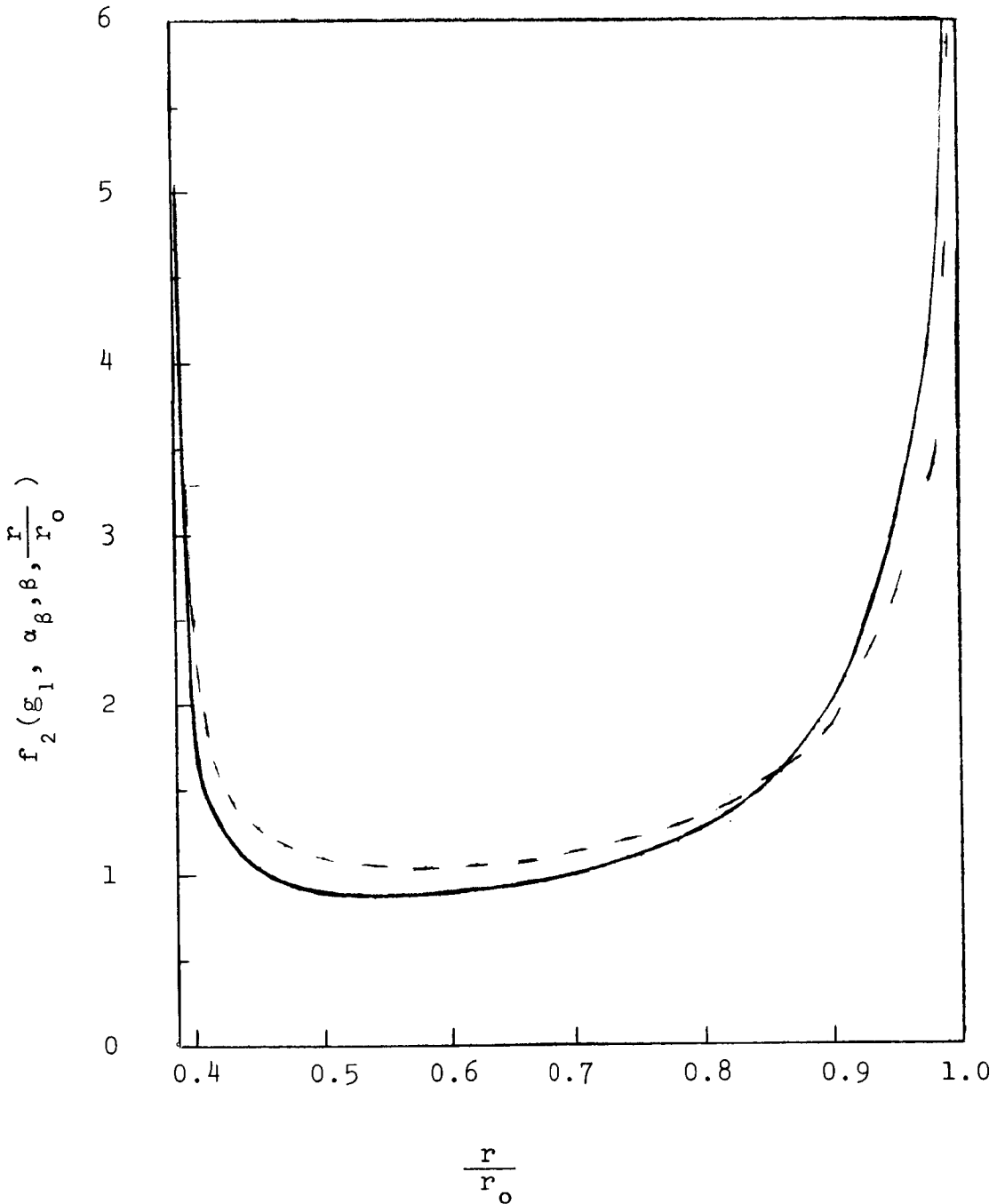
Fig. 6   2nd Approximation to the Charge Density
           Distribution.

Note: The 1st approximation, $f_1(\alpha_o, \frac{r}{r_o})$, is
           shown dashed for comparison. The rela-
           tively small difference between $f_1(\alpha_o, \frac{r}{r_o})$
           and $f_2(g_1, \alpha_\beta, \beta, \frac{r}{r_o})$ implies that the
           iteration process converges rapidly.

45

$g_2(g_1, \alpha_\beta, \beta, \frac{r}{r_o})$. These functions may then be used, in the same way as above, to generate the third approximation to the charge density distribution. $\rho_3(r)$ may now be used to begin the third iteration, and so on... The development of a self-consistent solution having the required accuracy is finally completed if the result of the last iteration $\rho_n(r)$ differs from the result of the previous iteration $\rho_{n-1}(r)$, by less a prescribed amount over the entire range of the electron motion $(r_i \leq r \leq r_o)$. From a study of the form of Eq.(80), it is clear that the charge boundaries in $\rho_3(r)$ will be the same as they are in $\rho_2(r)$. Thus, no further adjustment in α_β and β will be required in subsequent iterations.

At this point, the first approximation to the number of electrons in unit length of the rotating electron cloud, $(N_L)_1$, may be obtained immediately from Eq.(61). Using Eqs.(75) and (78) to evaluate the left side of this equation, eliminating $\log \frac{R_o}{R_i}$ on the right in terms of β from Eq.(65), and substituting for $I'(r_o)$ and $I(r_o)$ on the right from Eqs.(75) and (76) gives (after rearranging)

$$(N_L)_1 = \frac{4\pi \, \varepsilon_o \, \beta \, T(r_o)}{\alpha_\beta^2 \, e^2 [\log \frac{r_o}{r_i} - g_1(\alpha_o, 1)]}. \tag{82}$$

All the parameters on the right side of this equation are prescribed except $g_1(\alpha_o, 1)$, the value of which has already been calculated. Substituting into Eq.(82) the numerical values of the prescribed parameters given in Eqs.(69),(70) and (71), and the numerical value of $g_1(\alpha_o, 1)$ from Fig.5 gives

$$(N_L)_1 = \frac{4\pi \, \varepsilon_o \, T(r_o)}{(0.422) \, e^2}. \tag{83}$$

50 eV is about the minimum outer turning point kinetic energy consistent with an acceptable ionization probability (for most gases). The inner turning point kinetic energy is given by, from Eqs. (20) and (56),

$$T(r_i) = \left(\frac{r_o}{r_i}\right)^2 T(r_o) , \tag{84}$$

which from Eq.(69) yields $T(r_i) = 6.7\ T(r_o)$. From this result, it is clear that the minimum acceptable $T(r_o)$ should be used to avoid the penalty of a reduced ionization probability in the neighborhood of the inner turning point. The outer turning point kinetic energy is therefore prescribed such that

$$T(r_o) \simeq 50 \text{ eV}. \tag{85}$$

Substituting this value into Eq.(83) gives the first approximation for the number of electrons per unit length of the rotating electron cloud (for $R_i \simeq r_i, \alpha_o^2 = \frac{1}{3}$, $\beta = 1$, $T(r_o) = 50\text{eV}$).

$$(N_L)_1 = 0.825 \times 10^9 \text{ cm}^{-1}. \tag{86}$$

Referring again to Fig.6, it can be inferred that the function $g_2(g_1, \alpha_\beta, \beta, \frac{r}{r_o})$, which will result from the second iteration, has the property $g_2 < g_1$. Combining this with Eq.(82) implies that the second approximation to N_L will yield a number which is smaller than $(N_L)_1$, since the denominator of Eq.(82) will increase. Thus, it may be concluded that

$$(N_L)_2 < (N_L)_1. \tag{87}$$

However, since g_1 is only of the order of $\frac{1}{3}$ of $\log \frac{r_o}{r_i}$ and

the difference between g_1 and g_2 should not be large, $(N_L)_2$ probably will not differ substantially from $(N_L)_1$.

The method of deriving a self-consistent value for the ratio of the electrode radii is discussed in the following paragraph. The Hamiltonian, H, of an orbiting electron is simply its total energy. Therefore,

$$H = T(r) + U(r), \qquad (88)$$

where $U(r)$ is the electron potential energy, given by

$$U(r) = -e\phi_{21}(r), \qquad (89)$$

and thus

$$H = T(r) - e\phi_{21}(r). \qquad (90)$$

Since the Hamiltonian is constant over the entire electron trajectory, it may be evaluated at any point along the trajectory. However, it is convenient to evaluate H at the outer turning point. $\phi_{21}(r_o)$ is given by Eq.(77) after evaluating at $r=r_o$. Substituting Eqs.(75),(76) and (78) into Eq.(61) and using the result to eliminate N_L in $\phi_{21}(r_o)$ gives

$$\phi_{21}(r_o) = \frac{2T(r_o)}{\alpha_\beta^2 e} \log \frac{R_o}{R_i}. \qquad (91)$$

Substituting Eq.(91) into Eq.(90) gives (after rearranging)

$$\log \frac{R_o}{r_o} = \frac{\alpha_\beta^2}{2} \left[1 - \frac{H}{T(r_o)} \right]. \qquad , \qquad (92)$$

48

Thus, instead of prescribing $\frac{R_o}{r_o}$ (which is equivalent to pre-
scribing $\frac{R_o}{R_i}$ since $\frac{r_o}{R_i}$ is already prescribed) it is prefer-
able to prescribe H, since it is one of the more important
physical parameters concerning the dynamics of the electron.
For example, suppose that $H = T(r_o)$: From Eq.(92), it is ob-
vious that the outer turning point then occurs at R_o, the
surface of the outer cylinder. For certain applications, it
may be preferable to operate the orbitron in this mode.
However, for $r_o \simeq R_o$ (actually $r_o = R_o - \delta'$, where δ' is small
compared to R_o), it is probable that a large fraction of the
orbiting electrons could be collected at the outer cylinder.
This condition should be avoided in both ion gages and ion
pumps. Therefore, H should be sufficiently small that it is
improbable that electrons can reach the outer cylinder. This
occurs for H=0, which implies that if all the outer turning
point kinetic energy (angular mode) were converted (in an
elastic collision) to radial mode kinetic energy (an improb-
able event), the electron would reach the outer cylinder as
$\dot{r} \rightarrow 0$. Thus, setting H=0 in Eq.(92) and using Eqs.(69) and
(70) (and recalling that it has been prescribed that $r_i \simeq R_i$)
gives $\frac{R_o}{R_i} = 3.65$. This is the minimum value that may be pre-
scribed for $\frac{R_o}{R_i}$ (See Appendix E). From the above discussion,
it may be seen that to completely avoid the possibility of elec-
trons reaching the outer cylinder, a negative energy must be pre-
scribed for H. It is convenient (although somewhat arbitrary)
to prescribe

$$H = -T(r_o).$$
(93)

Substituting this into Eq.(92) gives

$$\log \frac{R_o}{r_o} = \alpha_\beta^2 ,$$
(94)

and using Eqs.(69),(70) and (71) yields the ratio of the electrode radii,

$$\frac{R_o}{R_i} = 5.13. \tag{95}$$

The only way this number can be increased is to decrease H (prescribe a larger negative value).

The method of deriving the self-consistent anode potential is described in the following paragraph. From Eq.(65), after substituting from Eq.(94) and recalling that $r_i \simeq R_i$, the self-consistent anode potential is given by

$$eV = \frac{2T}{\alpha_\beta^2} (r_o) \left(\alpha_\beta^2 + \beta + \log \frac{r_o}{r_i} \right). \tag{96}$$

Using Eq.(68), this may be written in the form

$$eV = T(r_o) \frac{r_o^2}{r_i^2} - H. \tag{97}$$

Using Eq.(93), this equation becomes

$$eV = T(r_o) \left[\frac{r_o^2}{r_i^2} + 1 \right] . \tag{98}$$

Substituting into Eq.(96),(97), or (98) (which are simply different forms of the same statement) from the numerical values given in Eqs.(69),(70),(71),(85) and (93) gives the self-consistent anode voltage

$$V = 385 \text{ volts.} \tag{99}$$

The method of deriving the launcher bias voltage is described in the following paragraph. The electrons may be inserted into orbit at any point along their trajectory, however at the turning points only a fraction of the space occupied by the launcher need protrude into the space occupied by the electron trajectories, but if the launcher is located at any other point along the electron trajectory the entire launcher is within the space charge cloud. Thus, orbit insertion should be accomplished at either the inner or outer turning points. At either turning point, there are two principal methods of inserting the electrons into orbit: (1) The electrons may be accelerated within the launcher, which is biased to the local space charge dependent potential, such that they are emitted from the launcher with the prescribed turning point kinetic energy (angular momentum) and with their velocity vectors coinciding with the θ-direction. (2) The electrons may be emitted from the launcher with negligible kinetic energy, but constrained to move in the θ-direction only, from a launcher which is biased below the local space charge dependent potential such that they are accelerated up to the prescribed turning point kinetic energy by the local field as they leave the launcher. It is, of course, possible to combine the two methods. The first method is, in principle, more flexible and the accurate control of the launch (insertion) parameters is simpler and more positive. Of the two turning points, the more suitable location for the launcher is the outer turning point, r_o, since this location gives the lowest probability for electrons colliding with the launcher on subsequent passes (for moderate to high eccentricity trajectories). For electrons emitted from a launcher at r_o, in the θ-direction, and with kinetic

energy $T(r_o)$ $(\ell=[2 \, m \, r_o^2 \, T(r_o)]^{\frac{1}{2}})$, the launcher bias voltage must be such that it matches the local space charge dependent potential $\phi_{21}(r_o)$. From Eqs.(77),(61),(75),(76),(85),(92) and (93), it follows that the launcher bias voltage is given by

$$eV_{b_1} = e\phi_{21}(r_o)$$

$$= 2 \, T(r_o), \qquad (100)$$

or

$$V_{b_1} = 100 \text{ volts}, \qquad (101)$$

where the subscript b_1 indicates that this bias applies to the first launch method. (It is interesting to observe that for a space charge free potential distribution, and all other parameters held fixed, the local potential would be ~ 160 volts.) If the electrons are emitting with negligible kinetic energy, the launcher must be biased such that

$$e[\phi_{21}(r_o) - V_{b_2}] = T(r_o) , \qquad (102)$$

from which it follows that

$$V_{b_2} = 50 \text{ volts}, \qquad (103)$$

where the subscript b_2 indicates that this bias applies to the second launch method. (For a space charge free potential distribution, the required bias would be ~ 110 volts). In the second launch method, the application of the correct bias to the launcher is not sufficient to assure that the electrons are correctly inserted into orbit since the potential difference

through which the electrons fall depends on the direction which
the electrons leave the launcher since the potential hill sur-
rounding an acceleration-biased launcher is not symmetrical,
being steeper on the inside (toward the anode) than it is on
the outside. The acceleration-biased launcher cannot be located
at r_o (the outer turning point) since the electron must
arrive at r_o with $\dot{r}(r_o)=0$ and at this point have kinetic
energy $T(r_o)$ (a prescribed parameter). The only way that an
acceleration-biased launcher can satisfy these conditions is
for the electrons to be emitted from the launcher in a direction
which makes an angle somewhat less than $\frac{\pi}{2}$ with the radius vec-
tor (emitted outward) such that the electrons pick up angular
momentum and kinetic energy in falling down the potential hill.
The electrons then continue to coast outward (against the field)
until the radial component of the momentum goes to zero. This
point is r_o, however for insertion into the correct orbit the
launcher bias and the direction of emission must have been such
that the electrons arrive at this point with the proper angular
momentum $(\ell=[2\ m\ r_o^2\ T(r_o)]^{\frac{1}{2}}$, where $T(r_o)$ is prescribed, say
50 eV). The important conclusion is that an acceleration-biased
launcher is completely within the space charge cloud since the
cloud outer boundary (trajectory outer turning point) is well
outside the launcher location. A similar argument applies to
acceleration-biased launcher locations in the neighborhood of
the inner turning point and a similar conclusion is obtained.
It is obvious that a potential hill 50 volts high produces a
substantial perturbation in the space charge dependent potential
distribution. It is not only a large perturbation locally, but
it is non-negligible over a substantial fraction of the volume
of the space charge cloud in the z-neighborhood of the launcher
since its decay is quasi-logarithmic. It thus appears that the

only acceptable method of launching is the first, with launcher locations restricted to either the inner or outer turning points, since this method produces no perturbation of the space charge dependent potential distribution, and only a fraction of the volume of the launcher protrudes into the space charge cloud volume.

Under certain conditions, the orbitron principle contains a natural feedback mechanism which may be used to maintain the number of electrons in the space charge cloud constant. This feedback mechanism is discussed in the following paragraph.

Suppose the electrons are inserted into orbit at the outer turning point with kinetic energy $T(r_o)$ from a launcher biased to match the local space charge dependent potential. Thus, the outer turning point is fixed at r_o (the launcher location), the electron emission angle is fixed at $\frac{\pi}{2}$ (with respect to the radius vector), and the electron emission energy, T_e, is fixed since

$$T_e = T(r_o). \tag{104}$$

Now, suppose that the electron injection rate into the space charge cloud is perturbed such that it exceeds, by a small fraction, the total electron loss rate from the cloud. It necessarily follows that N_L must begin to increase. The immediate effect of increasing N_L is to lower the potential distribution within the space charge cloud, see Eq.(77). Thus, $\phi_{21}(r_o)$ must decrease or, considering the potential a function of N_L, it follows that

$$\phi_{21}(r_o, N_L + \Delta N_L) < \phi_{21}(r_o, N_L). \qquad (105)$$

Since $r_i = R_i + \delta$ (and δ is negligible), the potential at the inner turning point is nearly identical with the anode potential and is, therefore, constant. Thus, at the inner turning point, the potential must satisfy

$$\phi_{21}(r_i, N_L + \Delta N_L) = \phi_{21}(r_i, N_L). \qquad (106)$$

Therefore, the potential difference appearing in the numerator of Eq.(57), which gives the ratio of the turning point radii, must increase as N_L increases. Now, concerning the denominator of Eq.(57), before the injection rate perturbation, the launcher bias must satisfy Eq.(100), that is

$$V_{b_1} = \phi_{21}(r_o, N_L), \qquad (107)$$

and after the perturbation begins, the launcher bias is greater than the local space charge dependent potential since the bias is fixed and the potential at the outer turning point decreases as N_L increases, see Eq.(105). Thus, the electrons are emitted from the launcher into a retarding field. The outer turning point kinetic energy, after the beginning of the perturbation of the injection rate, is given by

$$T(r_o, N_L + \Delta N_L) = T_e - e[V_{b_1} - \phi_{21}(r_o, N_L + \Delta N_L)], \qquad (108)$$

which may be written, using Eqs.(104) and (107)

$$T(r_o, N_L + \Delta N_L) = T(r_o, N_L) - e[\phi_{21}(r_o, N_L) - \phi_{21}(r_o, N_L + \Delta N_L)]. \qquad (109)$$

From this equation and Eq.(105), it is obvious that

$$T(r_o, N_L + \Delta N_L) < T(r_o, N_L). \tag{110}$$

Thus, the perturbation which increased N_L, resulted in a decrease of the outer turning point kinetic energy. Using Eqs.(106) and (109) to evaluate Eq.(57) after the beginning of the perturbation gives

$$\left. \frac{r_o^2}{r_i^2} \right|_{N_L + \Delta N_L} = 1 + e \frac{[\phi_{21}(r_i, N_L) - \phi_{21}(r_o, N_L + \Delta N_L)]}{T(r_o, N_L) - e[\phi_{21}(r_o, N_L) - \phi_{21}(r_o, N_L + \Delta N_L)]} . \tag{111}$$

From Eq.(105), it follows that increasing N_L by ΔN_L has increased the numerator and decreased the denominator of the term on the right in Eq.(111). Therefore, it follows that

$$\left. \frac{r_o^2}{r_i^2} \right|_{N_L + \Delta N_L} > \left. \frac{r_o^2}{r_i^2} \right|_{N_L} , \tag{112}$$

and since r_o is fixed, it necessarily follows that r_i must decrease. But decreasing r_i implies that electrons collide with the anode, since $r_i \approx R_i$. These collisions increase the total electron loss rate from the space charge cloud which produces a decrease in N_L (and incidentally a decrease in the mean orbiting life time). It is, therefore, concluded that the variation in the space charge dependent potential distribution as a function of N_L is such that it has the effect of closing a feedback loop around N_L and tends to hold N_L constant (provided, of course, that the orbit injection parameters, electrical parameters, and geometrical parameters all belong to a self-consistent set).

1.8 ION PRODUCTION RATE

The average number of ions produced in unit time by the electrons in unit length of the rotating space charge cloud, $(\dot{N}_+)_L$, is given by

$$(\dot{N}_+)_L = <v> N_L \eta \sigma_+, \tag{113}$$

where $\sigma_+ \equiv$ gas ionization cross section for electrons having a mean kinetic energy $<T> = \frac{m}{2}<v>^2$,

   $<v> \equiv$ mean electron velocity,

   $\eta \equiv$ gas member density.

N_L has already been calculated and σ_+ has been repeatedly measured for many gases by numerous experimenters and is available in the literature. Thus, it remains to calculate the mean electron velocity, $<v>$.

There are several useful definitions of the mean electron velocity, each differing slightly from the others. The definition of $<v>$ considered most useful in this application is that electron velocity properly associated with the mean radial position of the electron, $<r>$. Therefore, it is first necessary to derive a self-consistent expression for $<r>$, then evaluate it for the particular set of parameters under consideration in this first self-consistent solution and, finally, compute the electron velocity at this mean radial position, that is to compute $v(<r>)$.

The second approximation to the mean radial position of the electrons is given by

$$\left\langle \frac{r}{r_o} \right\rangle = \frac{1}{r_o \tau_1} \int_o^\tau r \, dt \qquad (114)$$

$$= \frac{2}{r_o \tau_1} \int_{r_i}^{r_o} \frac{r \, dr}{\dot{r}_1} \quad .$$

Integrating by parts gives

$$\left\langle \frac{r}{r_o} \right\rangle = \frac{2}{r_o \tau_1} \left\{ r \int \frac{dr}{\dot{r}_1} \Big|_{r_i}^{r_o} - \int_{r_i}^{r_o} dr \int \frac{dr}{\dot{r}_1} \right\} \quad . \qquad (115)$$

Equations (53) and (54) may be used to evaluate the first integral, with the result

$$\left\langle \frac{r}{r_o} \right\rangle = 1 - \frac{2}{r_o \tau_1} \int_{r_i}^{r_o} dr \int \frac{dr}{\dot{r}_1} \quad . \qquad (116)$$

The second integral may be written, using Eqs.(52), (79), (80) and (81), as

$$\left\langle \frac{r}{r_o} \right\rangle = 1 - \int_{r_i}^{r_o} \frac{dr}{r_o} \int f_2 \left(g_1, \alpha_\beta, \beta, \frac{r}{r_o} \right) \frac{dr}{r_o} \quad , \qquad (117)$$

and from an equation similar to Eq.(75), but applying to the 2nd approximation to the charge integral I!(r), Eq.(117) may be written

$$\left\langle \frac{r}{r_o} \right\rangle = 1 - \int_{r_i}^{r_o} g'_2 \left(g_1, \alpha_\beta, \beta, \frac{r}{r_o} \right) \frac{dr}{r_o} \quad . \qquad (118)$$

This integral has been evaluated numerically (for $\alpha_o = \frac{1}{3}$, $\beta = 1$, $r_i \approx R_i$) and the result is

$$\langle \frac{r}{r_o} \rangle = 1 - 0.254$$

$$= 0.746. \tag{119}$$

The electron velocity at any point along its trajectory is given by

$$v(r) = \{\dot{r}^2 + r^2 \dot{\theta}^2\}^{\frac{1}{2}} \tag{120}$$

and using Eqs.(20) and (56), this may be written

$$v(r) = \{\dot{r}^2 + \frac{2T(r_o)}{m} \frac{r_o^2}{r^2}\}^{\frac{1}{2}} \tag{121}$$

and substituting for $\dot{r}$ from Eq.(79) gives the 2nd approximation to the electron velocity

$$v_2(r) = \left(\frac{2T(r_o)}{m}\right)^{\frac{1}{2}} \left\{1 + \frac{2}{\alpha_\beta^2} \left[\log \frac{r_o}{r} + \beta \frac{[\log \frac{r_o}{r} + g_1(\alpha_o, \frac{r}{r_o}) - g_1(\alpha_o, 1)]}{[\log \frac{r_o}{r_i} - g_1(\alpha_o, 1)]}\right]\right\}^{\frac{1}{2}}$$

$$\tag{122}$$

Evaluating this expression at $\langle \frac{r}{r_o} \rangle$ given by Eq.(119), taking $\frac{r_o}{r_i}$ from Eq.(69), β from Eq.(70), α_β from Eq.(71), $g_1(\alpha_o, \langle \frac{r}{r_o} \rangle)$ from Fig.5, and $g_1(\alpha_o, 1)$ from Fig.5, yields

$$\langle v_2 \rangle \equiv v_2(\langle \frac{r}{r_o} \rangle) = (2.38)^{\frac{1}{2}} \left[\frac{2T(r_o)}{m}\right]^{\frac{1}{2}}. \tag{123}$$

Digressing for a moment, the electron mean kinetic energy may be immediately calculated from Eq.(123), since

$$<T> = \frac{m}{2} <v>^2, \qquad (124)$$

which gives

$$<T> = 2.38 \ T(r_o), \qquad (125)$$

and substituting from Eq.(85) for $T(r_o)$ gives

$$<T> = 119 \ eV. \qquad (126)$$

Thus, for the set of parameters chosen, the electron mean kinetic energy is about the center of the kinetic energy range corresponding to the ionization probability maxima for a large group of common gasses. From Eqs.(85) and (123), it follows that the mean electron velocity is

$$<v_2> = 6.45 \times 10^8 \ \frac{cm}{sec}. \qquad (127)$$

Returning now to the ion production rate (Argon is used throughout as a typical gas wherever gas properties are required in detail calculations) given by Eq.(113) and taking N_L from Eq.(86), $<v_2>$ from Eq.(127) and the ionization probability for Argon (the average of many values from the literature applicable to Eq.(126)) as

$$\sigma_{Ar+} = 3.8 \times 10^{-16} \ cm^2 \qquad (128)$$

yields

$$(\dot{N}_{Ar+})_L = 6.6 \times 10^{18} \ P_T, \left(\frac{Ar^+}{sec} \right), \qquad (129)$$

for each centimeter of space charge cloud (the T-subscript
on P_T indicates that pressure is measured in Torr). This
result should be considered a first approximation since the
value of N_L used is a first approximation even though the
value of $<v_2>$ is a second approximation. The ion current
produced (per cm of space charge cloud) is simply $e(\dot{N}_{Ar^+})_L$
($-e \equiv$ electronic charge), and from Eq.(129) this is

$$(i_{Ar^+})_L = 1.06 \, P_T, \quad \text{(Amp)}. \qquad (130)$$

The electron injection rate required in two typical
modes of operation is computed in the following paragraphs.
One of the simplest modes of operation is that in which the
electrons drift slowly away from the launcher (in the z-
direction) until they reach $z=L$ where they leak out of the
coaxial cylindrical structure through a weak mirror field.
This mode of operation tends to minimize the x-ray induced
residual current since the electrons which do not collide
with a gas atom are eventually collected outside the orbitron
structure. Suppose that the potential of the mirror electrode
is such that the mean velocity in the z-direction is $<\dot{Z}>$.
Thus, the current leaving the neighborhood of the launcher in
the z-direction is $-eN_L<\dot{Z}>$ (none of which returns). There-
fore, the electron injection rate required to maintain N_L
constant in the neighborhood of the launcher is

$$\dot{N}_e = N_L <\dot{Z}> . \qquad (131)$$

It is assumed that the electrons are inserted into orbits
which are sufficiently eccentric to miss the launcher during
the interval of time required to drift out of the z-neighbor-
hood of the launcher. For a launcher biased to match the local

space charge dependent potential, this may be of the order of five orbit periods (or more). However, for an acceleration biased launcher, this interval is probably of the order of one orbit period. Thus, $<\dot{Z}>$ must be larger (in this mode of operation) for an acceleration biased launcher than for a potential matched launcher. This implies that the electron injection rate must be larger for the acceleration biased launcher than for a potential matched launcher.

For a potential matched launcher, the electrons must move a distance $\Delta Z = L'$ (L' is the launcher length) in a time interval of the order of 5τ. This yields the approximate relation

$$\frac{<\dot{Z}>}{<v>} \geq \frac{L'}{10\pi <r>} \quad .\tag{132}$$

For L'=0.5 cm (a small but yet practicable value) and $R_o = 2.5$cm(implying from previous results that $<r> \simeq 0.94$ cm) gives

$$\left.\frac{<\dot{Z}>}{<v>}\right|_{min} \simeq 10^{-2} \quad .\tag{133}$$

This constraint places an upper limit on the parameter $\frac{\dot{N}_+}{P\dot{N}_e}$ somewhere in the neighborhood of 10^3. For an acceleration biased launcher, this upper limit would be smaller since Eq.(133) gives a larger minimum value for $\frac{<\dot{Z}>}{<v>}$.

An important mode of operation involves a relatively strong mirror field at Z=L such that all electrons are reflected. By properly restricting the maximum value of operating pressure, the ratio $\frac{L}{R_e}$, and $\frac{<v>}{<\dot{Z}>}$, N_L may be maintained approximately uniform over the full range of Z (this was not necessarily the case in the previous mode of operation). For

where $\sigma_+ \equiv$ ionization collision cross section of the atom for electrons having a mean kinetic energy $<T>$.

The number of non-ionizing collisions per unit time is therefore

$$\nu - \nu_+ = <v> L\, N_L\, \eta(\sigma - \sigma_+). \qquad (136)$$

This also may be taken as the number of elastic collisions per unit time, since the excitation cross section is generally very small compared to σ . In some fraction of the elastic collisions, there is sufficient electron kinetic energy loss or momentum change such that the electrons are left in an unstable orbit after the collision and, subsequently, collide with the anode. The number of electrons lost from the space charge cloud in unit time by this mechanism is therefore

$$h\, \nu_e = h(\nu - \nu_+) = <v> L\, N_L\, \eta h(\sigma - \sigma_+) , \qquad (137)$$

where h is in the interval $0 \leq h \leq 1$, the exact value of which is not essential.

A small fraction of the electrons orbiting in the z-neighborhood of the launcher, continuously collide with the launcher. The electron-launcher collision frequency is worked out below for a launcher located at r_o and biased to match the local space charge dependent potential (the necessary procedural modifications for treating the acceleration biased launcher are rather obvious). Consider a cylindrical launcher of radius R_L, the axis of which is parallel to the orbitron axis and located at r_o (electrons are ejected from a central slit, parallel to the launcher axis, which is orthogonal to the radius vector passing through the center of the launcher).

Obviously, the launcher radius should be as small as practicable. From practical considerations of the operations involved in the assembly of the various launcher electrodes, a near minimum launcher radius is considered to be

$$R_L = 0.05 \text{ cm.} \tag{138}$$

The effective launcher length, L', protruding into the end of the space charge cloud, is taken as

$$L' = 0.5 \text{ cm.} \tag{139}$$

The electron collision frequency with the launcher is given by

$$\nu_L = \frac{1}{-e} \int_{A_L} j_\theta(r) \, dA, \tag{140}$$

where $A_L \equiv$ that part of the launcher projected area onto a radial plane passing through it, which is within the space charge cloud,

$$= L'R_L.$$

The current density is given by

$$j_\theta(r) = \rho(r) \, v_\theta(r) \ . \tag{141}$$

But since $R_L \ll r_o$ and $v_\theta(r)$ is a slowly varying function in the neighborhood of r_o , the approximation may be made that

$$v_\theta(r) \simeq v_\theta(r_o), \quad r_o - R_L \leq r \leq r_o. \tag{142}$$

64

a launcher biased to match the local space charge dependent potential, electrons that collide with the launcher have a kinetic energy of 50 eV (for a launcher located at the outer turning point). If the launcher were located at the inner turning point, the electrons would collide with a kinetic energy of 335 eV, which is another reason for avoiding an inner turning point location for the launcher. The electron launcher collisions produce soft x-rays, a fraction of which radiate from the launcher to the ion collector surface (outer cylinder) where they eject photoelectrons. Thus, in this mode of operation, it is necessary, in the interest of reducing the residual current for ion gage applications, to separate that portion of the outer cylinder which surrounds the launcher from the remainder of the outer cylinder and use only the latter for ion collection. This substantially reduces the photoelectron emission from the ion collector, since the substantial fraction of the soft x-rays and photoelectrons leave the surface in a direction near the surface normal and thus do not reach the ion collector.

Under the above conditions, the total number of electron-atom collisions in unit time is

$$\nu = \langle v \rangle L N_L n\sigma \ , \qquad (134)$$

where $\sigma \equiv$ total collision cross section of the atom for electrons having a mean kinetic energy $\langle T \rangle$.

Similarly, the total number of ions generated in unit time is

$$\nu_+ = \langle v \rangle L N_L n\sigma_+ \ , \qquad (135)$$

From this approximation and Eqs.(124) and (125), the current density may be written

$$j_\theta(r) \simeq \frac{<v>}{\sqrt{2.38}} \rho(r). \qquad (143)$$

Substituting this back into Eq.(140) and taking $\rho(r)$ from Eq.(52) and noting that $dA=L'dr$, the electron-launcher collision frequency becomes

$$\nu_L = \frac{<v>}{\sqrt{2.38}} \frac{L'N_L}{\pi \tau} \int_{r_o-R_L}^{r_o} \frac{dr}{r \, \dot{r}(r)}. \qquad (144)$$

The strong variable in this integrand is $\dot{r}(r)$ since $\dot{r}^{-1} \to \infty$ as $r \to r_o$. Further $r_o - R_L \simeq r_o$ which implies that the range of integration is sufficiently small that r may be set equal to r_o and factored out of the integrand. From Eqs.(71), (94) and (138), and taking

$$R_o = 2.5cm, \qquad (145)$$

it follows that

$$r_o - R_L = 0.96 \, r_o, \qquad (146)$$

and that

$$r_o = 1.26 \text{ cm } . \qquad (147)$$

Therefore Eq.(144) may be written

66

$$\nu_L = \frac{<v>}{\sqrt{2.38}} \frac{L'N_L}{\pi \tau r_o} \int_{r_o - R_L}^{r_o} \frac{dr}{\dot{r}(r)} . \qquad (148)$$

Using Eq.(53) and Fig.4 to evaluate this expression, the electron-launcher collision frequency is

$$\nu_L = \frac{<v>}{\sqrt{2.38}} \frac{L'N_L(0.185)}{2\pi r_o} , \qquad (149)$$

and from Eqs.(139) and (147)

$$\nu_L = 7.58 \times 10^{-3} <v> N_L . \qquad (150)$$

The total number of electrons lost per unit time from the space charge cloud by elastic, inelastic and launcher collisions, is the sum of Eqs.(135), (137) and (150). A necessary condition for maintaining N_L = constant is that the electron launcher rate, $\dot{N}_e$, must be equal to this loss rate. Therefore

$$\dot{N}_e = <v>N_L\left\{L\eta\sigma[(1-h)\frac{\sigma+}{\sigma} + h] + 7.58 \times 10^{-3}\right\} . \quad (151)$$

At low pressure (small η) the dominant term in this expression is obviously the last term. Thus, maintaining N_L constant at low pressures requires a constant electron launch rate, independent of P. This launch rate is given by

$$\dot{N}_e = <v>N_L[7.58 \times 10^{-3}], \qquad (152)$$

dropping all but the last term in Eq.(151). Substituting from Eqs.(86) and (127) for N_L and $<v>$, implies that the emission

current (required to maintain the total charge in the rotating electron cloud constant) is

$$i_e = 0.645 \text{ ma,} \tag{153}$$

(again, for the specific set of parameters used in this first development of a self-consistent solution). The pressure above which the electron launch rate (required to maintain N_L= const.) depends on P , may be evaluated by determining that pressure above which the last term in Eq.(151) is no longer dominant (suppose it is only of the order of 90% of the total). Thus

$$\eta_{max} \leq \frac{8.5 \times 10^{-3}}{L\sigma[(1-h)\frac{\sigma_\pm}{\sigma} + h]} \, , \tag{154}$$

and again taking Argon as a typical gas, for which

$$\sigma_{Ar} = 9.5 \times 10^{-16} \text{ cm}^2, \tag{155}$$

and from Eq.(128) $\frac{\sigma_{Ar^+}}{\sigma_{Ar}} = 0.4$, and taking

$$L = 10 \text{ cm,} \tag{156}$$

gives the pressure above which the launch rate required to maintain N_L= const. is dependent on pressure

$$(P_T)_{max} \leq \begin{cases} 2.64 \times 10^{-5} \text{ Torr, } (h=1), \\ 6.6 \times 10^{-5} \text{ Torr, } (h=0). \end{cases} \tag{157}$$

A reasonably accurate estimate of h is a rather laborious computation which involves not only quantum collision mechanics but also the specific geometrical parameters of the orbitron, the space charge dependent potential distribution, and the electron trajectory parameters. The computation of h is not done here, but from Appendix A, it may be seen that $h \to 1$ as $\alpha_\beta^2 \to \frac{1}{3}$ and that $h \to h_{limit}$ as $\alpha_\beta^2 \to 1$. Although $h_{limit} > 0$ for all useful electron kinetic energies.

The parameter $\frac{\dot{N}_+}{\dot{N}_e P_T}$ may now be calculated from Eqs. (135) and (152), which gives

$$\frac{\dot{N}_+}{\dot{N}_e P_T} = \frac{L \, \eta \, \sigma_+}{7.58 \times 10^{-3} P_T} \, , \qquad (158)$$

and taking L from Eq.(156) and σ_+ from Eq.(128) (for Argon), gives

$$\frac{\dot{N}_{Ar^+}}{\dot{N}_e P_T} = 1.63 \times 10^4 \, , \, (Torr^{-1}) \, . \qquad (159)$$

The ionic pumping speed, S_+ , associated with the ion production rate is given by

$$S_+ = C_\perp \frac{\nu_+}{\eta} \, , \qquad (160)$$

where $C_\perp \equiv$ ion capture probability at normal incidence for ions having kinetic energy $T_+(R_0) = e\phi_{21}(<r>)$, ($\approx 170$ eV).

Substituting Eq.(135) into Eq.(160) gives

$$\frac{S_+}{C_\perp} = <v> \ L \ N_L \sigma_+, \tag{161}$$

and using Eqs.(86), (127), (128) and (156), gives the ionic pumping speed for Argon

$$\frac{S_{Ar^+}}{C_\perp} = 2 \times 10^3 \ \frac{cm^3}{sec} \ . \tag{162}$$

The rotating electron cloud corresponds to a circulating current which is given (approximately) by

$$i_\theta = eN_L \ \frac{<v> \ L}{2\pi <r>} \ . \tag{163}$$

Thus, the ratio of emission current to circulating current is given by, from Eqs.(152) and (163),

$$\frac{i_e}{i_\theta} = (7.58 \times 10^{-3}) \ \frac{2\pi <r>}{L} \ ,(P<P_{max}), \tag{164}$$

and using Eqs.(119), (147) and (156) gives

$$\frac{i_e}{i_\theta} = 4.47 \times 10^{-3}. \tag{165}$$

This result validates the use of the time-independent continuity equation, an assumption made earlier in deriving the charge density distribution, see Eq.(29).

It was assumed earlier that the charge distribution is nearly uniform along the Z-axis. The validity of this assumption may be determined for the maximum pressure for which the orbitron response is a linear function of emission current, Eq.(157). The electron mean free path in Argon is given by

$$\lambda(e,Ar) = \frac{1}{\eta \, \sigma_{Ar}}$$

$$= \frac{0.032}{P_T}, \text{ (cm)}, \tag{166}$$

and substituting $(P_T)_{max}$ for P_T from Eq.(157), gives

$$\lambda(e,Ar)\big|_{min} = 5.8 \times 10^2 \text{cm, (h=0)}. \tag{167}$$

The distance traveled by an electron along its trajectory during one orbit is of the order of

$$s = \sqrt{2} \, \pi \, <r> \text{ , (see Appendix C),} \tag{168}$$

and using Eqs.(119) and (147) gives

$$s = 5.0 \text{ cm.} \tag{169}$$

Thus, in one mean free path, an electron executes

$$\frac{\lambda(e,Ar)}{s} = 116 \text{ orbits,} \tag{170}$$

which is adequate to assure nearly uniform charge distribution along the Z-axis since in this number of orbits the electron could have traversed the full Z-range several times.

This entire orbitron analysis has been based (in part) on the working hypothesis that the space charge was completely electronic. The validity of this hypothesis may be determined by calculating that pressure above which the ionic component of the space charge is no longer negligible. Since the mean radial position of the electrons is $<r>$, the most probable radial position at which ions are formed is also $<r>$. The mean ion life time, $<\tau_+>$, is therefore the time required for an ion to traverse the distance from $<r>$ to R_0. The ionic acceleration is given by

$$\ddot{r} = \frac{e}{m_+} E(r).$$ (171)

Integrating this equation gives the ionic velocity

$$\dot{r} = \begin{cases} \left(\frac{2e}{m_+}\right)^{\frac{1}{2}} \left[\phi_{21}(<r>)-\phi_{21}(r)\right]^{\frac{1}{2}}, & <r> \le r \le r_0, \\ \left(\frac{2e}{m_+}\right)^{\frac{1}{2}} \left[\phi_{21}(<r>)-\phi_{31}(r)\right]^{\frac{1}{2}}, & r_0 \le r \le R_0, \end{cases}$$ (172)

where the initial ion velocity is assumed negligibly small. Integrating this result again gives the mean ion life time

$$<\tau_+> = \left(\frac{m_+}{2e}\right)^{\frac{1}{2}} \left\{ \int_{<r>}^{r_0} \frac{dr}{\left[\phi_{21}(<r>)-\phi_{21}(r)\right]^{\frac{1}{2}}} + \int_{r_0}^{R_0} \frac{dr}{\left[\phi_{21}(<r>)-\phi_{31}(r)\right]^{\frac{1}{2}}} \right\}$$ (173)

$\phi_{21}(r)$ is given by Eq.(77), and from Eqs.(15), (54), (55), (75), (76) and (78), it follows that

$$\phi_{31}(r) = \left\{ V - \frac{eN_L}{2\pi\epsilon_0} \left[\log \frac{r_0}{r_i} - g_1(\alpha_0,1)\right] \right\} \frac{\log \frac{R_0}{r}}{\log \frac{R_0}{R_i}}.$$ (174)

Making the appropriate potential substitution in Eq.(173), taking the limits of integration from previously defined parameters, taking $g_1(\alpha_o, \frac{r}{r_o})$ from Fig. 5, and performing the indicated integrations numerically, gives

$$<\tau_+> = 1.45 \; R_o \; \left(\frac{m_+}{2 \; eV}\right)^{\frac{1}{2}}. \tag{175}$$

Taking R_o from Eq.(145) and V from Eq.(99), the mean Argon ion life time is

$$<\tau_{Ar^+}> \approx 8.4 \times 10^{-7} \; \text{sec.} \tag{176}$$

The number of ions in unit length of the interelectrode space is given by

$$(N_+)_L = (\dot{N}_+)_L \; <\tau_+>. \tag{177}$$

Substituting from Eq.(129) for $(\dot{N}_{Ar^+})_L$ and from Eq.(176) for $<\tau_{Ar^+}>$ gives (again for Argon)

$$(N_{Ar^+})_L = 5.5 \times 10^{12} \; P_T. \tag{178}$$

For the space charge to be considered completely electronic (as has been done in the analysis)

$$(N_{Ar^+})_L << N_L. \tag{179}$$

Therefore from Eqs.(86) and (178), it follows that

$$P_T\big|_{\text{max}} \ll 1.49 \times 10^{-4} \text{ Torr.} \qquad (180)$$

This result implies that the space charge may be considered completely electronic below about 1.5×10^{-5} Torr. Therefore, from Eq.(157) (for any value of h), it follows that over the entire linear dynamic range of the orbitron, the assumption that the space charge is completely electronic, is valid.

1.9 CONCLUSIONS

The development of the 1st approximation to a self-consistent solution for the electron motion, charge density distribution and charge dependent potential distribution in an orbitron, used the following assumptions:

0. The space charge is completely electronic.

1. The charge density distribution is sufficiently uniform in the Z-direction that its variation with Z may be neglected.

2. The charge density distribution is independent of θ .

3. Allowed orbits are members only of the orbit subset which satisfies the stability criteria; excluding, however, although members of this subset, that part of the discrete series of closed trajectories for which η is small.

4. The time dependent component of the charge density corresponding to the collision loss rate and the balancing injection rate is negligible, compared to the equilibrium charge density.

These assumptions are shown to be valid for practicable configurations and modes of operation.

Under these assumptions, the consistent set of differential equations describing the space charge dependent potential distribution, the charge density distribution, and the electron radial velocity are:

$$\frac{d}{dr}\left(r\ \frac{d\phi}{dr}\right) = -\frac{r\ \rho(r)}{\varepsilon_o} \qquad \text{(Poisson Equation)},$$

$$\frac{d}{dr}\left[r\ \dot{r}\ \rho(r)\right] = 0 \qquad \text{(Continuity Equation)},$$

and

$$\dot{r}\ \frac{d\dot{r}}{dr} = \frac{\ell^2}{m^2 r^3} + \frac{e}{m}\ \frac{d\phi}{dr} \qquad \text{(2nd Law)}.$$

The solution of which is applied to three concentric cylindrical regions, with space charge in the middle region only, by forcing the solution to satisfy two boundary conditions on the potential at the inner and outer electrode surfaces, and four continuity conditions on the potential and electric field at the two interfaces of the three regions. The solution is also constrained to satisfy

$$T(r_o) = \frac{\alpha^2}{2}\ e\left[\left.-r\ \frac{d\phi}{dr}\right|_{r=r_o}\right. \qquad \text{(Stability Constraint)},$$

for the allowed range of the stability parameter

$$\frac{1}{3} < \alpha^2 \leq 1 ,$$

which assures that the rotating electron cloud is populated with electrons having long probable life times.

The solution is developed by substituting the space charge free potential distribution into the 2nd Law, and solving numerically for $\dot{r}$. This function is then substituted into the Continuity Equation and a solution obtained for $\rho(r)$. This result is used in the Poisson Equation to obtain the 1st approximation to the space charge dependent potential distribution. This potential is substituted into the 2nd Law, and a 2nd approximation to $\dot{r}$ obtained numerically. Using this function in the Continuity Equation gives a 2nd approximation to the space charge distribution.

Since the above system of equations is non-linear and also non-integrable analytically, a particular solution may be obtained by numerical integration for a specific set of parameters only. To enhance the utility of this first development of a self-consistent solution, it is first determined where the rotating electron cloud inner boundary should be located to give maximum charge storage. It is found that the inner turning point should be near the anode surface. This result permits the introduction of a valid approximation which, in turn, makes it possible to retain some generality in the sense that the numerical integrations apply not to one particular solution only, but rather to a subset of particular solutions.

The following table gives the prescribed parameters and the derived parameters in order of progress:

Prescribed Parameters $\qquad$ Derived Parameters

$$r_i \simeq R_i$$

$$\alpha_o^2 = \frac{1}{3}$$

$$\beta = 1$$

$$\frac{r_o}{r_i} = 2.59$$

$$\alpha_\beta^2 = 0.684$$

$$N_L = \frac{4\pi\,\varepsilon_o\,\beta\,T(r_o)}{\alpha_\beta^2\,e^2\left[\log\frac{r_o}{r_i} - g_1(\alpha_o,1)\right]}$$

Prescribed Parameters	Derived Parameters

- -

| $T(r_o) = 50$ eV | $N_L = 0.825 \times 10^9$ cm^{-1} |

- -

$H = -T(r_o)$

$\dfrac{R_o}{R_i} = 5.13$

$V = 385$ Volts

$V_{b_1} = 100$ Volts

$\left\langle \dfrac{r}{r_o} \right\rangle = 0.746$

$\langle v \rangle = 6.45 \times 10^8 \dfrac{cm}{sec}$

$\langle T \rangle = 119$ eV

$\left(\dot{N}_{Ar^+} \right)_L = 6.6 \times 10^{18} \, P_T \left(\dfrac{Ar^+}{sec} \right)_L$

$\left(i_{Ar^+} \right)_L = 1.06 \, P_T \, (amp)_L$

- -

| $R_o = 2.5$ cm | $r_o = 1.26$ cm |

$r_i = 0.49$ cm

- -

Prescribed Parameters

$L = 10$ cm

$R_L = 0.05$ cm

$L' = 0.5$ cm

Derived Parameters

$(P_T)_{max} < 6.6 \times 10^{-5}$ Torr

$i_e = 0.645$ ma

$\dfrac{i_e}{i_e} = 4.47 \times 10^{-3}$

$\dfrac{\dot{N}_{Ar^+}}{\dot{N}_e P_T} = 1.63 \times 10^4$ Torr^{-1}

$\dfrac{S_{Ar^+}}{C_\perp} = 2$ liters/sec.

$<\tau_{Ar^+}> = 8.4 \times 10^{-7}$ sec.

$(N_{Ar^+})_L = 5.5 \times 10^{12} \; P_T \; (A_{Ar^+})_L$

The following conclusions may be drawn from the results developed in the preceding orbitron analysis:

The space charge dependent potential distribution, for maximum charge stored stably in the rotating electron cloud, is substantially lower than the space charge free potential distribution. This confirms the suspicion that a space charge free analysis has limited utility.

The maximum charge that may be stored stably in the rotating electron cloud is about the same as may be stored on one plate of a cylindrical capacitor of the

same dimensions at the same anode potential.

The maximum charge stored stably is approximately a linear function of anode potential (other parameters fixed).

The ion production rate (per unit length of electron cloud) increases slower than the anode potential (other parameters fixed).

Maximizing the charge stored stably requires that the electron trajectory inner turning point be very near the anode surface.

The charge stored stably increases with increasing anode radius and decreasing outer cylinder radius (however for all other parameters fixed, the outer cylinder radius cannot be less than a certain lower limit).

The feedback mechanism, which regulates the total population of the electron cloud at its maximum value consistent with stability requirements, is operative only for an inner turning point location very near the anode surface. For all larger inner turning point locations the cloud population must be regulated by other (external) mechanisms. The possibility of over populating the electron cloud presents a grave hazard if the inner turning point is not near the anode surface.

Orbit insertion parameters must be accurately controlled to achieve optimum charge storage. Deviation in orbit insertion parameters results in unstable trajectories, short orbiting life times, and low ion production rate.

For many configurations or modes of operation, the ratio of emission current to ion current increases with increasing anode potential.

Ion gage sensitivities of the order of 10^4 to 10^5 Torr^{-1} can be achieved for conventional size devices.

Several modes of operation are possible, for orbitron ion gages, which are substantially free of residual current.

Relatively high ionic pumping speeds are attainable in orbitron ion pumps. For example: an orbitron pump about the size of the magnetron gage (Redhead) and operated at the same anode potential would have an Argon speed of about 2 liters/sec. Similarly, a 5 cm diameter, 20 cm length orbitron pump operated at 10KV would have an Argon speed of about 65 liters/sec.

The computational task associated with obtaining a precise solution to the orbitron problem appears to be less formidable than was suspected at first, since the comparison presented in Fig. 6 implies that the iteration process converge rapidly.

The numerical data presented in Fig. 3 thru 6 may be applied to geometrical and electrical configurations which differ from the configuration worked out in section VII and VIII by using the computational procedures developed in these sections, provided only that α_β and β are held fixed.

2.0 DESIGN AND CONSTRUCTION OF AN EXPERIMENTAL
ORBITRON GAGE

The analytical results obtained in the preceeding section have been applied to the design of an orbitron ion gage which is discussed in the following paragraphs. Schematics of the device are presented in Fig. 7 and 8 where electrode materials are indicated and important dimensions are given.

The design is such that either mode of electron launching may be used, that is from a potential matched launcher or from an acceleration biased launcher. The ion collector portion of the outer cylinder is electrically separated from the end section of the outer cylinder and the launcher is located within this end section to minimize the residual current at the ion collector. The launcher is located near one of the electron mirrors to provide for control of the ratio of z-axis drift velocity to orbital velocity. In this configuration, launching is anticipated only in the neighborhood of the outer turning point. It is further supposed that operating parameters will always be such that the inner turning point is in the neighborhood of the anode surface since optimum charge storage in the electron cloud is of principal interest. The launcher is mounted on a bellows assembly to provide for some adjustment in the ratio of outer turning point radius to inner turning point radius by adjusting the radial position of the launcher. This mounting system also provides for some adjustment in the z position of the launcher and as well as some variation in launch angle about $\frac{\pi}{2}$ (applicable to an acceleration biased launcher). Electrically isolated electron mirrors and anode guard electrodes are provided to control the axial flow of electrons and adjust the axial position of the electron cloud.

An enlarged schematic of the electron launcher is shown in Fig. 8. The cathode is centrally located in a slited tube. The tube serves as one heater current lead and supports one end of the cathode, and the axial slit limits the width of the electron stream drawn from the cathode assembly. The launcher anode

82

Auxiliary Outer Cylinder (Ta)

Electron Mirror (Ta)

Anode Guard (Ta)

To
Ceramic
Passthrus
on Flange

Electron Launcher

Ion Collector (Ta)

$r_0 = 1.26$ cm

$r_1 = 0.5$ cm

$R_0 = 2.5$ cm

Anode (Ta)

Support Posts (SS)

Enclosure

Al_2O_3 Insulation

Anode Support (W)
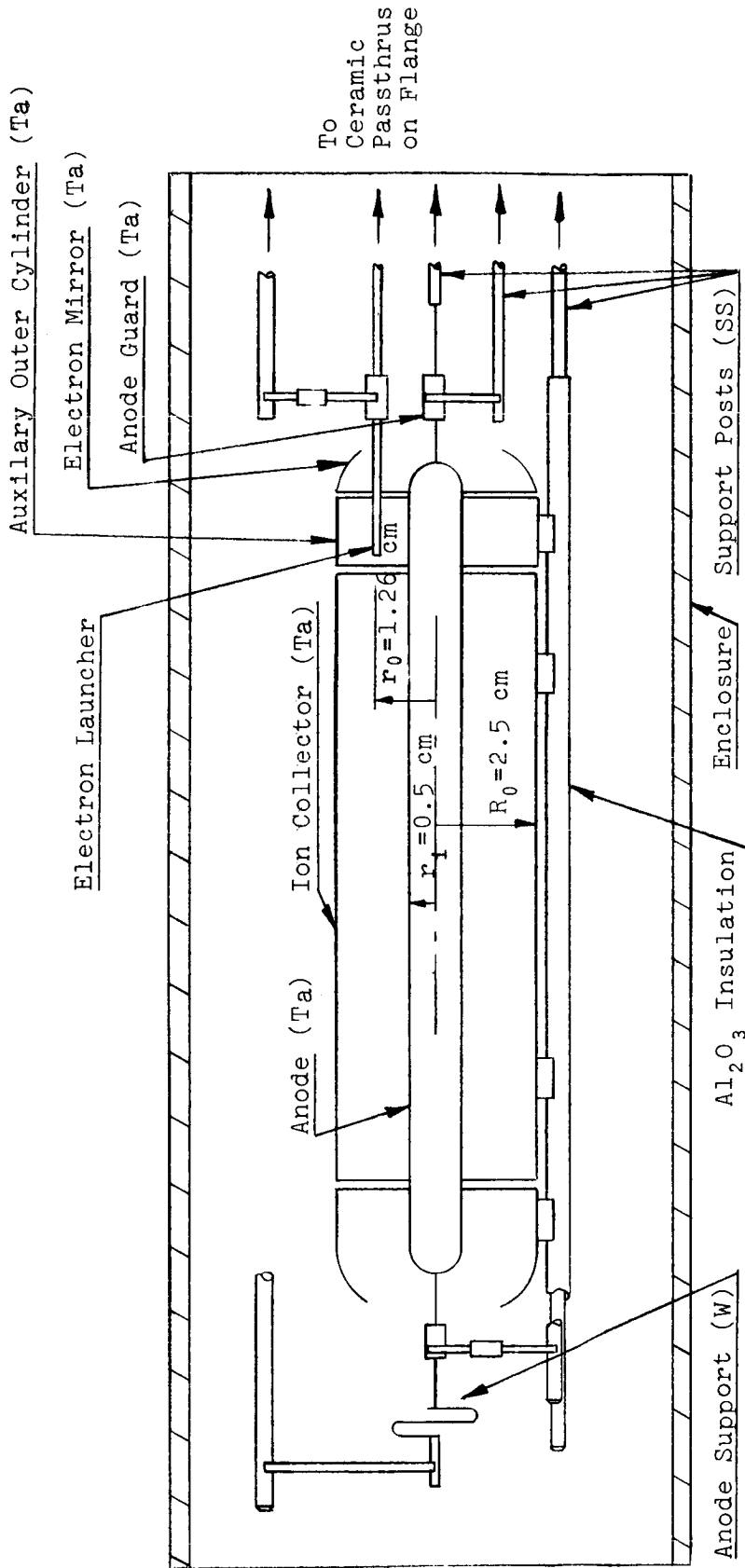
Fig. 7 Experimental Orbitron Gage [Schematic]

83

1.0 mm

0.1 mm

A–A

Anode (Ta)

0.5 cm

Cathode (W)

Collimator (Ta)

Al_2O_3

Al_2O_3

Anode Lead (Re)

Launcher Support
and Positioning Linkage
(SS)

To Bellows
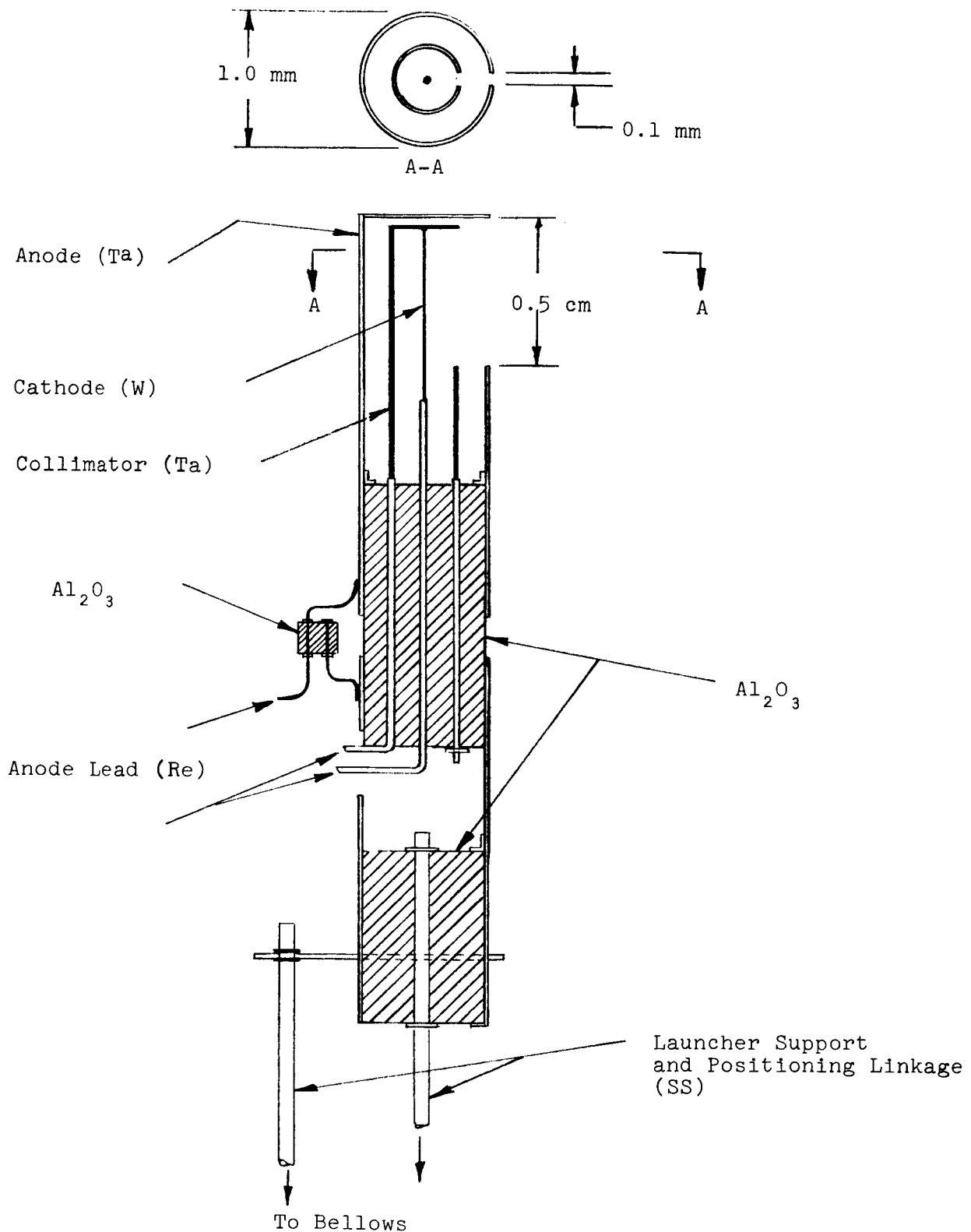
Fig. 8 Electron Launcher (Schematic)

surrounds the cathode assembly and has an axial slit which is aligned with the cathode assembly slit. This slit system results in the ejection of a narrow stream of electrons from the launcher. The center plane of the slit system is oriented at an angle of $\frac{\pi}{2}$ with respect to the radius vector of the orbitron. In the potential matched mode of launching the launcher anode is biased to match the local space charge dependent potential and the cathode assembly is biased below the anode such that the potential difference between them corresonds to the desired electron ejection kinetic energy (outer turning point kinetic energy). The electron launch rate is controlled by variation of the heater current only. In the acceleration biased launching mode, the launcher anode is biased below the local space charge dependent potential such that the potential difference corresponds to the desired electron kinetic energy in the neighborhood of the outer turning point. However, to minimize space charge limitations within the launcher and to assist in collimating the ejected electron stream the launcher cathode assembly should be biased somewhat below the launcher anode. Thus the electrons leave the anode slit in a well defined direction and with a few eV of kinetic energy.

All electrodes are mounted on support rods which pass through ceramic insulators located on a single flange thus making the entire assembly demountable.

With the above geometrical configuration and for anode potentials between 250 and 1000 volts corresponding to the mean electron kinetic energy range from about 75 to 300 eV, the orbitron ion gage performance may be experimentally studied and evaluated over the sensitivity range from about 10^3 to 10^5 Torr^{-1}.

APPENDIX A

Stability Analysis

If an electron is in a stable orbit, any small perturbation of its radial motion, resulting in an incremental displacement from its orbit, must be resisted by a force which tends to restore the electron motion to its original orbit. Thus, the incremental restoring force resulting from an incremental displacement of the electron from its orbit must have the following form if the orbit is to be stable

$$df = -k\, dr, \tag{A1}$$

where k is a positive constant. Taking the differential of both sides of Eq.(21) gives

$$d(m\ddot{r}) \equiv df = -\left(\frac{3\ell^2}{mr^4} + e\frac{d}{dr}E(r)\right)dr. \tag{A2}$$

For these two equations to be identical in form, it is necessary that

$$\frac{3\ell^2}{mr^4} + e\frac{d}{dr}E(r) > 0, \tag{A3}$$

for all points along the trajectory.

The least stable point in an ellipse-like trajectory is the outer turning point, where the electron is most distant from the force center, thus experiencing the smallest electric force, and also where the gradient of this force is smallest. Thus, a stability criteria which assures that the electron trajectory is stable at the outer turning point is sufficient to assure that the entire orbit is stable.

The outer turning point of an electron in an undisturbed orbit coincides with the outer boundary of the space charge cloud, the boundary between regions 2 and 3. However, if the electron trajectory has been perturbed such that the actual trajectory has been displaced radially by a positive increment from the original trajectory, its outer turning point will occur in region 3, beyond the space-charge boundary. Therefore, the field derivative appearing in Eq.(A3) must be evaluated immediately outside

the space-charge boundary in region 3. Since, in general, this region is charge free, Laplace's Equation applies, from which it follows

$$\frac{d}{dr} E_3(r)\bigg|_{r=r_0} = -\frac{E_3(r_0)}{r_0} = -\frac{E_2(r_0)}{r_0} \tag{A4}$$

Substituting this result into Eq.(A3) and evaluating the angular momentum term at r_0 also, gives (after rearranging)

$$\ell^2 > \frac{r_0{}^3}{3} me\, E_2(r_0). \tag{A5}$$

Thus, of all possible orbits, only those are stable for which the electron angular momentum is greater than this lower limit.

In the orbitron, only bound orbits are of any interest, thus, the repulsive term (positive) in Eq.(21) must not be so large (relative to the electric field term) that it forces the electron to escape radially from the interelectrode space. The repulsive term has its largest allowed value when it exactly balances the attractive electric field term. The repulsive term is related to the angular momentum. Therefore, the angular momentum must have an upper limit if the orbit is to remain bound. This limit is obtained by setting the left side of Eq.(21) to zero, which gives

$$\ell^2 = r_0{}^3 me\, E(r_0), \tag{A6}$$

where $r^3 E(r)$ has been evaluated at a radius equal to the outer turning point radius of an ellipse-like orbit, thus occupying the same region of the interelectrode space.

Thus for stable, bound orbits the angular momentum has an upper and lower limit according to

$$\frac{r_0{}^3}{3} me\, E_2(r_0) < \ell^2 \leq r_0{}^3 me\, E_2(r_0). \tag{A7}$$

This expression may be converted to an equation, for insertion into the analysis, an operation which assures the selection of only the stable subset of orbits for further study. Converting the relation (A7) to an

Thus the effect of the perturbation, independent of the form of the perturbation interaction, is that the electron oscillates about its original trajectory at the frequency given by Eq.(A14) and with the amplitude given by Eq.(A16). The oscillation will continue for a very long time since the only damping in the system is radiation damping of the electron which has been neglected in Eq.(A13) since it is extremely small. The energy radiated during one orbit is typically of the order of 10^{-10} $T(r_i)$ to 10^{-15} $T(r_i)$ where $T(r_i)$ is the kinetic energy of the electron at the inner turning point (maximum kinetic energy). Since the system is nonlinear ω is not a constant. In fact, ω increases as r decreases (as the electron proceeds along its trajectory from r_0). The oscillatory period, $\frac{2\pi}{\omega}$, is of the same order of magnitude as the orbit period. Thus, the oscillatory electron response actually distorts the entire orbit.

For $k<0$ in Eq.(A10), the response of the electron to a perturbation is essentially different from the above results. The solution to Eq.(A13) is then

$$x(t) = x_0 \cosh \omega t + \frac{\dot{x}_0}{\omega} \sinh \omega t, \qquad (A18)$$

where

$$\omega^2 = \frac{(1-3\alpha^2) \, E_2(r_0)}{mr_0}, \; \alpha^2 < \frac{1}{3}. \qquad (A19)$$

Thus, for $\alpha^2 < \frac{1}{3}$, a perturbation which produces either a displacement from the original trajectory or an increment in the radial velocity (or both), no matter how small, yields an electron response which diverges from the original trajectory without limit.

A-5

where

$$\omega^2 = \frac{k}{m} = \frac{(3\alpha^2 - 1) \ e \ E_2(r_o)}{mr_o} \tag{A14}$$

The solution to this equation describes the electron response to the perturbation. Since the form of the perturbation forcing function is unknown, the most general method of proceeding with the solution to Eq.(A13) is to assume that at the end of the perturbation, the electron has been displaced by χ_o and given a velocity increment $\dot{\chi}_o$, where $\frac{1}{2}m\dot{\chi}_o^2$ (the increase in radial mode kinetic energy) is assumed small compared to $\frac{\ell^2}{2mr_o^2}$. Taking the end of the perturbation as the zero-time reference, the parameters χ_o and $\dot{\chi}_o$ become the initial conditions necessary to specify the integration constants in the solution of Eq.(A13).

For $k>0$, the solution to Eq.(A13) is

$$\chi(t) = \chi_o \cos \omega t + \frac{\dot{\chi}_o}{\omega} \sin \omega t. \tag{A15}$$

For $k>0$, from Eq.(A14) it is obvious that ω decreases as α decreases. Therefore, the amplitude of the electron response in Eq.(A15) increases as α decreases and the frequency of the oscillatory response decreases as α decreases. The maximum displacement of the electron from its original trajectory is, from Eq.(A15),

$$\chi_{max} = \chi_o \left[1 + \frac{\dot{\chi}_o^2}{\chi_o^2 \omega^2} \right]^{\frac{1}{2}} . \tag{A16}$$

Using Eqs.(A8) and (A14), this may be rewritten in terms of the kinetic energy given to the electron during the perturbation ΔT, and the original electron kinetic energy at the outer turning point $T(r_o)$,

$$\left(\frac{\chi_{max}}{r_o} \right)^2 = \frac{\chi_o^2}{r_o^2} + \frac{\alpha^2}{(3\alpha^2-1)} \frac{\Delta T}{T(r_o)} . \tag{A17}$$

A-4

Thus the effect of the perturbation, independent of the form of the perturbation interaction, is that the electron oscillates about its original trajectory at the frequency given by Eq.(A14) and with the amplitude given by Eq.(A16). The oscillation will continue for a very long time since the only damping in the system is radiation damping of the electron which has been neglected in Eq.(A13) since it is extremely small. The energy radiated during one orbit is typically of the order of $10^{-10} T(r_i)$ to 10^{-15} $T(r_i)$ where $T(r_i)$ is the kinetic energy of the electron at the inner turning point (maximum kinetic energy). Since the system is nonlinear ω is not a constant. In fact, ω increases as r decreases (as the electron proceeds along its trajectory from r_0). The oscillatory period, $\frac{2\pi}{\omega}$, is of the same order of magnitude as the orbit period. Thus, the oscillatory electron response actually distorts the entire orbit.

For $k<0$ in Eq.(A10), the response of the electron to a perturbation is essentially different from the above results. The solution to Eq.(A13) is then

$$x(t) = x_0 \cosh \omega t + \frac{\dot{x}_0}{\omega} \sinh \omega t, \tag{A18}$$

where

$$\omega^2 = \frac{(1-3\alpha^2) E_2(r_0)}{mr_0}, \ \alpha^2 < \frac{1}{3}. \tag{A19}$$

Thus, for $\alpha^2 < \frac{1}{3}$, a perturbation which produces either a displacement from the original trajectory or an increment in the radial velocity (or both), no matter how small, yields an electron response which diverges from the original trajectory without limit.

APPENDIX B

Effective Eccentricity

The trajectory of a bound particle in a r^{-2} central force field is in general a closed ellipse[4] (provided wave effects and relativistic effects are negligable). The radial position of the particle as a function of the azimuth angle θ is given by

$$r = \cfrac{1}{\dfrac{km}{\ell^2} - \left(\dfrac{km}{\ell^2} - r_o^{-1}\right) \cos \theta} , \qquad (B1)$$

which is the standard form in polar coordinates of the ellipse sketch below,
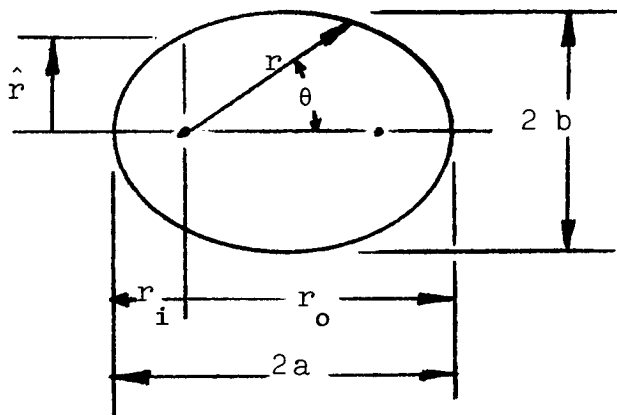
and where $k \equiv$ force constant,

$\ell \equiv$ particle angular momentum,

$m \equiv$ particle mass,

$r_o \equiv$ outer turning point,

$r_i \equiv$ inner turning point,

$\hat{r} \equiv$ semi-latus rectum of the ellipse.

The radial component of the particle acceleration is given by

$$\ddot{r} = \frac{\ell^2}{m^2 r^3} - \frac{k}{mr^2} \ .$$

$$(B2)$$

The radius at which the particle radial acceleration passes through zero is obtained from this equation by setting $\ddot{r} = 0$ and solving for r

$$r(\ddot{r}=0) \equiv \hat{r} = \frac{\ell^2}{km} \ .$$

$$(B3)$$

Substituting this value for $\hat{r}$ into Eq.(B1) and solving for $\theta(\ddot{r}=0) \equiv \hat{\theta}$ gives

$$\hat{\theta} = \pm\, n\, \frac{\Pi}{2} , (n \text{ odd}).$$

$$(B4)$$

Thus, the polar coordinates of the particle at the instant that the radial acceleration passes through zero are just the coordinates of the end points of the semi-latus recturn of the ellipse.

In terms of standard elliptical parameters, the radius to the outer turning point is given by

$$r_o = a(1+e_c),$$

$$(B5)$$

and the length of the semi-latus recturn is given by

$$\hat{r} = \frac{b^2}{a} \ ,$$

$$(B6)$$

and the ellipse eccentricity e_c must satisfy the relation

$$b^2 = a^2(1-e_c^2),$$

$$(B7)$$

where $2a \equiv$ major axis of the ellipse,

$2b \equiv$ minor axis of the ellipse.

Eliminating a and b in Eq.(B5) through (B7) gives

$$\frac{\hat{r}}{r_o} = 1-e_c .$$

$$(B8)$$

That is, the ratio of the radius at which the radial acceleration is zero to the outer turning point radius is a function only of the eccentricity of the ellipse. In retrospect, this may be demonstrated more

succintly by substituting Eqs.(B3) and (B8) into Eq.(B1) which gives the equation of an elliptical orbit in the form

$$\frac{\hat{r}}{r} = 1 - e_c \cos \theta, \tag{B9}$$

from which Eq.(B8) follows immediately for the coordinate pair $(r_0, n\pi)$ (n even).

By analogy with the closed elliptical orbit, an effective eccentricity may be defined for the electron trajectory in an orbitron even though it is not a closed ellipse. Equation(24), upon setting $r=0$, gives

$$\alpha^2 = \left(\frac{\hat{r}}{r_0} \right)^3 \frac{E_2(\hat{r})}{E_2(r_0)}. \tag{B10}$$

This equation is cumbersome to use if left in its general form, but becomes particularly elementary if only the space charge free potential distribution is considered. The space charge free field is simply

$$E(r) = \frac{V}{\log \frac{R_0}{R_i}} \frac{1}{r}. \tag{B11}$$

Substituting Eq.(B11) into (B10) gives

$$\frac{\hat{r}}{r_0} = \alpha. \tag{B12}$$

Thus, by analogy with Eq.(B8), the effective eccentricity e_c^* of an electron trajectory in the orbitron is given by

$$e_c^* = 1 - \alpha. \tag{B13}$$

Thus, the parameter originally introduced as an orbit stability label, turns out to be nothing more than an obscure way of writing the effective eccentricity of the open, ellipse-like electron trajectories in the orbitron.

Strictly, the elementary relation in Eq.(B13) applies only to negligibly low space charge distributions. A similar, but more complicated relation

may be derived for non-negligible space charge distributions. However, the essential conclusion is (and applies to any space-charge distribution) that α is simply a measure of the effective eccentricity of the ellipse-like electron trajectories.

APPENDIX C

θ-Dependent Charge Distributions

For this discussion it should be recalled that an orbit may be defined as that segment of the electron trajectory between two successive outer turning points (this definition is consistent with the conventional definition[4]). The azimuthal angle θ is the angle traversed in θ-space between two successive outer turning points. It is shown below that θ has an upper and lower bound (independent of charge density distribution). It is then shown that for certain values of θ the electron trajectory is stationary yielding a θ-dependent charge density distribution.

A bound electron having the maximum allowed angular momentum ($\alpha^2=1$) executes a constant radius trajectory about the anode such that $\ddot{r}=0$, $\dot{r}=0$ and the electron velocity along its trajectory is constant and given by

$$v_o^2 = \frac{e}{m} E(r_o)r_o = \left(\frac{\ell}{mr_o}\right)^2 \tag{C1}$$

where r_o is the constant radius of the trajectory and ℓ is the injection angular momentum. Suppose that a small radial perturbation is applied to the electron motion. If the perturbation is sufficiently small that nonlinear terms may be neglected, the resulting motion is a small amplitude harmonic oscillation about the original trajectory, the oscillatory part of which is given by Eq.(A15) after having set $\alpha^2=1$ in Eq.(A14). During the period of one oscillation $\tau=\frac{2\pi}{\omega}$, the electron advances along the trajectory $r=r_o$ a distance $v_o\tau$. Obviously then, the wave length of one oscillation, measured along the original trajectory, is given by

$$\Lambda = 2\pi \frac{v_o}{\omega} . \tag{C2}$$

Taking the period τ as the time between two successive maxima of the oscillatory part of the motion, it follows from the above definition of θ that (see sketch below)

$$\Lambda = r_0 \theta \tag{C3}$$

since the average value of the oscillatory amplitude is zero as may be seen from

$$\bar{r} = r_0 + \frac{1}{\tau} \int_0^\tau \chi(t)dt = r_0 \tag{C4}$$

upon substituting from Eq.(A15) for $\chi(t)$.
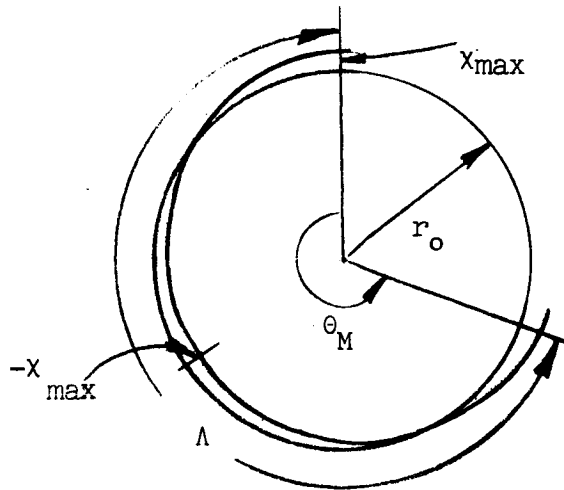
Eliminating Λ between Eq.(C2) and (C3), substituting from Eq.(C1) for v_0, and substituting from Eq.(A14) for ω (with $\alpha^2=1$), gives

$$\theta_M = \sqrt{2}\,\pi. \tag{C5}$$

The subscript M (for maximum) has been applied to θ since this value was obtained for the maximum angular momentum and as the angular momentum decreases θ must decrease. An important observation is that the result in Eq.(C5) is independent of electric field distribution and therefore of the charge density distribution.

The minimum angle traversed in one orbit is that associated with an $\ell=0$ trajectory (which of course violates the stability criteria and presents obvious practical difficulties). However, if practicable and if allowed, an $\ell=0$ electron would pass through the origin $(r=0)$ and proceed to $r=r_0$ on the opposite side of the anode. The angle between two successive outer turning points is Π and therefore

$$\Theta_m = \Pi, \qquad (C6)$$

where the subscript m (for minimum) has been applied since an angle smaller than this value would have no physical meaning.

From the above discussion, it follows immediately that all electron trajectories in an ortitron must satisfy

$$\Pi \leq \Theta \leq \sqrt{2}\,\Pi. \qquad (C7)$$

Since the derivation of these limits did not involve the form of the electric field distribution, Eq.(C7) is applicable to any charge density distribution provided only that the charge is uniformly distributed in θ-space.

It is immediately obvious that the $\ell=0$ trajectory results in a non-uniform θ-distribution of the space charge, since on a time average the charge is mostly in the neighborhood of the turning points where $\dot{r}=0$. The $\ell=0$ trajectory thus yields two charge clusters, each in the neighborhood of $r=r_0$ but one at $\theta=\theta_0$ and the other at $\theta=\theta_0 + \Pi$. Thus for all θ not near θ_0 or $\theta_0+\Pi$, $\rho \equiv 0$. An important observation concerning this charge distribution is that it is stationary in θ-space. As the number of $\ell=0$ electrons are increased, the charge density approaches saturation in only two regions while in the remainder of the interelectrode space the charge density is zero. Such trajectories then make very inefficient use of the interelectrode space and the applied potential.

A sequence of possible trajectories exists having $\ell>0$ which like the $\ell=0$ trajectory, tend to produce localized stationary charge clusters. The trajectories belonging to this series are those for which the angle between successive outer turning points satisfies the relation

A-12

$$n\Theta = 2m\Pi \quad (n{>}m), \qquad\qquad (C8)$$

where n and m are positive integers containing no common factor (and of course Θ must satisfy Eq.(C7).) The n=2, m=1 trajectory has already been discussed (ℓ=0). The n=3, m=2 and the n=5, m=3 trajectories are sketched below.
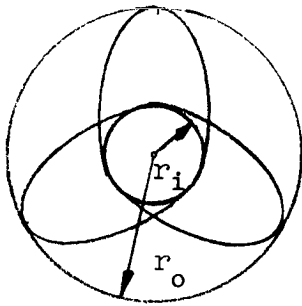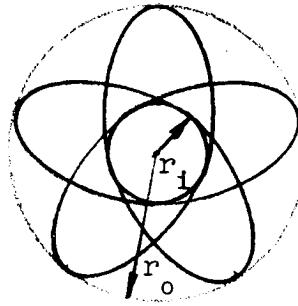
The important property of this series of trajectories is that after n orbits (or m circuits of the anode) each closes on itself and repeats indefinitely. Thus, the n-orbit trajectory considered integrally is stationary. The n-orbit closed trajectory produces 2n stationary charge clusters in the neighborhoods of the 2n turning points of the integral, closed trajectory. All the members of this series of trajectories make more or less inefficient use of the interelectrode space, approaching saturation in a discrete set of small regions. The maximum charge that can be stored in the interelectrode space under these conditions is substantially less than that corresponding to a uniform approach to saturation over all θ-space. As n becomes large, the charge clusters begin to overlap and the charge distribution in θ-space begins to smooth, eventually becoming approximately uniform.

From the above discussion, it is clear that the n-orbit closed trajectories, in which n is small, should be avoided in the orbitron. This may be

accomplished by disallowing those values of α within the stability range which correspond to stationary, closed trajectories. It turns out that the specification of this discrete set of α's involves considerable numerical computation and a complete solution to the electron motion in the space charge dependent potential distribution.

For all trajectories which do not satisfy Eq.(C8), θ is an irrational multiple of 2Π, the trajectories never close, the orbits continue to precess, and the charge density is uniform in θ-space.

APPENDIX D

Interpretation of β

The electric field distribution in Region 3, outside the space charge cloud, is obtained from Eq.(15) by taking the negative derivative with respect to r. Applying Eqs.(54) and (55) and evaluating at R_o gives the electric field at the outer boundary

$$E_3(R_o) = \left\{V + I'(r_o)\log\frac{r_o}{R_i} - I(r_o)\right\} \frac{1}{\log\frac{R_o}{R_i}} \cdot \frac{1}{R_o} \, . \tag{D1}$$

The space charge free electric field at the outer boundary is obtained from this same equation by setting all the charge integrals to zero

$$E_{cf}(R_o) = \frac{V}{\log\frac{R_o}{R_i}} \cdot \frac{1}{R_o} \, . \tag{D2}$$

The change in electric field at the outer boundary resulting from the charge insertion is

$$E_{cf}(R_o) - E_3(R_o) = +\left\{-I'(r_o)\log\frac{r_o}{R_i} + I(r_o)\right\} \frac{1}{\log\frac{R_o}{R_i}} \frac{1}{R_o} \, . \tag{D3}$$

The fractional change in electric field, relative to the final value, is

$$\frac{E_{cf}(R_o) - E_3(R_o)}{E_3(R_o)} = \frac{-I'(r_o)\log\frac{r_o}{R_i} + I(r_o)}{V + I'(r_o)\log\frac{r_o}{R_i} - I(r_o)} \, . \tag{D4}$$

Substituting from Eq.(61) for $I'(r_o)$ gives

$$\frac{E_{cf}(R_o) - E_3(R_o)}{E_3(R_o)} = \frac{E_{cf}(R_o)}{E_3(R_o)} - 1 = \left\{\frac{\alpha^2 eV}{2T(r_o)} - \log\frac{R_o}{R_i}\right\} \frac{1}{\log\frac{R_o}{R_i}} \, . \tag{D5}$$

Therefore by comparison with Eq.(65), it follows that

$$\beta = \left\{ \frac{E_{cf}(R_o)}{E_3(R_o)} - 1 \right\} \log \frac{R_o}{R_i} . \tag{D6}$$

From this equation it is obvious that β is positive for all nonzero charge densities and approaches zero as the charge density approaches zero. β is essentially a measure of the fractional reduction in electric field at the outer boundary relative to its final value after charge insertion.

An informative alternate form of Eq.(D6) is

$$E_3(R_o) = \frac{V}{R_o (\beta + \log \frac{R_o}{R_i})} , \tag{D7}$$

from which it follows that

$$\lim_{\beta \to \infty} E_3(R_o) = 0. \tag{D8}$$

Thus, the electric field at the outer boundary is always greater than zero for acceptable values of β.

APPENDIX E

Charge Optimization

It follows immediately from Eqs.(16), (52), (53) and (54) that

$$-I'(r_o) = - \int_{r_i}^{r_o} \frac{\rho(r)}{\varepsilon_o} r \, dr = \frac{eN_L}{\pi \tau \varepsilon_o} \int_{r_i}^{r_o} \frac{dr}{\dot{r}} = \frac{eN_L}{2\pi\varepsilon_o} . \qquad (E1)$$

Therefore Eq.(61) may be written

$$eN_L = 2\pi\varepsilon_o V \frac{\left[1 - \frac{2T(r_o)}{\alpha^2 \, eV} \log \frac{R_o}{R_i} \right]}{\left[\log \frac{r_o}{R_i} - \frac{I(r_o)}{I'(r_o)} \right]} . \qquad (E2)$$

Since

$$\log \frac{r_o}{R_i} = \log \frac{r_o}{r_i} + \log \frac{r_i}{R_i} , \qquad (E3)$$

Eq.(E2) may be written

$$eN_L = 2\pi\varepsilon_o V \frac{\left[1 - \frac{2T(r_o)}{\alpha^2 \, eV} \log \frac{R_o}{R_i} \right]}{\left[\log \frac{r_i}{R_i} + \log \frac{r_o}{r_i} - \frac{I(r_o)}{I'(r_o)} \right]} . \qquad (E4)$$

The left side of this equation is the total charge stored in unit length of the rotating electron cloud. Optimizing N_L involves several operations: Maximizing N_L with respect to r_i; maximizing N_L with respect to α^2 but consistent with the other requirements that α^2 must satisfy; and determining the behavior of N_L as a function of other prescribed parameters such that values are prescribed which tend to optimize N_L.

Maximizing N_L with respect to r_i involves minimizing the denominator of Eq.(E4) with respect to r_i. Although the ratio $\frac{r_0}{r_i}$ is fixed by prescribing α^2 and β, either r_0 or r_i may be prescribed independently. Full advantage may be taken of this degree of freedom by prescribing that

$$r_i = R_i + \delta, \qquad (E5)$$

such that

$$\frac{\delta}{R_i} \simeq \frac{\delta}{r_i} \ll 1. \qquad (E6)$$

This prescription is equivalent to locating the inner turning point immediately outside the anode surface such that the electrons pass by the anode at a distance just sufficient to assure that they do not collide with the anode surface. Under this condition δ may frequently be neglected in the analysis (for α^2 not close to 1). This simplifies the denominator of Eq.(E4) and removes any explicit dependence on R_i since the first term may be written

$$\log \frac{r_i}{R_i} = \log \left(1 + \frac{\delta}{R_i}\right) \simeq \log \left(1 + \frac{\delta}{r_i}\right) \simeq \frac{\delta}{r_i} \ll 1 . \qquad (E7)$$

This operation maximizes N_L with respect to r_i while leaving the ratio $\frac{r_0}{r_i}$ unchanged and without substantially affecting the value of $\frac{I(r_0)}{I'(r_0)}$.

Maximizing N_L with respect to α^2 is not so elementary. A plausibility argument may be constructed, based on an approximation to $\frac{I(r_0)}{I'(r_0)}$ obtained by using the radial component of

the electron velocoty applicable to negligibly low charge densities. Although this approximation does not contain some of the important parameters (for example β), it must indicate correctly at least the direction of the variation in N_L as a function of α^2. That is, the result must correctly indicate, even for non-negligible charge densities, whether N_L is an increasing or decreasing function of α^2 (it turns out this is the only information required to maximize N_L with respect to α^2). This conclusion follows from the fact that $\rho(r)$ has the same general shape for any value of N_L. The principal influence of N_L upon $\rho(r)$ is that variations in N_L raise or lower $\rho(r)$ and only secondarily increase or decrease the distance between turning points (space charge boundaries). The shape of $\rho(r)$ is principally determined by the form of the function (which is generally similar for any N_L) and α^2. The first integral of the charge density is independent of the shape of $\rho(r)$. The ratio $\frac{I(r_o)}{I'(r_o)}$ is independent (explicitly) of N_L and is principally a function of the shape of the charge density distribution. Therefore, conclusions based on the shape of one charge density distribution must be generally applicable to other similar charge density distributions since their shapes do not differ substantially.

The derivation of the analytical expressions necessary to expose the way that the ratio $\frac{I(r_o)}{I'(r_o)}$ depends on α^2, is connected intimately with the trajectory analysis in Appendix F, which is therefore used freely in the following analysis.

Equation (F13) may be used to obtain an approximate value for the charge integrals $I'(r_o)$ and $I(r_o)$. Substituting Eq.(F13) into Eq.(52), substituting the result into Eq.(16) and applying Eqs.(54) and (F16) gives

$$I'(r) = - \frac{eN_L}{2\pi\varepsilon_o} \cdot \frac{1}{\pi} \int_o^x \frac{dx}{[2ax - x^2]^{\frac{1}{2}}}$$

$$= \frac{-eN_L}{2\pi\varepsilon_o} \cdot \frac{1}{\pi} \cos^{-1}(1-\frac{x}{a}),$$

where a is defined by Eq.(F14). Evaluating this equation at r_o, (x = 2a), gives the expected result

$$I'(r_o) = - \frac{e N_L}{2\pi\varepsilon_o} , \tag{E9}$$

which is the same for all charge density distributions since $I'(r_o)$ is independent of the shape of $\rho(r)$.

Substituting Eq.(E8) into Eq.(17), performing the co-ordinate transformation of Eq.(F3) on $\frac{dr}{r}$ and applying Eq.(55) gives

$$I(r) = - \frac{eN_L}{2\pi\varepsilon_o} \cdot \frac{1}{\pi} \int_o^x \cos^{-1}(1-\frac{x}{a}) \frac{dx}{(\gamma+x)} , \tag{E10}$$

where γ is defined in Eq.(F4) or (F12). It is convenient to make a new coordinate transformation such that

$$\zeta = \cos^{-1}(1-\frac{x}{a}) , \tag{E11}$$

with the limits

$$\left. \begin{matrix} x = 0 , \zeta = 0 \\ x = x_o, \zeta = \pi \end{matrix} \right\} . \tag{E12}$$

Equation (E10) may then be written

$$I(r) = -\frac{eN_L}{2\pi\varepsilon_0} \cdot \frac{b}{\pi} \int_o^\zeta \frac{\zeta \sin \zeta \, d\zeta}{1 - b \cos \zeta} \, , \qquad\qquad (E13)$$

where

$$b = \frac{1}{2}\left(\frac{\alpha^2 - \gamma^2}{2\alpha^2 - \gamma^2}\right). \qquad\qquad (E14)$$

Integrating Eq.(E13) by parts gives

$$I(r) = -\frac{eN_L}{2\pi\varepsilon_0}\left\{\frac{\zeta}{\pi}\log(1-b\cos\zeta) - \frac{1}{\pi}\int_o^\zeta \log(1-b\cos\zeta)d\zeta\right\}. \qquad (E15)$$

Since $b << 1$ (the leading term in its expansion as a function of Δ is $\frac{\Delta}{2}$) (see Eqs.(F8) and (F12)), the logarithms in Eq.(E15) may be expanded in powers of $(b \cos \zeta)$. Second order and higher terms may be neglected for the present purpose. After performing these operations, Eq.(E15) becomes

$$I(r) \cong -\frac{eN_L}{2\pi\varepsilon_0} \cdot \frac{b}{\pi}(\sin\zeta - \zeta \cos\zeta). \qquad\qquad (E16)$$

Evaluating this expression at r_o, $(\zeta = \pi)$, gives

$$I(r_o) = -\frac{eN_L}{2\pi\varepsilon_0} b \, . \qquad\qquad (E17)$$

From Eqs.(E9) and (E17)

$$\frac{I(r_o)}{I'(r_o)} = b \, , \qquad\qquad (E18)$$

and from Eq.(E14)

$$\frac{I(r_o)}{I'(r_o)} = \frac{1}{2} \left(\frac{\alpha^2 - \gamma^2}{2\alpha^2 - \gamma^2}\right) ,$$ (E19)

and applying Eq.(F12) gives

$$\frac{I(r_o)}{I'(r_o)} = \frac{1}{2} \left(\frac{1 - \alpha^2}{2 - \alpha^2}\right) \simeq \frac{\Delta}{2} .$$ (E20)

Therefore the denominator of Eq.(E4) may be written (for α^2 near 1)

$$\log \frac{r_i}{R_i} + \log \frac{r_o}{r_i} - \frac{I(r_o)}{I'(r_o)} \cong \log \frac{r_o}{r_i} - \frac{\Delta}{2} ;$$ (E21)

and from Eqs.(F4) and (F12) it follows that

$$\log \frac{r_o}{r_i} \simeq \Delta;$$ (E22)

from which Eq.(E21) becomes

$$\log \frac{r_i}{R_i} + \log \frac{r_o}{r_i} - \frac{I(r_o)}{I'(r_o)} = \frac{\delta}{r_i} + \frac{\Delta}{2}$$
$$= \frac{\delta}{r_i} + \frac{1}{2}(1 - \alpha^2).$$ (E23)

Therefore, under the condition expressed in Eq.(E5) and for α^2 near 1, the limiting value of the total charge stored in unit length of the rotating electron cloud is

$$\lim_{\alpha^2 \to 1} eN_L = \frac{2\pi\varepsilon_0 V r_i}{\delta} \left[1 - \frac{2T(r_o)}{eV} \log \frac{R_o}{R_i}\right].$$ (E24)

Using Eq.(65) to eliminate $\log \frac{R_o}{R_i}$, which in this discussion is an unimportant parameter, Eq.(E24) may be written in the alternate form

$$\lim_{\alpha^2 \to 1} N_L = \frac{4\pi\epsilon_o \beta T(r_o)}{e^2} \frac{r_i}{\delta} \qquad (E25)$$

from which it is obvious that N_L increases with increasing r_i and decreases with increasing δ. This limiting charge corresponds to a thin, high density charge sheet immediately outside the anode surface, the electrons of which execute circular trajectories.

$\alpha^2 = 1$ leads to serious practical difficulties since the electron launcher cannot be made infinitesimally small. Long electron life times can be achieved only if the electron trajectory is sufficiently eccentric that the electrons miss the launcher during the first few passes after injection (it is assumed that after the first few passes, the electron has drifted far enough along the z-axis to miss the launcher altogether). Therefore, optimization of N_L is not a simple maximization operation. The optimum N_L is that associated with the largest α^2 for which the trajectory is sufficiently eccentric that the probability of collision with the launcher during the first few orbits is negligibly small. It is only under this condition that the charge density can be pumped up to its equilibrium value all along the z-axis and a uniform charge density cahieved in z-space (if the electrons returned to the launcher at the end of the first circuit of the anode, all the charge would be concentrated in the z-neighborhood of the launcher).

Concerning the remaining parameters in Eq.(E4), it is obvious that N_L increases with V and increases with decreasing $\frac{R_o}{R_i}$.

APPENDIX F

Trajectory Analysis for Low Charge Density (Approximate)

If the total charge stored in the rotating electron cloud is sufficiently low that the space charge dependent potential distribution does not differ substantially from the space charge free potential distribution, and if the electrons are injected into trajectories which are not very eccentric, then Eq.(26) may be approximated by an integrable function. The results obtained are not strictly applicable to the more interesting and useful high density, moderate eccentricity space charge configuration, however the results provide considerable insight into the low density electron dynamics and may be used to clarify and assist the correct interpretation of other results which are directly applicable to moderate eccentricity, high density space charge distributions.

Under the above restrictions, the radial component of the electron velocity is given by

$$\dot{r} = \kappa^{\frac{1}{2}} \left\{ \log \frac{r_o}{r} + \frac{\alpha^2}{2}(1 - \frac{r_o^2}{r^2}) \right\}^{\frac{1}{2}}, \tag{F1}$$

where

$$\kappa = \frac{2 \, eV}{m \, \log \frac{R_o}{R_i}} . \tag{F2}$$

For mathematical convenience, let

$$\frac{r}{r_o} = \gamma + x , \tag{F3}$$

where

$$\gamma = \frac{r_i}{r_o} \qquad (F4)$$

The trajectory turning points then occur at

$$r = r_i \ , \ x = x_i = 0 \ , \ (\text{inner turning point}) \ , \qquad (F5)$$

and

$$r = r_o \ , \ x = x_o = 1-\gamma, (\text{outer turning point}) \ . \qquad (F6)$$

Recalling that the trajectories considered in this Appendix are not very eccentric, γ is near 1 and for even the maximum value of x,

$$x_o \ll 1 \ . \qquad (F7)$$

Similarly, α^2 is not much less than 1 and may be written

$$\alpha^2 = 1 - \Delta \ , \qquad (F8)$$

where

$$0 \leq \Delta \ll 1 \ . \qquad (F9)$$

From Eqs. (F1) and (F4), it follows that

$$\log \frac{1}{\gamma} + \frac{\alpha^2}{2}(1 - \frac{1}{\gamma^2}) = 0. \qquad (F10)$$

The logarithmic term in this equation may be approximated by the first two terms of the well known Taylor expansion in the neighborhood of 1,

$$\log \frac{1}{\gamma} \cong (\frac{1}{\gamma}-1)-\frac{1}{2}(\frac{1}{\gamma}-1)^2 . \qquad (F11)$$

Substituting Eq.(F11) into Eq.(F10) and solving the resulting quadratic equation for γ gives

$$\gamma = \frac{1+\alpha^2}{3-\alpha^2} = \frac{2-\Delta}{2+\Delta} \simeq 1-\Delta = \alpha^2, \qquad (F12)$$

a result which is needed frequently later on.

Using Eq.(F3) to eliminate r in Eq.(F1) and performing an expansion similar to Eq.(F11) and taking account of Eq.(F10) yields an approximate analytical expression for the radial component of the electron velocity

$$\dot{r} = \frac{\kappa^{\frac{1}{2}}}{\gamma^2} \left(\frac{3\alpha^2-\gamma^2}{2}\right)^{\frac{1}{2}} [2ax-x^2]^{\frac{1}{2}}, \qquad (F13)$$

where

$$a = \gamma \left(\frac{\alpha^2-\gamma^2}{3\alpha^2-\alpha^2}\right) \simeq \frac{1}{2}(1-\alpha^2) \simeq \frac{\Delta}{2}. \qquad (F14)$$

The solution to this differential equation gives the electron radial position as a function of time. Taking the zero time reference to correspond to the inner turning point of the electron trajectory and integrating Eq.(F13) gives

$$t = \int_1^r \frac{dr}{\dot{r}}$$

$$\simeq \frac{r_o \gamma^2}{\kappa^{\frac{1}{2}}} \left(\frac{2}{3\alpha^2 \gamma^2}\right)^{\frac{1}{2}} \int_0^x \frac{dx}{[2ax-x^2]^{\frac{1}{2}}}$$

$$\simeq \frac{r_o \gamma^2}{\kappa^{\frac{1}{2}}} \left(\frac{2}{3\alpha^2-\gamma^2}\right)^{\frac{1}{2}} \cos^{-1}(1-\frac{x}{a}). \qquad (F15)$$

From this equation, the orbit half-period τ' is found immediately by setting $r=r_0$ ($x=x_0$),

$$\tau' = \frac{\pi \, r_0 \gamma^2}{\kappa^{\frac{1}{2}}} \left(\frac{2}{3\alpha^2 - \gamma^2}\right)^{\frac{1}{2}}. \tag{F16}$$

Using this result, Eq.(F15) may be written

$$x = x_0 \sin^2 \frac{\pi t}{2\tau'}, \tag{F17}$$

and transforming from x-space back to r-space, the radial position of the electron as a function of time is given by

$$\frac{r}{r_0} \approx 1 - (1-\gamma) \cos^2 \frac{\pi t}{2\tau'}. \tag{F18}$$

The position of the electron in θ-space may be obtained as a function of time by substituting Eq.(F18) into Eq.(20) and integrating (again taking the zero – θ reference to correspond to the inner turning point),

$$\theta = \frac{\dot{\theta}_0 \tau'}{\pi} \left(\frac{2}{1+\gamma}\right)^2 \int_0^t \frac{d\left(\frac{\pi t}{\tau'}\right)}{\left[1-\left(\frac{1-\gamma}{1+\gamma}\right) \cos \frac{\pi t}{\tau'}\right]^2}, \tag{F19}$$

where τ' is again the half-period and $\dot{\theta}_0$ is the angular velocity at the outer turning point and is given by

$$\dot{\theta}_0 = \left[\frac{2T(r_0)}{m \, r_0^2}\right]^{\frac{1}{2}}, \tag{F20}$$

and the outer turning point kinetic energy, $T(r_0)$, is given by

$$T(r_0) = \frac{\alpha^2 \, e \, V}{2 \, \log \frac{R_o}{R_i}} \; . \tag{F21}$$

The coefficient of $\cos \frac{\pi t}{\tau'}$ in the denominator of Eq.(F19) is small compared to 1 since

$$\frac{1-\gamma}{1+\gamma} \simeq \frac{\Delta}{2} \; . \tag{F22}$$

Therefore a satisfactory approximation of the integrand in Eq.(F19) is obtained by applying the binomial expansion theorem and retaining only the first two terms. This operation gives

$$\theta = \frac{\dot{\theta}_0 \tau'}{\pi} \left(\frac{2}{1+\gamma}\right)^2 \int_0^t \frac{d(\frac{\pi t}{\tau'})}{[1 - 2(\frac{1-\gamma}{1+\gamma}) \cos \frac{\pi t}{\tau}]} \; . \tag{F23}$$

Performing the integration indicated in this equation gives the θ-coordinate of the electron along its trajectory as a function of time (both measured from the inner turning point),

$$\theta = \frac{\dot{\theta}_0 \tau'}{\pi} \left(\frac{2}{1+\gamma}\right)^2 \frac{2}{[1 - 4(\frac{1-\gamma}{1+\gamma})^2]^{\frac{1}{2}}} \tan^{-1}\left\{ \left(\frac{3-\gamma}{3\gamma-1}\right)^{\frac{1}{2}} \tan \frac{\pi t}{2\tau'} \right\} \; . \tag{F24}$$

Using Eqs.(F2), (F16), (F20) and (F21), this may be written

$$\theta = 2 \left(\frac{\alpha^2}{3\alpha^2 - \gamma^2}\right)^{\frac{1}{2}} \left(\frac{2\gamma}{1+\gamma}\right)^2 \tan^{-1}\left\{ \left(\frac{3-\gamma}{3\gamma-1}\right)^{\frac{1}{2}} \tan \frac{\pi t}{2\tau'} \right\} \; . \tag{F25}$$

where the approximation has been made

$$[1-4\left(\frac{1-\gamma}{1+\gamma}\right)^2]^{\frac{1}{2}} \simeq 1 \qquad\qquad (F26)$$

because of Eq.(F22). Setting $t=\tau'$ in this equation gives
the azimuthal half-angle of the electron trajectory

$$\theta' = \pi\left(\frac{\alpha^2}{3\alpha^2-\gamma^2}\right)^{\frac{1}{2}}\left(\frac{2\gamma}{1+\alpha}\right)^2 . \qquad\qquad (F27)$$

Using this result, Eq.(F25) may be written in the alternate
form

$$\theta = \frac{2\theta'}{\pi}\tan^{-1}\left\{\left(\frac{3-\gamma}{3\gamma-1}\right)^{\frac{1}{2}}\tan\frac{\pi t}{2\tau'}\right\} . \qquad\qquad (F28)$$

Using Eq.(F12), γ may be eliminated from Eq.(F27) in favor of
α^2 which gives

$$\theta' = \frac{\pi}{(3-\alpha^2)^{\frac{1}{2}}}\left(\frac{2\alpha^2}{1+\alpha^2}\right)^2 , \qquad\qquad (F29)$$

from which it follows that

$$\lim_{\alpha^2 \to 1} \theta' = \frac{\pi}{\sqrt{2}} , \qquad\qquad (F30)$$

a result which was derived from other considerations in
Appendix C.

Considering Eqs.(F18) and (F25) as a set of parametric equations in t, r may be expressed as a function of θ by eliminating t. The result of this operation (after using Eq.(F12) to eliminate γ) is

$$\frac{r-r_i}{r_o-r} = \left(\frac{3\alpha^2-1}{3-\alpha^2}\right)\tan^2\left\{\left(\frac{1+\alpha^2}{2\alpha^2}\right)^2(3-\alpha^2)^{\frac{1}{2}}\frac{\theta}{2}\right\}. \qquad (F31)$$

An immediate application of this equation is to compute the values of α^2 for which the electron trajectories are closed and stationary so that these α's may be rejected in prescribing the launch parameters. From Appendix C, the first non-degenerate stationary trajectory has $n=3$, $m=2$. Therefore at $r=r_o$, $\theta=\frac{2\pi}{3}$. Substituting these values into Eq.(F31) gives

$$\left(\frac{1+\alpha^2}{2\alpha^2}\right)^2(3-\alpha^2)^{\frac{1}{2}}\frac{\pi}{3} = \frac{\pi}{2} , \quad (n=3, m=2) \quad ; \qquad (F32)$$

from which it follows that

$$\alpha^2 = 0.95 , \quad (n=3, m=2). \qquad (F33)$$

Similarly, the second closed, stationary trajectory occurs for

$$\alpha^2 \simeq 0.93 , \quad (n=5, m=3). \qquad (F34)$$

The separation in α-space between successive stationary trajectories decreases as n increases. This implies that either the launch parameters must be controlled very precisely or α^2 must be sufficiently small that n is large and the charge clusters in the neighborhood of the 2n turning points

overlap sufficiently to yield an approximately uniform charge density distribution in θ-space.

PART II MAGNETRON GAUGE

1.1 INTRODUCTION

In the initial description of the magnetron gauge using auxiliary cathodes, Redhead[6] showed that the gauge could be used to 10^{-12} Torr but that it was non-linear below about 5×10^{-10} Torr. Later work[7],[8], using different calibration techniques and extending the measured low pressure limit to 3×10^{-13} Torr, confirmed Redhead's work. However, in total, very little work has been carried out at pressures below 10^{-10} Torr where the aim has been to characterize the performance of the magnetron gauge over the range of the many variables which exist. For instance, in his original paper, Redhead[6] used an anode voltage of 6000 v and a magnetic field of 1000 gauss in measuring the variation of the cathode current with pressure. Similarly, later work[9] has tended to use similar values for the anode voltage and magnetic field. However, work at the National Research Corporation[10] has shown that below 10^{-10} Torr, the sensitivity ($S = i^+/P$) of the normal magnetron goes through a maximum as the anode voltage is varied from 1000 to 7000 volts. More recently[11] Redhead has investigated changes in both anode voltage and magnetic field over a range of pressures extending down to 1.3×10^{-11} Torr. This work has shown that the magnetron discharge exists in two states which may be characterized by the nature of the radio frequency oscillations exhibited by the gauge. In the pressure range 1×10^{-10} Torr to 10^{-6} Torr and at low magnetic fields (State I), the low frequency noise was large and stable r-f oscillations were not observed. At higher magnetic fields (State II), stable oscillations of very narrow band width were observed in the frequency range 15 - 100 Mc/s. (When used as a pressure gauge, the magnetron is operated under the conditions corresponding to State I.) In addition, Redhead reported

86

that oscillations were not observed below 10^{-10} Torr and it appeared that two separate states did not exist at these pressures. These results suggested that the change in oscillatory behavior may be closely related to the transition from linear to nonlinear operation at approximately 2×10^{-10} Torr. They also suggested that the oscillations might provide an indication as to whether or not a gauge was operating under linear conditions. The question also arose as to whether the gauge was linear when operated in State II. In general, it appeared that a wider range of variables than hitherto investigated should be studied - particularly the effect of anode voltage, magnetic field strength, and pressure on gauge sensitivity. The results of this work are discussed below in section 1.2: Performance Characteristics of Experimental Gauge. Several other aspects of magnetron performance which were studied included further experiments on the oscillatory behavior, the effects of ultra-violet radiation and electron injection and a study of some of the possible causes for anomolous currents in the magnetron gauge. A photographic study of the discharge within a magnetron gauge was also made. The results are reported in the following sections.

1.2 PERFORMANCE CHARACTERISTICS OF EXPERIMENTAL GAUGE

Previous work[8],[10] had shown that accurate, direct calibration procedures below 10^{-10} Torr required great care and considerable effort. In order to cover a wide range of such variables as anode voltage, magnetic field strength, and pressure, it was decided that it would be more efficient to use a simpler system involving comparison of the experimental magnetron gauge with a standard Redhead gauge (NRC 552). The reference Redhead gauge was operated at fixed conditions - anode voltage 4800 v, magnetic field strength, 1035 gauss.

The experimental apparatus constructed for the magnetron studies is shown schematically in Fig. 9. The basic vacuum system consisted of a mechanical pump backing two oil diffusion pumps in series, a 2 in. diffusion pump being used to "back" a 4 in. diffusion pump (NRC HK4-750). Dow Corning 705 Silicone oil was used in both pumps.

A specially adapted liquid nitrogen trap was mounted on the 4 in. diffusion pump. The trap was optically black and contained an anti-migration barrier. An R.C.A. high vacuum valve was mounted on the trap. The pressure above the liquid nitrogen trap was measured with a standard Redhead gauge (NRC 552). The R.C.A. valve was modified so that both the experimental magnetron gauge and the reference gauge could be tubulated onto the valve above the valve seat in such a way that there was high conductance- approximately 20 liters/sec - between the gauge volumes.

In order to extend the low pressure performance capabilities of the system to below 10^{-11} Torr, a liquid helium cryopump was installed below the high vacuum valve. The cryopump was designed to have a high conductance for gases not condensed at 4.2^{O}R. In addition, it produced low pressures

HELMHOLTZ MAGNETS

REDHEAD GAUGES

HIGH VACUUM VALVE

LIQUID NITROGEN
LIQUID HELIUM COLD
TRAP

EXPERIMENTAL
GAUGE
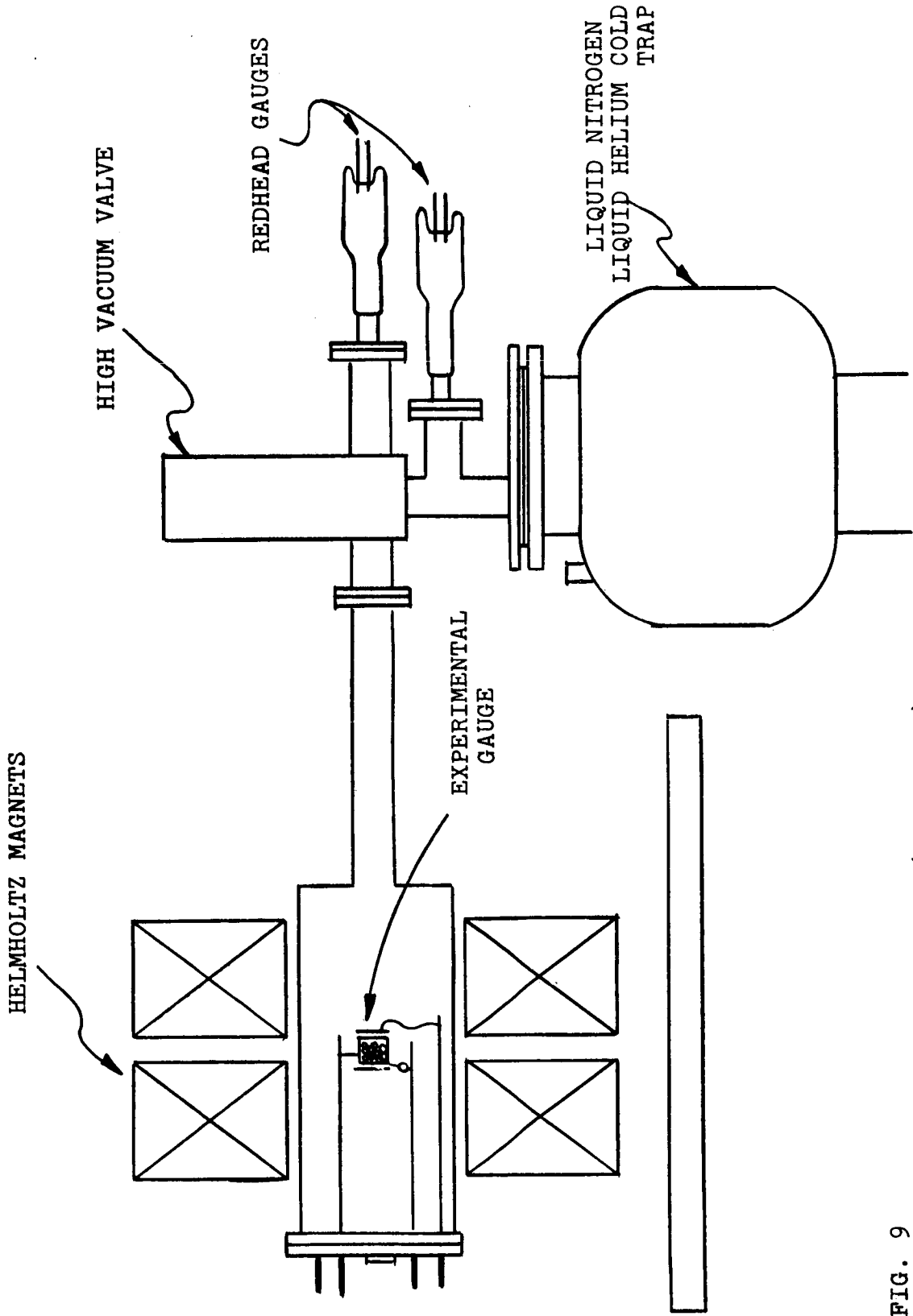
FIG. 9
MAGNETRON EXPERIMENTAL SETUP (SCHEMATIC)

which were stable for many hours of operation because of low heat losses and exceedingly small temperature variations over the cryopumping surface.

The gauge structure of the experimental magnetron was mounted on relatively heavy (0.100 in. diameter) stainless steel support posts, which also formed the electrical feed-through. Eight high impedance alumina feedthroughs were mounted in a 4 3/4 in. OD stainless steel (304) flange. The general arrangement of the magnetron is shown in Fig.10. A number of special features were included in the design and construction of this gauge. Some of the more important were:

i) The entire gauge assembly was mounted on the feed-through posts on a single flange. The arrangment facilitated the assembly and accurate alignment of the magnetron elements. It also permitted relatively rapid changes to be made in the gauge construction without major disassembly of the gauge-vacuum system.

ii) A radial slot (width 0.040 in.) was cut in the cathode end-plate and a mirror mounted close to the anode of the gauge. These arrangements were required for the photo-graphic measurements aimed at defining the spatial distri-bution of the discharge within the magnetron volume. See Section 1.6.

iii) A tungsten filament (0.007 in. diameter) was mounted opposite the anode. This filament was installed in order that the entire gauge assembly could be degassed by electron bombardment.

iv) A small hole (0.125 in. diameter) was drilled in one of the cathode end plates at a position one third of the distance from the cathode to the anode. In addition, a small tungsten coil filament was mounted opposite the hole outside

END VIEW

ELECTRON
INJECTION HOLE

VIEWING
SLIT

CATHODE

AUXILLIARY
CATHODE

DEGASSING
FILAMENT

MIRROR

ANODE

SHIELDING
SKIRTS

INJECTION
FILAMENT

FLANGE
SUPPORTS
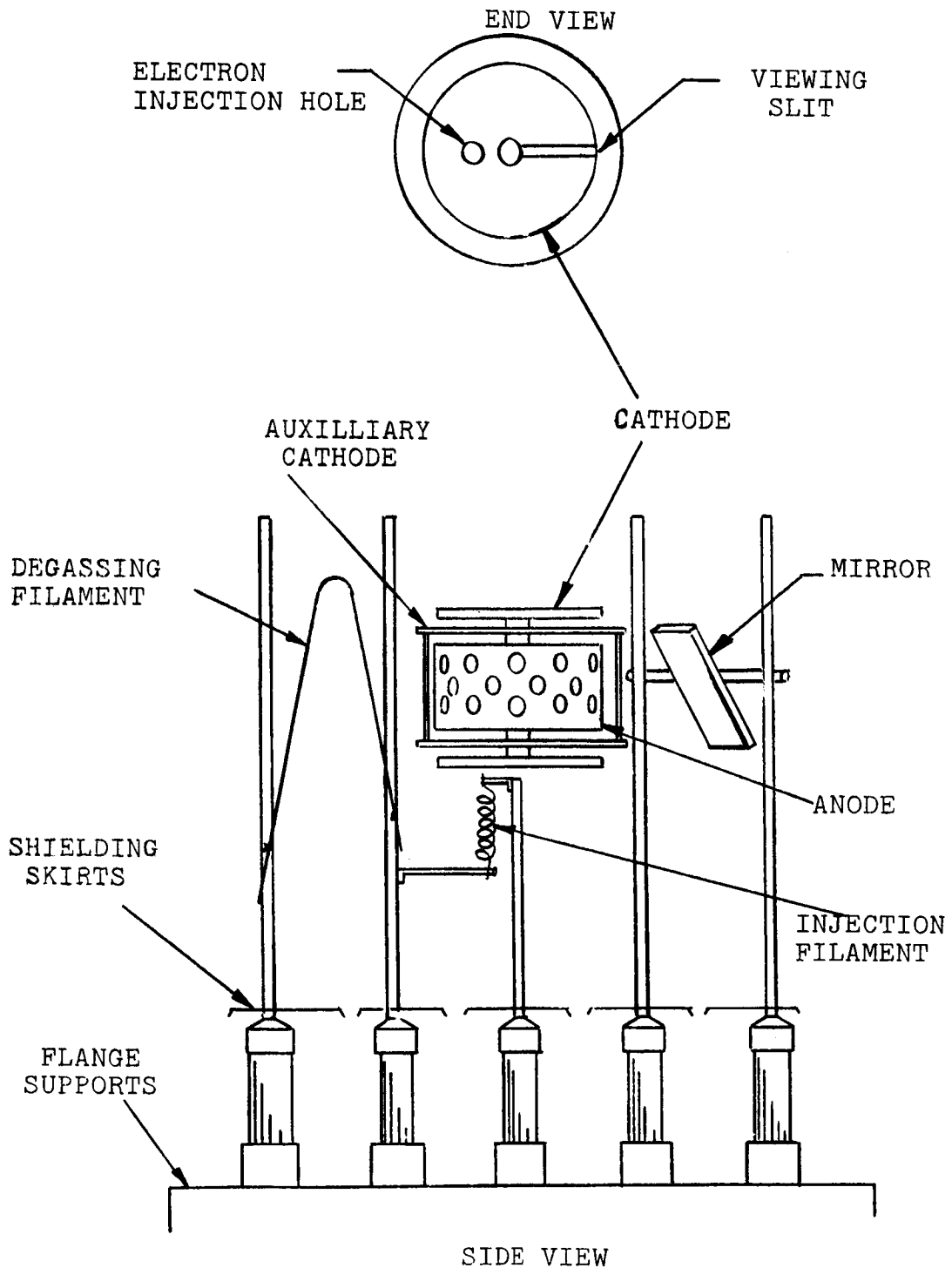
SIDE VIEW

FIG. 10

EXPERIMENTAL MAGNETRON SCHEMATIC

91

the magnetron volume. The purpose of this arrangement was
to permit the addition of electrons to the discharge. See
Section 1.5.

v) The magnetron was enclosed in a metal gauge volume
to provide adequate shielding. Only single conductor
ceramic feedthroughs were used. Since these were mounted
in the metal flange, a high degree of isolation and
shielding was achieved between each of the electrical feed-
throughs. In addition, metal skirts were placed around
the ceramic insulators on the vacuum side of the flange.
The purpose of these skirts was to prevent the build up
of a conductive coat on the ceramic during high tempera-
ture degassing of the metal elements of the gauge.

A Granville-Phillips variable leak valve was tubulated
to the chamber of the experimental gauge. High purity gases
could be added to the system through this valve or the
magnetron volume could be pumped out through it.

The entire system above the main diffusion pump, in-
cluding the liquid nitrogen trap, helium cryopump, high
vacuum valve and the three magnetron gauges could be
baked to 450°C. Gold seals were used for all flange
seals. Elastomeric materials were excluded from the entire
system.

The magnetic field for the experimental magnetron was
supplied by means of two electromagnets arranged as an
Helmholtz pair. This arrangement was chosen because of
the high degree of field homogeneity that it produces. For
example, the magnitude of the magnetic field varied less
than 0.1% over a spherical volume of 2 in. diameter in the
experimental setup used in the present work. The field
ripple, as detected by a Hall effect probe, was also less
than 0.1%. The magnetic field could be varied over the

range of 0 - 2200 gauss with the power supplies available.
In general, however, field variations over the range 400 -
2000 gauss were adequate for most of the experimental work.

The procedure used for determining the main performance
characteristics of the experimental magnetron gauge was as
follows. After thorough degassing of the system and gauge,
a known pressure was established in the experimental gauge.
This was usually done by admitting argon into a section of
the system above the high vacuum valve. The pressure was
measured by the reference Redhead gauge. The cathode current
from this gauge was converted to pressure (Torr N_2) by means
of Fig. 11. Since the latter takes into account the non-
linearity of the gauge below 2×10^{-10} Torr, the reference
pressures quoted in the following discussion correspond to
actual Torr N_2. After establishing a definite pressure,
the experimental gauge was operated at 1000 gauss and
10,000 v for a period of at least 45 minutes before starting
a series of measurements at lower anode voltages. This
procedure was found to give more reproducible results -
particularly at the lower pressures. It is not unlikely
that the gauge may tend to clean itself at the higher
ionization rates.

In the major part of the work, emphasis was not placed
on the measurement of low pressure. It was more to the
purpose to investigate a wide range of variables around
the region where the gauge changes from linear to non-linear.
The main conditions investigated were:

Pressures (Torr N_2): 5.2×10^{-8}, 5.2×10^{-10}
2.7×10^{-11}, 1.2×10^{-11}.

Anode Voltages: 1000 - 8000 in 1000 volt steps.

Magnetic Field Strength: 400 - 2000 gauss in 100 gauss steps.

This program thus covered some 500 combinations of pressure,
anode voltage and magnetic field. The data apply to a magnetron

FIG. 11
CALIBRATION CURVE 552 GAUGE
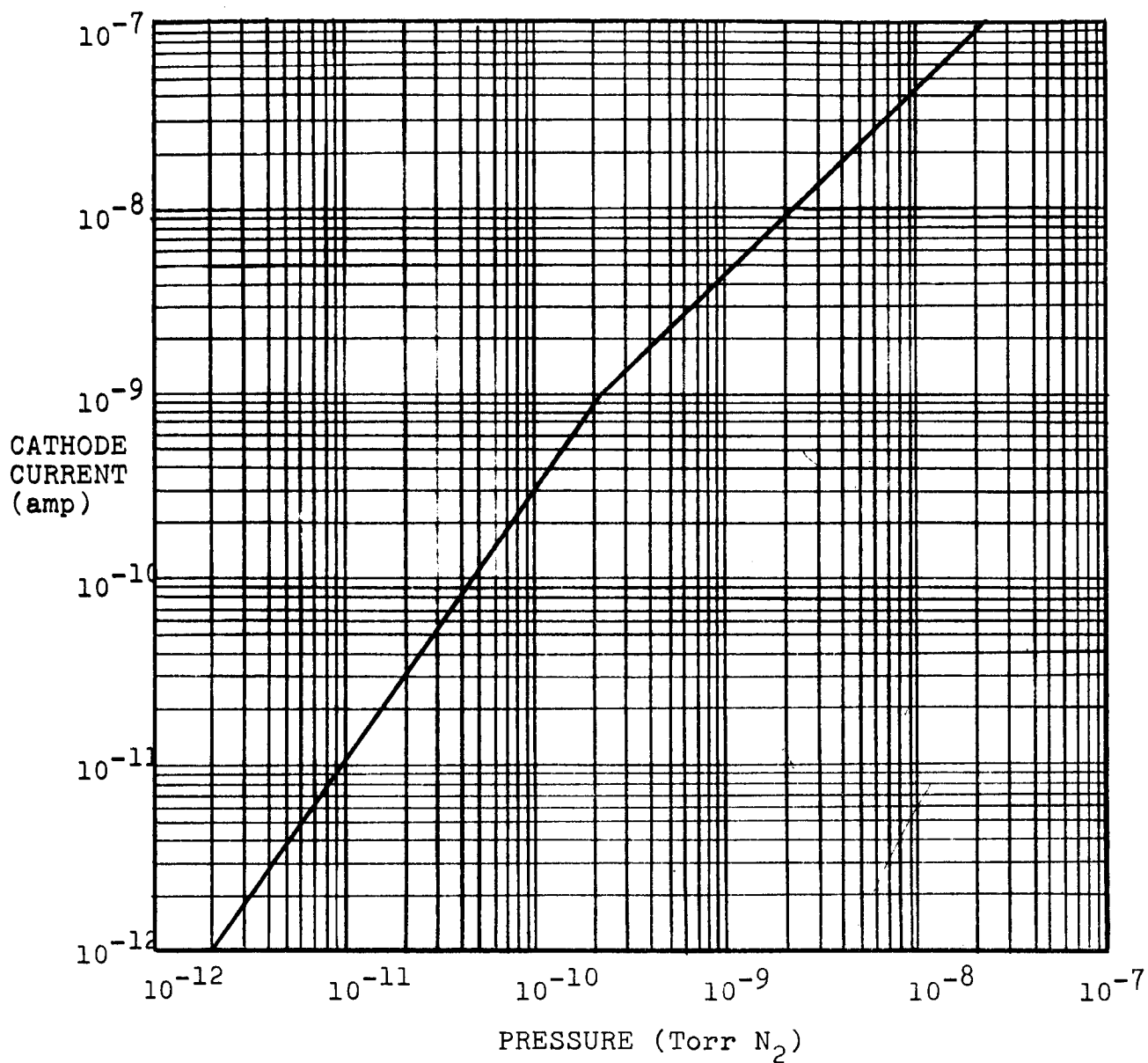
with a geometry essentially the same as that described by Redhead[6] and previously tested[8],[10]. It is considered very unlikely that the cathode hole and slits and method of support of the gauge elements would make the performance characteristics of this experimental gauge different from those previously investigated. Differences - and perhaps improved performance - were more likely to be associated with such factors as shielding by the metal envelope, magnetic field homogeneity and isolation of the high impedance feedthroughs. The results obtained are summarized in Tables I through IV. The performance characteristics have been specified in terms of gauge sensitivity, S, measured as amps/Torr N_2. One of the reasons for presenting the results in terms of the sensitivity, S, is that, other things being equal, S should be proportional to the average number of electrons trapped in the magnetron volume. In the tables, it will be noticed that in some cases two sensitivity values are given at particular values of V_a and B. The values refer to the minimum and maximum values recorded when the output of the gauge was oscillatory and very noisy. These results will be discussed in more detail in a later section (1.3).

Some of the data have also been plotted in Figs. 12, 13 and 14. Some of the points worthy of note are discussed below.

At pressures (above 2×10^{-10} Torr) where the gauge is linear for normal operating conditions, the gause sensitivity at any particular anode voltage increases with magnetic field once the magnetic field is above that required to maintain stable operation. Further increases in magnetic field result in a maximum sensitivity being reached after which the sensitivity decreases. At relatively low anode voltages (1000 - 2000 volts), the maximum is relatively flat with the sensitivity changing little with B. The sensitivity

TABLE I

SENSITIVITIES OF MAGNETRON GAUGE AT AN AVERAGE PRESSURE OF 5.2×10^{-8} (TORR N_2)

(Sensitivity, $S = 1^+/P$ amp/Torr N_2)

Magnetic Field Strength B (Gauss)

Anode Voltage	400	500	600	700	800	900	1000	1100	1200	1300	1400	1500	1600	1700	1800	1900	2000
1000	.56 / .63	.42 / .50	.40	.30	.20	.25	.23	.17	.13	.115	.124	.19	.15 / .17	.15	.14	.14	.14 / .16
2000	1.22 / 1.42	1.62 / 1.95	1.66 / 1.70	1.35 / 1.43	1.41	1.21	1.04	.65	.612	.53	.49	.52	.51	.49	.49 / .55	.14	.14 / .16
3000	2.01	2.3 / 2.0	3.35 / 2.47	3.06	2.49 / 2.20	2.49	2.35	2.0	1.92	1.37 / 1.27	1.39	1.11	1.00	.98	1.01	.98	.98
4000	out	3.2 / 2.75	3.3 / 2.48	4.63 / 4.22	4.3	3.95	3.12	3.67	3.30	1.81	2.70	2.0	1.48	1.83	1.59	1.54	1.60
5000	out	3.2 / 4.13	3.75 / 4.45	4.68 / 5.43	6.18	5.81	5.34	4.32	5.25	4.0 / 4.5	4.0	2.9	3.1	2.7	2.8	2.2	2.1
6000	out	out	4.5	5.25 / 5.63	6.13 / 6.52	7.37	7.42	6.74	5.9	5.8	5.0	5.3	5.0	4.8	4.1	5.42	4.2
7000	out	out	5.81	5.8	6.2	7.37	8.5	8.32	8.02	5.9	6.3 / 6.7	6.5	6.35	6.23	5.93	3.60	3.0
8000	out	out	5.95 / 6.72	6.5	6.5 / 7.3	7.82	10.0	9.7	8.9	6.5 / 7.2	6.7	7.36 / 7.77	7.4	6.85 / 7.56	4.2	4.7	5.65

Where two values of sensitivity are given they represent the maximum and minimum values recorded during oscillations.

TABLE II

SENSITIVITIES OF MAGNETRON GAUGE AT AN AVERAGE PRESSURE OF 5.2×10^{-10} TORR

(Sensitivity, $S = i^+/P = i_{Ext}/i_{Ref} \times 4.5$ = amps/Torr N_2)

Anode Voltage	Magnetic Field Strength B (Gauss)																
	400	500	600	700	800	900	1000	1100	1200	1300	1400	1500	1600	1700	1800	1900	2000
1000	2.85	.43	.50	.50	.48	0.40	.37	.34	.31	.32	.36	.33	.31	.35	.35	.35 / .21	.32 / .18
2000	.63	1.02	1.20 / 1.03	1.65	1.79	1.70	1.02 / .12	1.20 / 1.02	1.37	.065 / .03	.05	.12 / .029	.16 / .038	1.06	.11	.18	.16
3000	.47	1.43	2.0	2.72	3.37	3.42	3.38	1.66 / .35	3.32	.36 / .17	2.64	.31 / .14	.31 / .12	.24 / .11	.14	.14	.16
4000	out	1.36	2.14	3.16	4.14	5.1	4.95	5.33	5.43	1.88 / .38	1.88 / .48	.50 / .31	.45 / .31	.49 / .26	.49 / .26	.57 / .28	.50 / .26
5000	out	.88	2.52	3.92	4.30	5.48	5.67	6.65	6.45	3.2 / 1.07	2.58 / .86	.71 / .51	.84 / .54	.66 / .47	6.0	5.8	.66 / .46
6000	out	out	2.25	4.08	5.21	5.72	6.60	6.70	8.68	8.0	8.28 / 7.78	3.68 / 1.22	.78 / .60	3.27 / .82	.88 / .65	.78 / .63	.92 / .59
7000	out	out	1.60	3.64	5.68	5.76	7.52	5.45	10.2	10.0	9.5	8.8 / 2.2	8.8 / 1.8	.86 / .74	4.0 / 1.0	3.8 / 1.0	8.3
8000	out	out	0.60	3.45	5.33	6.75	6.92	4.82	6.27	10.4	11.2	10.2	6.7 / 1.9	8.6 / 2.12	.96 / .79	1.15 / .79	3.8 / .78

Where two values of sensitivity are given they represent the maximum and minimum values recorded during oscillations.

97

TABLE III

SENSITIVITIES OF MAGNETRON GAUGE AT AN AVERAGE PRESSURE OF 2.7 x 10⁻¹¹ TORR

(Sensitivity, $S = 1^+/P = \dfrac{1 + \text{Exp}}{1 + \text{Ref}} \times 2.04$ amp/Torr N_2)*

Anode Voltage	Magnetic Field Strength B(Gauss)																
	400	500	600	700	800	900	1000	1100	1200	1300	1400	1500	1600	1700	1800	1900	2000
1000	.059 / .092	.15 / .167	.266 / .281	.298 / .313	.32 / .33	.286	.27	.227	.211	.16 / .194	.185	.176	.168	.149	.147	.14	.113
2000	.055 / .070	.20 / .215	.465	.65	.92	1.15	1.26	1.43	1.48	1.27 / 1.46	1.43	1.48	1.51	1.50	1.53	1.50	1.52
3000	.02	.019 / .022	.42	.81	1.15	1.42	1.82	2.15	2.38	2.61 / 2.96	2.93	2.97	3.12	3.16	3.18	3.22	3.23
4000	.02 / .021	.13 / .15	.51	.69	1.26	1.62	2.06	2.58	2.97	3.30 / 3.65	3.73 / 3.90	4.3	4.55	4.74	4.83	4.71	2.15 / 2.90
5000	.006 / .008	.013 / .015	.28 / .296	.725	1.09	1.69	2.09	2.70	3.18	3.95	4.5	4.83	5.37	6.00	6.19	6.20	6.70
6000	.007 / .009	.009 / .011	.017 / .018	0.50	0.97	1.57	2.13	2.77	3.37	4.16	4.85	5.36	5.86	6.34	6.90	7.55	7.73
7000	.021	.021	.104	.46	1.11	1.38	2.22	2.77	3.48	4.25	5.17	5.90	6.28	6.65	7.02	8.13	8.50
8000	.009 / .014	.007 / .011	.011 / .11	.18 / .40	.63 / .89	1.33 / 1.55	2.04	2.70	3.33	4.62	5.07	6.00	6.77	7.02	7.80	8.55	9.30

*Average reading Reference Gauge 5.5 x 10⁻¹¹ Amp. Slope of sensitivity curve 1.50 below 2 x 10⁻¹⁰ Torr N_2.
Therefore pressure = 2.7 x 10⁻¹¹ Torr N_2.

Where two values of the sensitivity are given they represent the maximum and minimum values recorded during oscillations.

98

TABLE IV

SENSITIVITIES OF MAGNETRON GAUGE AT AN AVERAGE PRESSURE OF 1.2×10^{-11} TORR
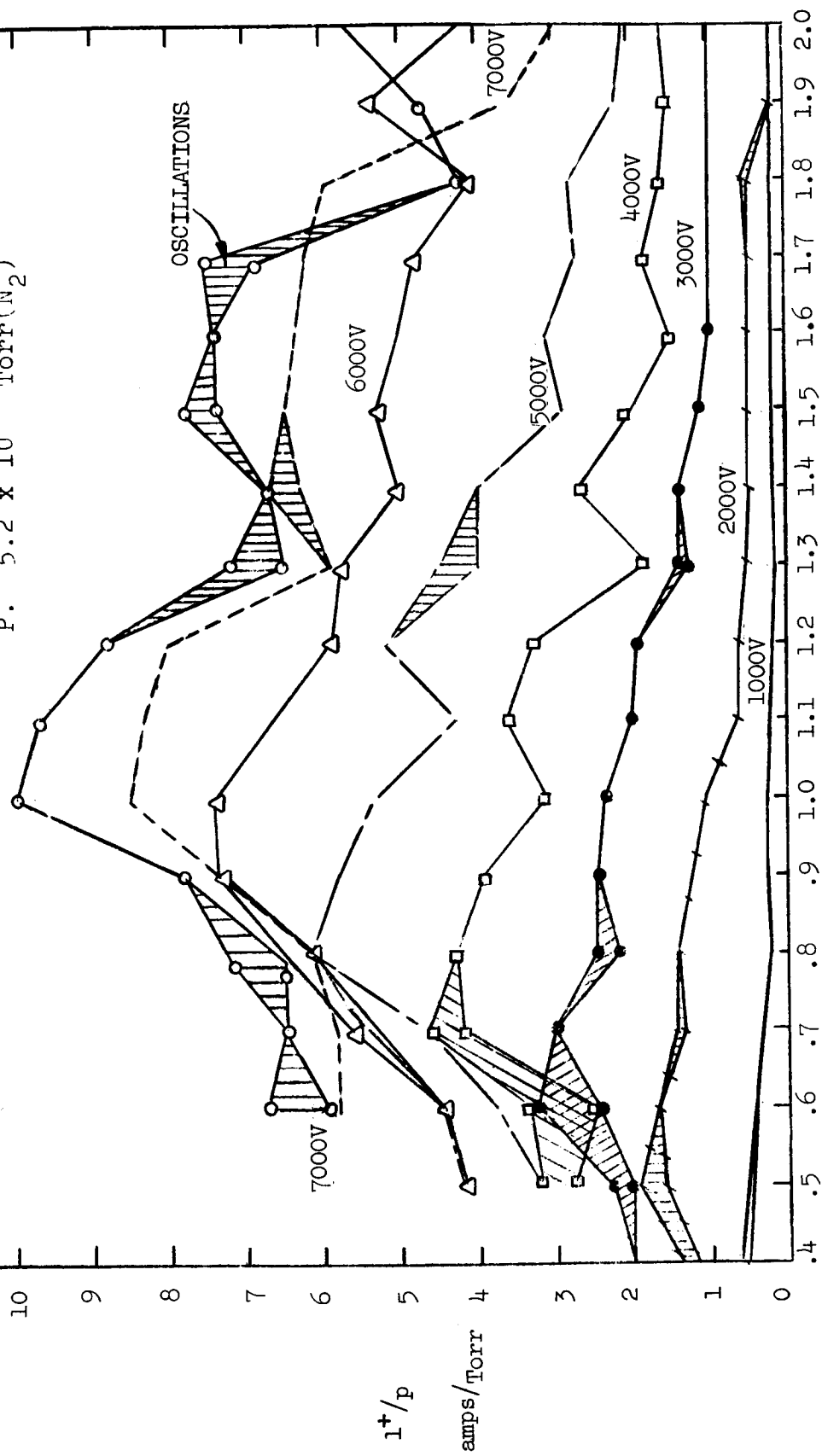
(Sensitivity, $S = \dfrac{1 + \text{Exp}}{P}$ amp/Torr N_2)

Magnetic Field Strength B (Gauss)

Anode Voltage	600	700	800	900	1000	1100	1200	1300	1400	1500	1600	1700	1800	1900	2000
1000	.124	.154	.165	.169	.164	.142	.134	.134	.143	.132	.120	.125	.109	.105	.096
2000	.141	.227	.363	.507	.595	.689	.750	.754	.754	.740	.715	.685	.675	.664	.684
3000	.126	.265	.386	.550	.768	1.00	1.12	1.55	1.68	1.73	1.58	1.61	1.64	1.63	1.61
4000	.130	.200	.412	.578	.787	1.02	1.31	1.81	2.07	2.43	2.66	2.79	2.90	2.99	3.08
5000	.094	.214	.313	.619	.786	1.02	1.29	2.03	2.50	2.84	3.14	3.55	3.83	3.97	4.07
6000	.085	.197	.349	.779	1.05	1.33	1.75	n.d.	n.d.	n.d.	n.d.	n.d.	n.d.	n.d.	n.d.
7000		.173	.429	.596	1.06	1.32	1.66	n.d.	n.d.	n.d.	n.d.	5.22	5.25	6.12	6.46
8000			.344	.664	1.02	1.44	1.84	2.31	2.64	2.85	3.58	4.05	4.60	5.10	6.30

n.d. = not measured

FIG. 12

EFFECT OF MAGNETIC FIELD AND ANODE VOLTAGE ON MAGNETRON SENSITIVITY

P. 5.2×10^{-8} Torr(N_2)

I^+/p

amps/Torr

B. (Kilogauss)

100

FIG. 13

EFFECT OF MAGNETIC FIELD
AND ANODE VOLTAGE ON
MAGNETRON SENSITIVITY

$P = 5 \times 10^{-10}$ Torr

8000V

6000V

7000

5000V

4000V

3000V

2000V

1000V

REGION
OF
OSCILLATIONS

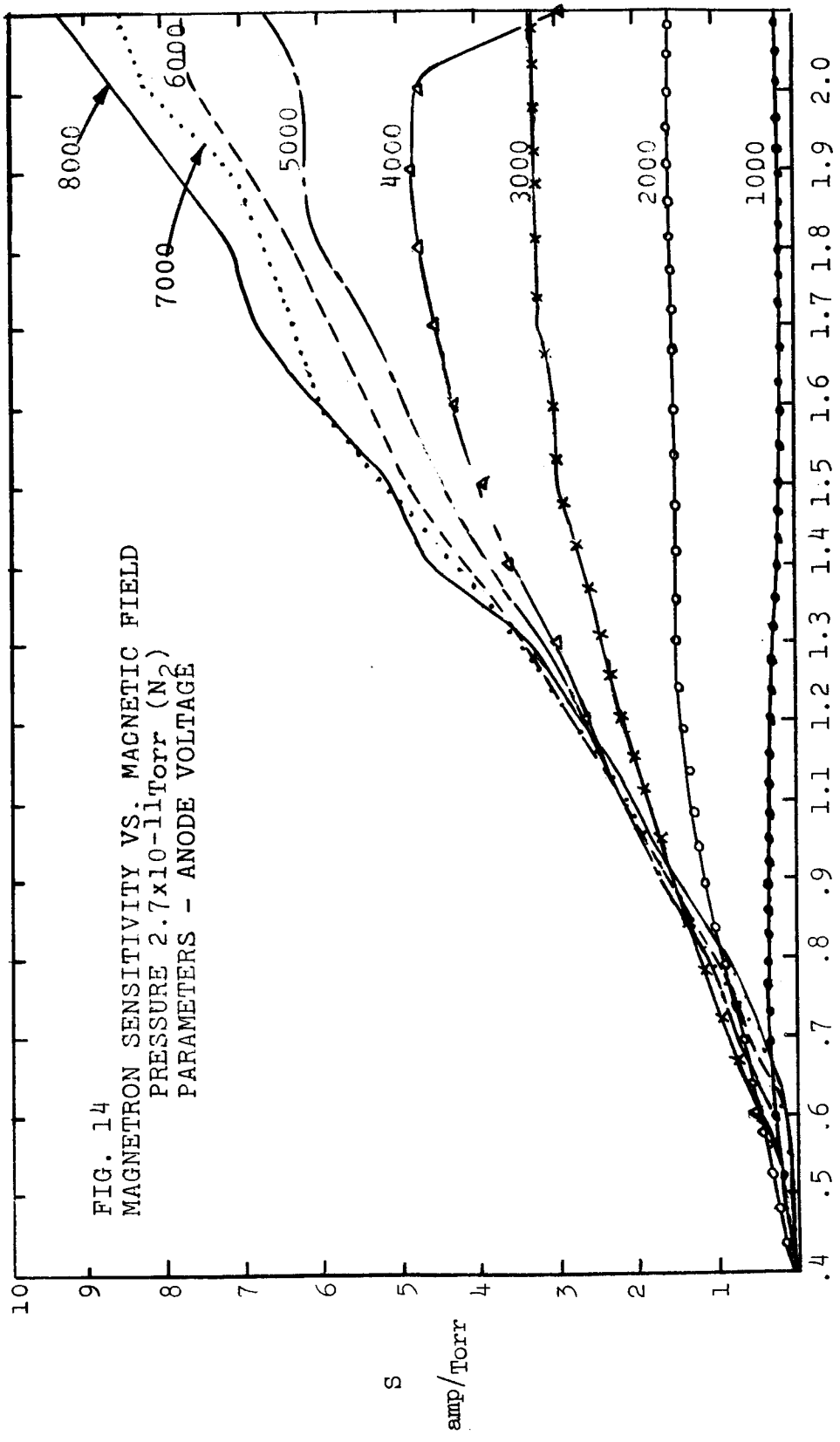$\frac{i^+}{P}$

amps/Torr

MAGNETIC FIELD B (KILOGAUSS)
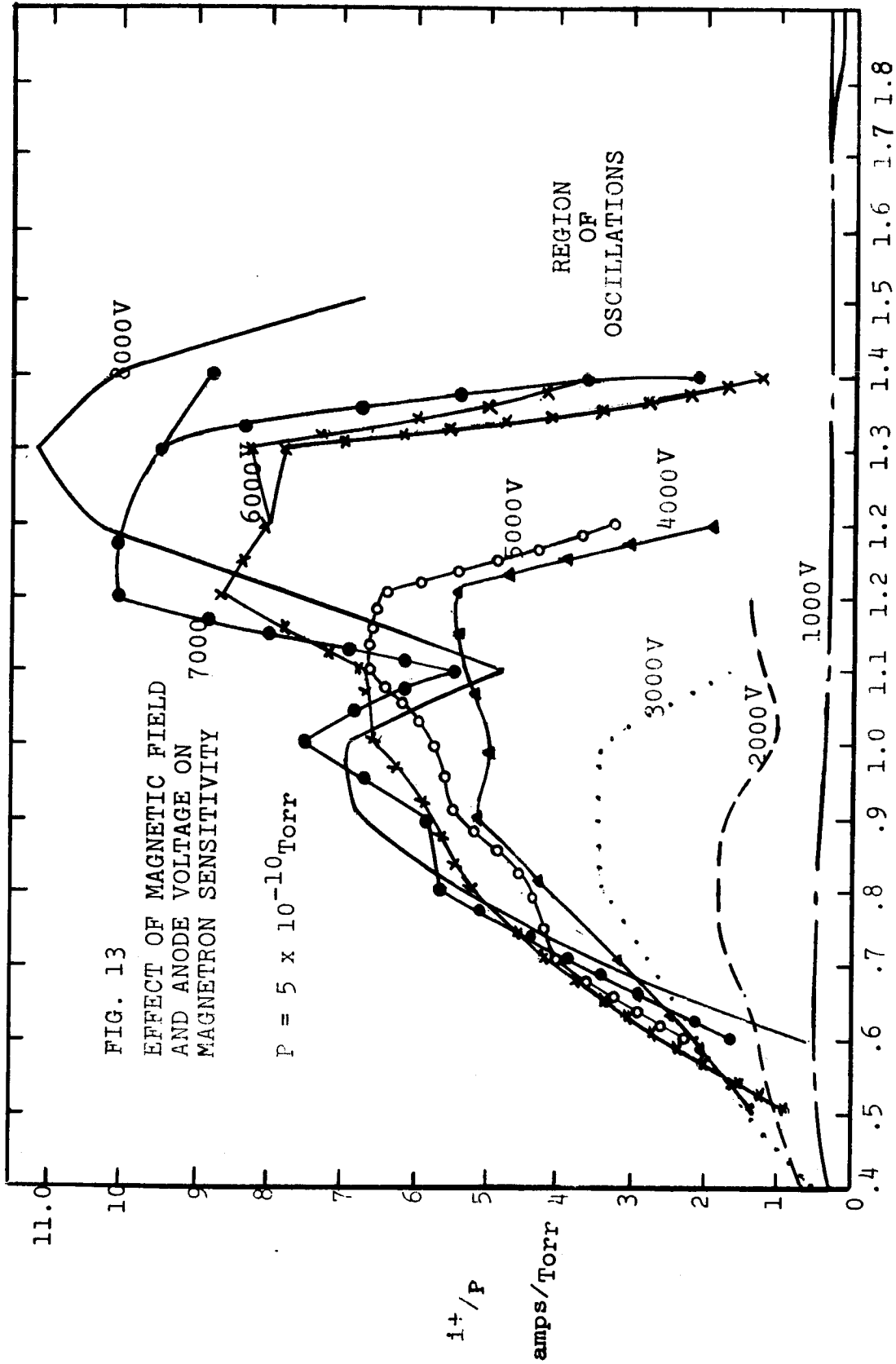
FIG. 14
MAGNETRON SENSITIVITY VS. MAGNETIC FIELD
PRESSURE 2.7×10^{-11} Torr (N_2)
PARAMETERS - ANODE VOLTAGE

MAGNETIC FIELD (KILOGAUSS)

S amp/Torr

102

also increases with anode voltage and the results presented in Figs. 12 and 13 suggest that there is an upper limit or envelope for the sensitivity at values of B less than those for maximum sensitivity at any particular anode voltage. This upper limit or asymptote is approximately linear with magnetic field. The slope appears to be somewhat higher at 5×10^{-8} than at 5×10^{-10} Torr. However, this may be associated with the fact that the gauge was much noisier at 5×10^{-8} Torr at low values of B than at 5×10^{-10} Torr. This contrasted sharply with the situation at higher magnetic fields after the maximum sensitivity values had been reached. At 5×10^{-8} Torr the sensitivity dropped relatively slowly and there were few conditions where noise and oscillations were noted. At 5×10^{-10} Torr, the sensitivity decreased abruptly after the maximum and there were many conditions where the sensitivity oscillated as indicated by the output from a Keithley 410 electrometer. There were, in addition, a few isolated conditions at high magnetic fields where the gauge returned to relatively high sensitivity. Some of the aspects of this oscillatory behavior will be described later under Section 1.3.

The above results follow the same general pattern as those of Redhead[11]. The high sensitivity region at low magnetic fields corresponds to Redhead's State I and the lower sensitivity at high magnetic fields corresponds to State II. The above results pertain to pressures above 2×10^{-10} Torr. At lower pressures where the gauge is non-linear, the general nature of the curves appears to change drastically (Fig. 14). The rate of increase of sensitivity with magnetic field is much lower than at the high pressures.

At 2000 volts and 3000 volts the sensitivity is constant for a large range of values of the magnetic field strength. There is also some evidence of a flat maximum in

sensitivity being achieved at 700 gauss and 1000 volts. The general nature of the curves in Fig. 14 suggests that at the higher anode voltages, e.g., 6000 - 8000 volts, magnetic fields in excess of 2000 gauss would produce a range of constant sensitivity. It is not unlikely that even higher magnetic fields would give decreased sensitivity. The effect of magnetic field and pressure on the sensitivity at an anode voltage of 5000 v is shown in Fig. 15. At 5×10^{-10} Torr, the sensitivity is a maximum at about 1100 gauss. (Note that at 5×10^{-8} Torr the maximum at 5000 volts was at about 800 gauss. See Fig. 4.) At both 2.7×10^{-11} Torr and 1.2×10^{-11} Torr no maximum is shown. The variation in sensitivity is approximately linear with magnetic field at 2.7×10^{-11} Torr and 1.2×10^{-11} Torr. The slope decreases with pressure.

It should also be noted (Fig. 13) that at a magnetic field strength of, say, 1500 gauss the gauge sensitivity is _greater_ at 2.7×10^{-11} Torr and 1.2×10^{-11} Torr than it is at 5×10^{-10} Torr. Similarly, at 1500 gauss and 5000 volts the sensitivity is greater at 2.7×10^{-11} Torr than at 5×10^{-8} Torr.

If it is assumed that the number of magnetically trapped electrons (N) is proportional to the sensitivity, the above results indicate that at the specific conditions taken above, N is lower at the higher pressures where the input _rate_ of electrons from the volumetric ionization process is greater. In general, it would be expected that the higher input rates would tend to add to rather than subtract from the number of trapped electrons. In this situation, one is tempted to seek an explanation in terms of the r-f oscillations which have only been detected at the higher pressures (Redhead).[11] It might be assumed that these oscillations effectively reduce the number of trapped electrons. However, as is shown by
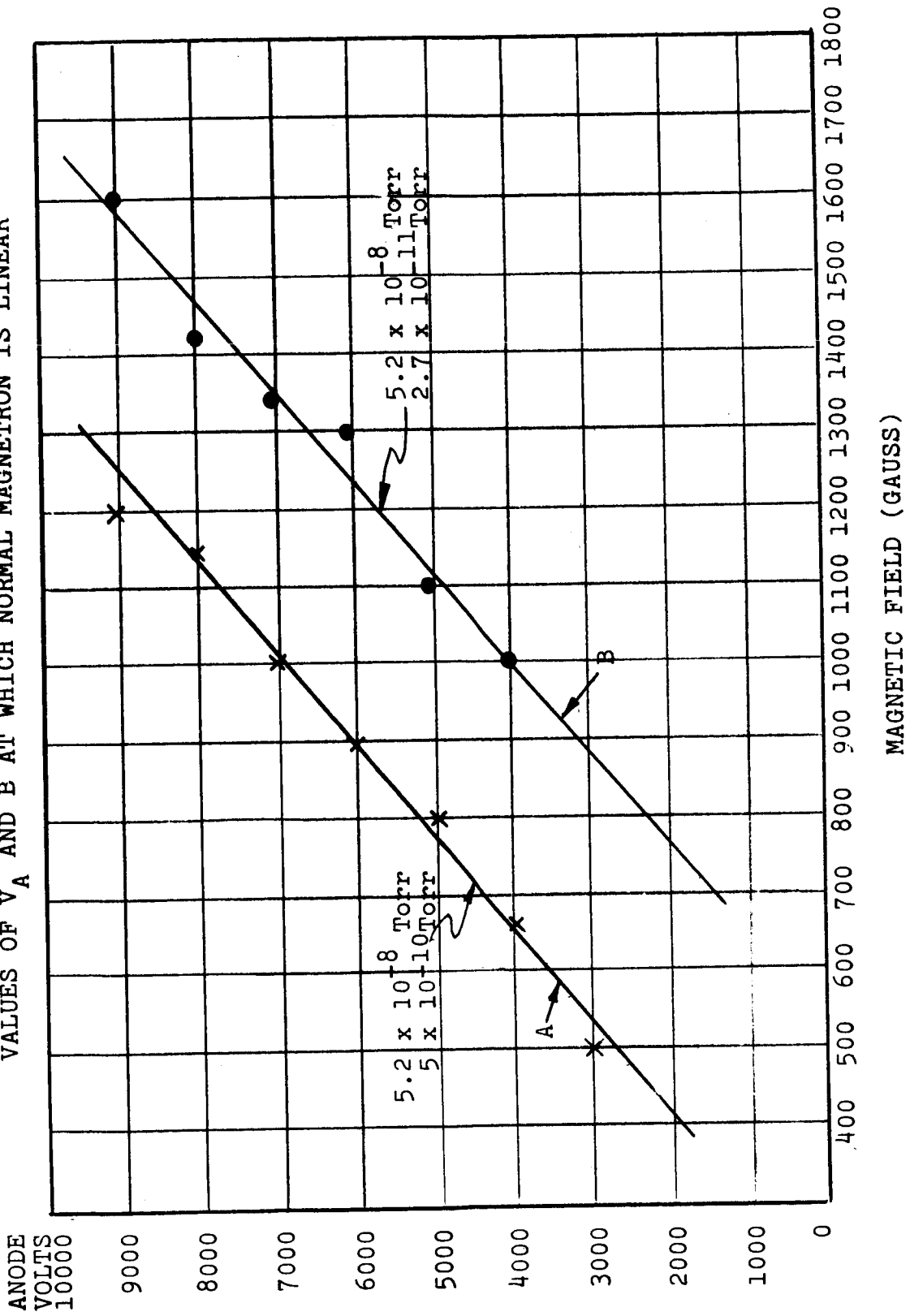
FIG. 15
EFFECT OF MAGNETIC FIELD AND PRESSURE
ON MAGNETRON SENSITIVITY

MAGNETIC FIELD (KILOGAUSS)
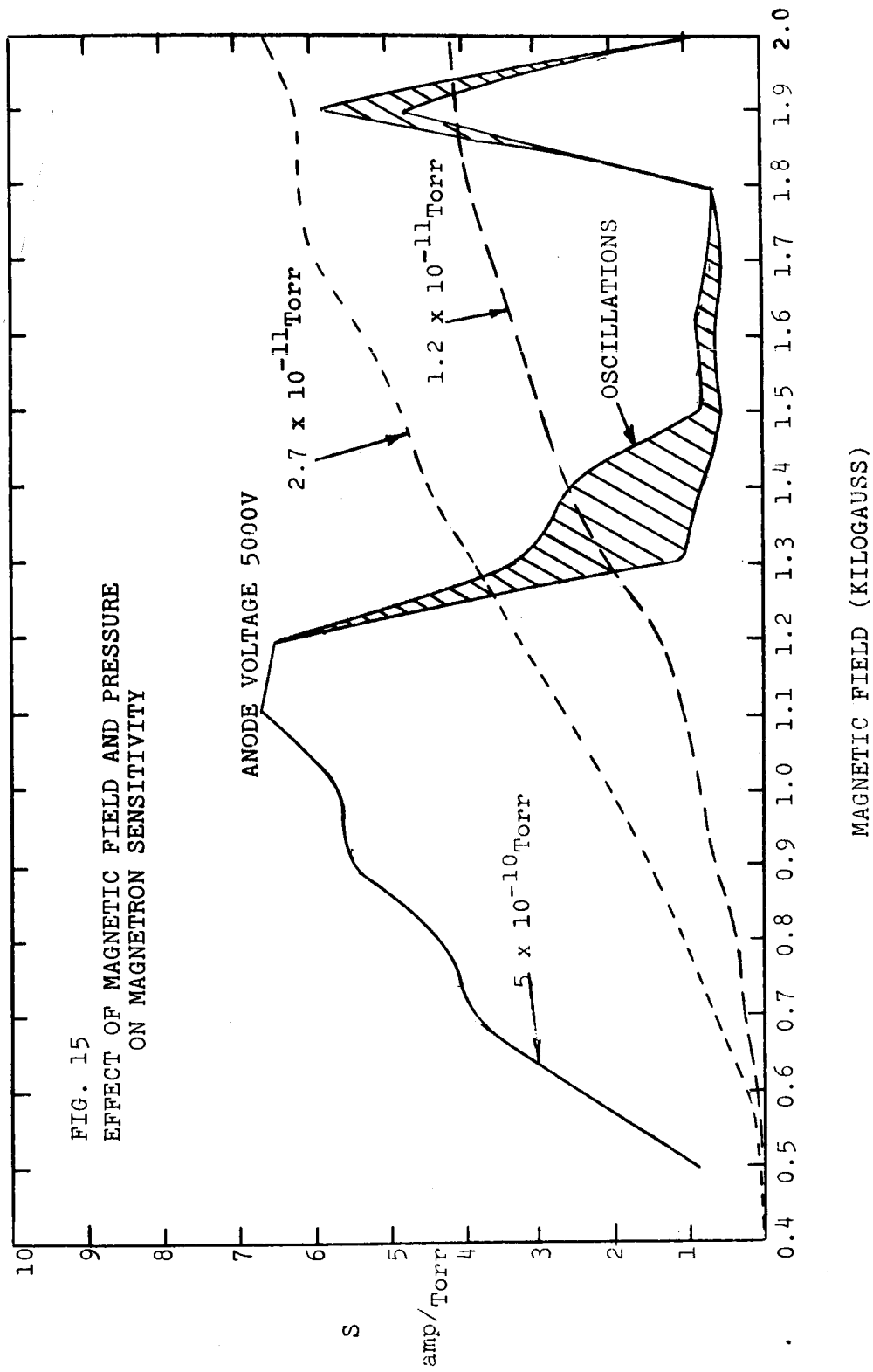
Redhead,[10] it is likely that the r-f oscillations are associated with the rotation of the electron cloud. Hence, at the same values of Va and B it is more difficult to see why increasing the electron production rate (and loss rate) by increasing the pressure should cause oscillations to develop in the electron cloud. The simpler explanation that the oscillations are dependent only on V_A and B and essentially independent of pressure - above 2×10^{-10} Torr - seems more acceptable. Further work should be carried out to measure the frequency and relative intensity of the oscillation under conditions of equal gauge sensitivity. It may well be that strong r-f oscillations do in fact exist at, say, 2.7×10^{-11} Torr, 1500 gauss and 5000 volts. It is, nevertheless, possible that the ion current is far from constant at any pressure and that there are growth and decay processes continually taking place in the electronic space charge. At high pressures (above 2×10^{-10} Torr), these processes which are probably associated with surface reactions at the cathode and anode possibly initiate or produce distortions in the electron cloud which result in stable r-f oscillations. At low pressures, the surface controlled initiation processes may be too small to produce oscillatory behavior.

From the data presented in Tables I through IV it is a simple matter to determine those sets of conditions at which the gauge has the same sensitivity at various pressure. That is, the conditions under which the gauge is linear. The results are presented in Fig. 16.

The data associated with line A in Fig. 16 where obtained by plotting those conditions at which the sensitivity at 5.2×10^{-8} equal that at 5×10^{-10} Torr. Line B was for conditions where the sensitivity at 5.2×10^{-8} Torr equaled that at 2.7×10^{-11} Torr. Along both line A and line B,

FIG. 16

VALUES OF V_A AND B AT WHICH NORMAL MAGNETRON IS LINEAR

ANODE VOLTS

MAGNETIC FIELD (GAUSS)

5.2 x 10^{-8} Torr
2.7 x 10^{-11} Torr

5.2 x 10^{-8} Torr
5 x 10^{-10} Torr

A

B

107

the sensitivities increased with anode voltage (and magnetic
field). Line A is approximately parallel to line B, and
at any anode voltage, line B is located at a magnetic field
strength which is approximately 350 gauss higher. The
normal operating conditions for the 552 magnetron gauge are
1000 gauss and 5000 volts. This lies on line A. The data
of line B then suggest that at, say, 3000 volts and 1100
gauge, the magnetron gauge would be linear down to at
least 2.7×10^{-11} Torr. This requires that the cathode
current vary monotonically over the pressure range
5.2×10^{-8} Torr - 2.7×10^{-11} Torr. A number of pressure
variation tests were carried out at 3000 volts and 1100
gauss and also at 4800 volts and 1250 gauss. The results
for 3000 volts and 1100 gauss are presented in Fig. 17.
The best line through the data gives a slope of 0.90 down
to approximately 1×10^{-10} Torr. At lower pressures there
is evidence that the slope increases to approximately 1.8.
The data for the lowest two pressures were taken from
separate experiments as recorded in Tables III and IV.
The slope obtained in this work in unusual in that it is
less than one. It is possible that the Reference gauge
changed from a slope of 1.0 to something less, but this is
unlikely. However, the decrease in sensitivity from 2.15
amps/Torr at 2.7×10^{-11} Torr to 1.0 at 1.2×10^{-11} Torr
(see Tables III and IV) indicates that operation in State II
is not likely to give high sensitivity performance at very
low pressures. The data taken at 4800 volts and 1250 gauss
also gave a slope of 0.90. Interpolating from the data in
Tables III and IV indicated that within experimental error
the slope remained constant down to the lowest pressure
measured, 1.2×10^{-11} Torr. However, a comparison of the
data in Tables III and IV at higher anode voltages and
magnetic fields shows that there is a decrease in sensitivity
at the lower pressures. This is also clearly shown in Fig. 15.

FIG. 17

NORMAL MAGNETRON CATHODE CURRENT
VS. PRESSURE (3000v, 1100 GAUSS)
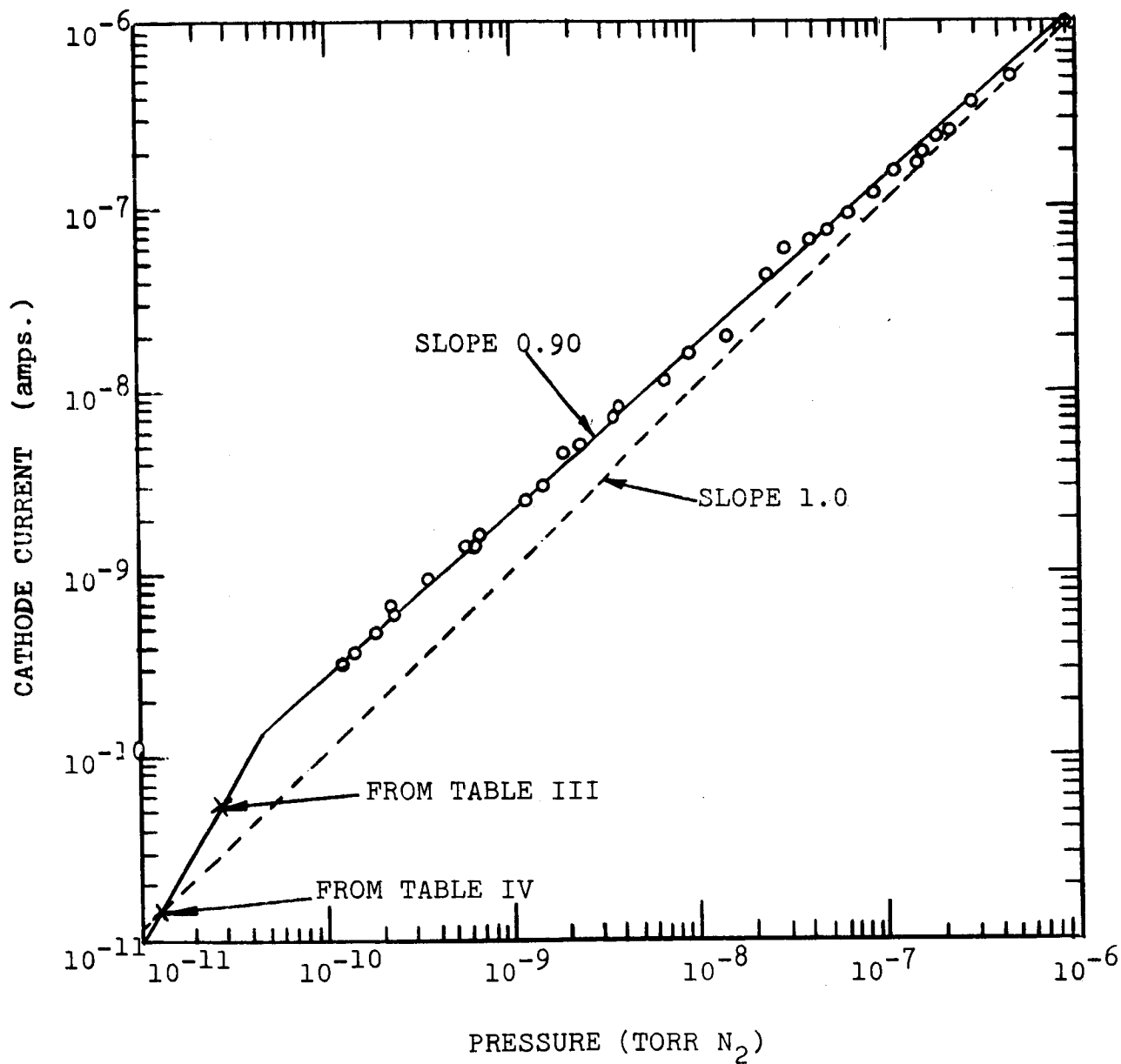
The data at 4800 volts and 1250 gauss showed considerably more scatter than the data of Fig. 17. Some of the scatter obtained in the early part of the experiment was found to be affected by the R, L, C of the electrometer circuit. For instance, at some specific pressures, particularly in the range 6×10^{-10} Torr to 2×10^{-9} Torr, a 410 Keithley electrometer would oscillate between specific values. A study of some of this oscillating behavior indicated that several types of oscillatory behavior may be observed when measuring pressures in State II. These are discussed more fully in the section below.

1.3 OSCILLATORY BEHAVIOR

Redhead[11] has given an extensive description of the
r-f oscillations which exist in the magnetron gauge when
operated in State II. Redhead's results on the effects of
magnetic field strength and anode voltage in the frequency
have been confirmed in the present program. The specific
frequencies have been observed in a number of ways including
field intensity meters, tuned r-f receivers and by means
of a high frequency oscilloscope. The coupling may be
carried out in a number of ways, including direct coupling
to the auxiliary cathode on main cathode, capacitive
coupling to the anode or by means of a small antenna
supported axially near the gause anode.

One of the aims of the present program was to measure
the variation in intensity of the r-f signal as a function
of pressure. Redhead has reported that the r-f oscillations
were not detected below 2×10^{-10} Torr. A number of attempts
were made to measure the effect of pressure on the signal
intensity but with little success. Using a tuned r-f
receiver and a signal intensity meter some data (Fig. 18)
were obtained which tended to suggest that the maximum signal
intensity at any pressure decreased as the pressure decreased.
At no time was an r-f signal detected below 2×10^{-10} Torr.
However, the data showed considerable scatter and cannot be
regarded as more than minimal evidence. In this part of the
work, experimental procedures were greatly hindered by an
exceedingly strong 80 Mc/s signal from an external source
beyond our control. The metal system Helmholtz coils,
electrical and cooling water systems all acted as antennae
for the signal. Attempts to filter the signal and its
harmonics were not successful and it was beyond the limita-
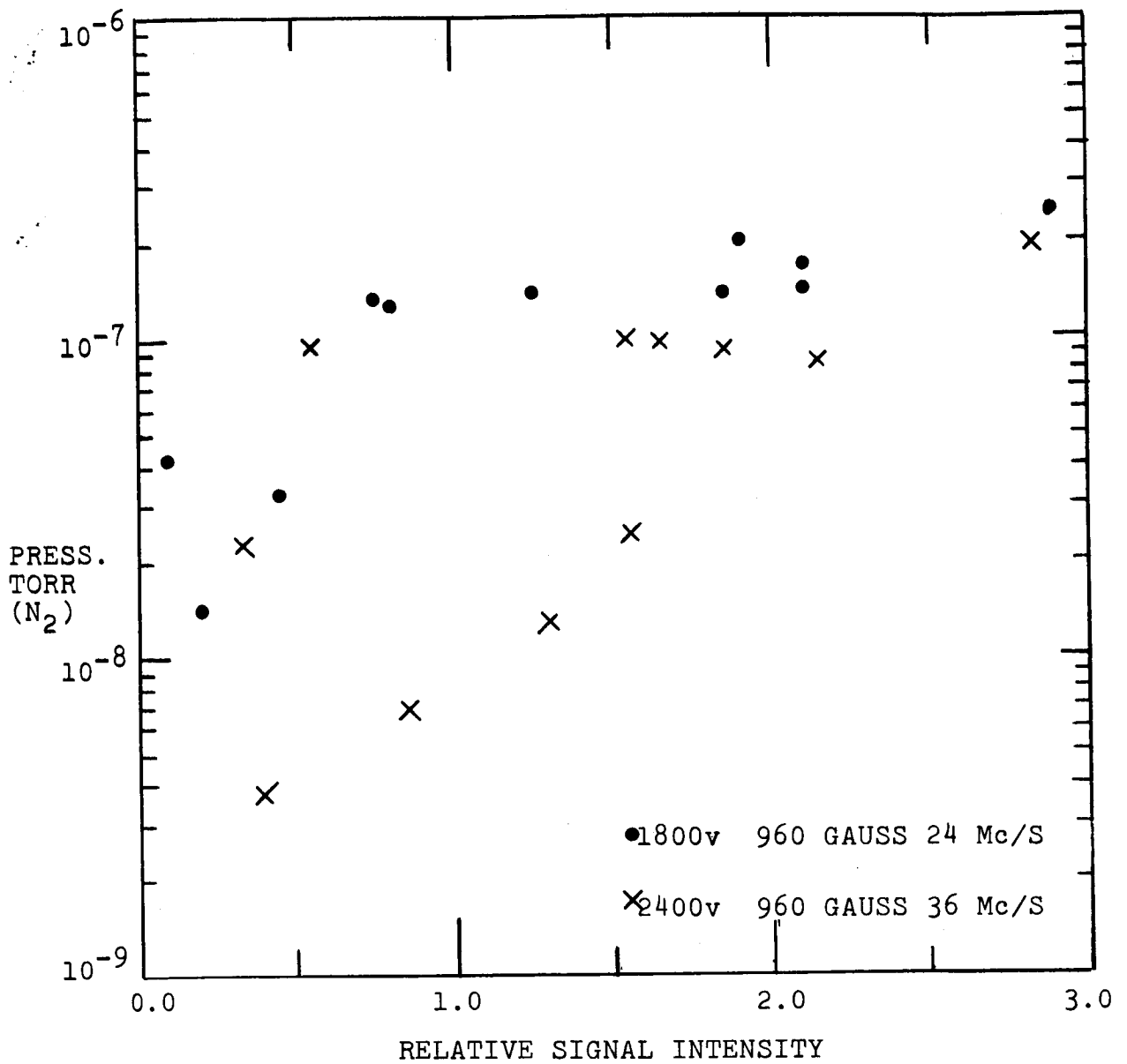tions of the program to install adequate shielding.

111

FIG. 18
EFFECT OF PRESSURE OF INTENSITY ON r-f SIGNAL
FROM MAGNETRON GAUGE

When operating in State II a different type of oscillatory behavior was noted. In this case, electrometer oscillations would develop above and below previous mean steady state values. The frequency was on the order of 0.1 - 1.0 cycles/sec. The period of the oscillation increased with decreasing pressures. These types of oscillations were often evident with an electrometer such as a Keithley 410. If the input capacitance of the electrometer was reduced, as with a Keithley 600 or 610 operating in the fast mode, oscillations did not occur. The R-C constants of the entire electrometer circuit should be such as to eliminate such low frequency oscillation. The use of a high quality vacuum capacitor to shunt high frequency components of the cathode current to ground is recommended.

1.4 EFFECTS OF ULTRA-VIOLET RADIATION

A convenient method of decreasing the starting time of
a magnetron gauge at low pressures is by irradiating the
gauge with ultra-violet. The mechanism by which photo-
radiation assists in initiating the build up of the discharge
has not been determined. One, or a combination, of the follow-
ing processes may play a part.

   i) Photo-emission of electrons from cathode.

   ii) Photo-desorption of neutral gas species previously
      adsorbed on gauge elements, walls, etc.

   iii) Photo-ionization of a neutral, free or absorbed gas
      species.

Experimentally, it is not easy to differentiate between
these processes and other effects - especially thermal de-
sorption effects associated with the radiation. However,
if the non-linearity of the magnetron gauge is caused by
a deficiency in the number of electrons in the discharge,
an increase in the number of electrons emitted by the
cathode should tend to make the gauge more linear. Bryant[7]
has shown that a cesiated magnetron gauge has a non-linear
characteristic, which has a lower slope than an uncesiated
gauge. Presumably, lowering the work function of the
cathode results in at least a partial increase in the number
of desired electrons in the discharge. As a practical
procedure for low pressure work the use of cesium has
obvious drawbacks. Another possibility of testing the
electron deficiency thesis appeared to lie in attempting
to stimulate photo-emission by the use of ultra-violet.
The radiation from a low-pressure mercury lamp, was shone
through the sapphire window of the experimental gauge.
The output of the mercury lamp peaked at 2537 $\overset{o}{A}$ and the
sapphire window had a limit of transmission of about
1400 $\overset{o}{A}$ (9 ev). Typical results were as follows: At a

pressure of 3.7×10^{-11} Torr the output current of the gauge rapidly rose from 6.8×10^{-11} amps to 9.8×10^{-11} amps. Within 5 minutes it decreased from this value and leveled off at 7.5×10^{-11} amps. It remained constant at this value for as long as the u.v. lamp was on (2 hrs.). However, this 10% increase in the output of the magnetron gauge was too small to be attributed to an increase in gauge sensitivity. Even though this was a steady increase in output current, it is more likely that it was caused by thermal desorption of gas which was temperature and not time dependent. In any case, even if it were all attributed to an increased gauge sensitivity, the increase is only 12% of that required to give a linear gauge. More work using a system in which a concentrated beam of ultra-violet radiation is focussed on specific areas within the gauge is recommended. In this work, temperature variations should be investigated to alter the effects of thermal and photodesorption of physically adsorbed gas. It is, however, likely that the magnetron discharge is already an efficient source of ultra-violet and X-ray radiation so that external sources may only have secondary effects.

1.5 ELECTRON INJECTION

As shown in Fig.10, the experimental magnetron was de-
signed so that an external filament could be used to inject
electrons through a small hole in one of the cathode end
plates and along the lines of magnetic flux. The hole in
the cathode end plate was 1/8 in. diameter and its center
was located 1/3 of the distance from the surface of the
central cathode rod to the anode diameter. The tungsten fila-
ment was coiled to an O.D. of about 0.08 in. In order to
prevent electrons moving directly to the cathode, it was
first necessary to determine the bias required on the
filament supply to prevent this. This was done with the
magnetron gauge not operating (Va = 0) but with the range
of B fields planned for experimental use. With the filament
at 1050°C, it was found that a bias of 4 volts was sufficient
to reduce the electron current to the cathode to less than
5×10^{-14} amps. The gauge was then degassed by electron
bombardment and the temperature of the filament raised to
1350°C for about 1 hour. The output current of the ex-
perimental gauge was then measured with the filament at
1050°C and biased 4 to 6 volts above ground. At a pressure
of 3×10^{-11}, these conditions caused an increase in the
cathode current of about 10%, but once again it is doubtful
whether this current could be attributed to an increase in
gauge sensitivity. Even though very careful degassing
procedures had been used, the magnitudes of the pressure
changes in the experimental and reference gauges were
commensurate with increased thermal desorption rates in the
gauge.

Since the electric fields within an operating magnetron
gauge are not known, it is difficult to inject electrons
into the discharge. If the electrons do not have sufficient
energy, they will not penetrate to the discharge. If they

have too much energy, they will pass through the discharge to the opposite cathode plate. In a later model of an experimental gauge, a small accelerating grid was placed between the filament and the cathode plate. It is anticipated that this may allow more control and perhaps permit adequate testing of electron injection techniques. It may be advantageous to place holes in both cathode plates so that electrons with excess energy would not be collected by the back cathode plate but would move on to a dummy cathode behind the hole in the true cathode.

1.6 PHOTOGRAPHIC STUDIES

If a normal magnetron gauge is allowed to operate at relatively high pressure - say 10^{-4} or 10^{-5} Torr - a characteristic purple glow is clearly visible within the gauge. In a darkened room, this glow is still discernible at much lower pressures, particularly if 10 or 15 minutes is allowed for eye accommodation. It was the aim of this part of the program, to attempt to determine the distribution of the discharge within the gauge by photographic techniques. It was hoped that not only would it be possible to map the discharge within the linear region of the gauge but that the techniques could be made sufficiently sensitive so that the distribution below 2×10^{-10} Torr could also be determined.

The experimental magnetron gauge, Figure 10, was assembled so that one of the cathode end plates could be viewed directly through the sapphire window in the flange of the magnetron chamber. A radial slot (1 mm wide) was cut in the cathode end plate from the outer edge to within 1.4 mm of the central cathode rod. A mirror was also mounted at approximately 45 degrees to the magnetron axis outside the anode screen. However, this mirror was of limited usefulness in measuring the axial distribution of the glow because of parallax problems associated with the relatively small sapphire window. It was experimentally easier to photograph the axial distribution directly through the glass of the reference gauge, a NRC 552 gauge.

Most of the photographs were taken with a Linhof Technika Camera, using Xenar 1:4.5/150 lens. For the major fraction of the work, Polaroid Type 57 film (ASA 3000 speed) was most suitable. At the lower light levels, Polaroid Type 410 (ASA speed 10,000) was also used. In general, the camera was operated with a lens opening of f 4.5 at approximately 7 in.

from the magnetron assembly. The resultant image had a magnification of 1.47. When taking photographs of the experimental magnetron, the shutter mechanism failed to operate in the high magnetic fields associated with the Helmholtz pair. However, time exposures were generally necessary so that it was entirely satisfactory to use plate slides to give the desired exposure.

The main part of the experimental work was devoted to the determination of the effects of pressure, magnetic field strength, anode voltage and gas composition in the shape, location and intensity of the discharge. The major results are summarized below.

A representative photograph of the radial variation of the intensity of the discharge is reproduced in Fig. 19. The figure is a view of the discharge at 4.2×10^{-6} Torr through the radial slot in the cathode end plate. The slot extended from the anode to within about 0.07 in of the surface of the central cathode rod. The photograph shows that the glow extends from the surface of the cathode rod to about half way out to the anode. The intensity appears to be relatively constant to approximately $1/2 \ (r_a - r_c)$ and it then drops rapidly to a negligible value. Photographs of the discharge as seen through the perforated anode were used to obtain an estimate of the axial distribution of the discharge. By taking a series of photographs at slightly different angles, various sections through the discharge could be photographed. This series of photographs, when taken in conjunction with the radial photographs, has suggested that the distributions within the gauge are as shown in Fig. 20.

The discharge extends out from the cathode rod to about half the anode distance. The axial length of the discharge is considerably less than the distance between the cathode end

SLOT WIDTH

ANODE

LENGTH
OF SLOT
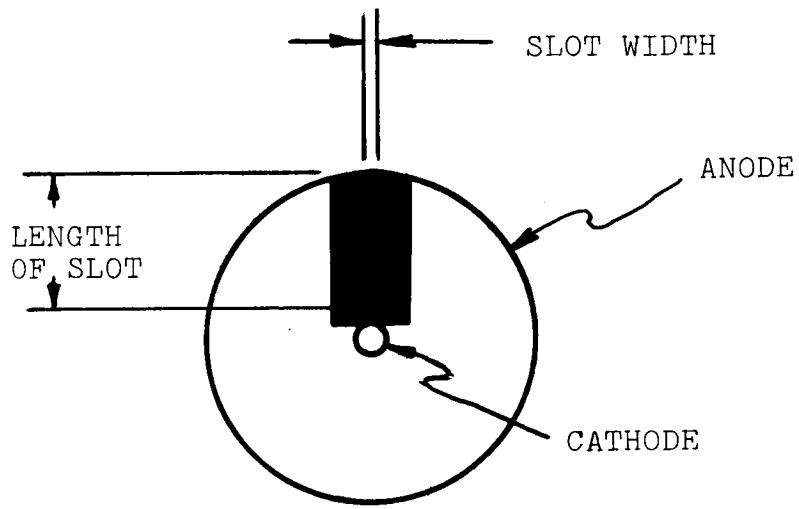
CATHODE

MAGNIFICATION 1.47

FIG. 19

VIEW OF DISCHARGE THROUGH RADIAL SLOT
IN CATHODE OF MAGNETRON GAUGE.

GAUGE CONDITIONS: ANODE: 4800V
MAGNETIC FIELD 1000 GAUSS
PRESSURE 4.2 x 10^{-6} TORR

ANODE

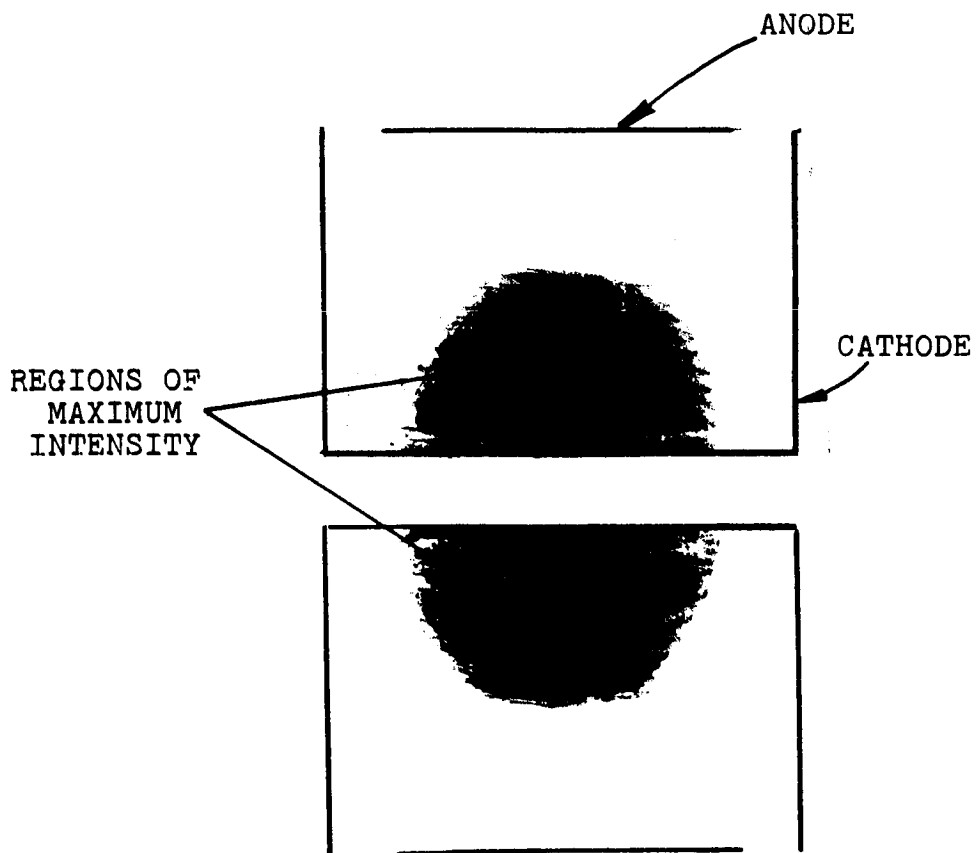CATHODE

REGIONS OF
MAXIMUM
INTENSITY

FIG. 20

DISTRIBUTION OF PHOTO-RADIATION FROM
MAGNETRON GAUGE

plates. That is, the discharge does not appear to extend to
the cathode end plates. The general shape of the discharge
resembles that of a doughnut around the cathode rod. There
was some evidence that the maximum light intensity was not
at the cathode rod but somewhat removed from it, as shown
in Figure 20. However, this increase in intensity was
relatively small. The axial length of the discharge appears
greatest at the cathode rod so that the radial sections
appeared to give an intensity which was either constant
out to $1/2$ $(r_a - r_c)$ or at a maximum at the surface of
the cathode rod.

The above results were obtained with the gauges operating
in Argon at 4.5×10^{-8} Torr (N_2) at normal conditions - anode,
4800 volts; magnetic field, 1000 gauss. The effects of
variations in pressure, magnetic field, anode voltage and
gas composition are summarized below.

Photographs obtained of 4.5×10^{-7} Torr, 4.5×10^{-8} Torr
and 4.5×10^{-9} Torr indicated that the intensity of the dis-
charge was directly proportional to the cathode current.
Quantitative densitometer measurements of the intensity of
the discharge were not made but by varying exposure times
at different pressures and using visual comparison of the
photographic density, a fair estimate of the degree of
proportionality could be obtained. Future work would be
greatly facilitated by densitometer measurements. In order
to obtain a reasonable picture of 4.5×10^{-8} Torr, an
exposure time of 10 minutes was required with the 3000 speed
film. Unfortunately, no photographs of the discharge
were obtained in the non-linear region below 2×10^{-10} Torr,
even though exposure times in excess of 12 hours with
10,000 speed were used. Unfortunately, the films used lose
reciprocity for exposure times greater than about 8 hours
so that larger exposure times are not beneficial.

The effect of varying the anode voltage was investigated at two levels of magnetic field - 1000 gauss and 500 gauss. The pressure was 4.5×10^{-8} Torr and the gas, argon. In order to compare the results, an arbitrary scale has been used to estimate and specify the intensity. A range of 1 through 10 was used for 10 minute exposures of 3000 speed film. Intensity 1 was barely discernible - and 10 was complete exposure of the film. Intensities outside this range were obtained with exposure times other than 10 minutes.

In some instances, considerable variations in film sensitivity were noted from pack to pack. In general, fresh packs were used for each series of experiments and there was then good consistency within a series. Where comparison between series was required, the estimated sensitivities were normalized so that intensities at 5000 volts and 1000 gauss were consistent. The results have been summarized in Table V. The distance which the discharge extends out from the cathode is specified in terms of R - the fraction of the cathode to anode distance from which light is emitted.

TABLE V
EFFECT OF ANODE VOLTAGE (V_A) VARIATIONS
ON INTENSITY OF DISCHARGE IN ARGON

Pressure (Torr N_2)	V_A (Volts)	B (Gauss)	i^+Exp. (Amps)	R	Relative Intensity
4.5×10^{-8}	8000	1000	7.4×10^{-7}	.53	15
	7000	1000	6.5×10^{-7}	.55	12
	6000	1000	5.0×10^{-7}	.51	9
	5000	1000	3.6×10^{-7}	.52	7.5
	4000	1000	3.1×10^{-7}	.52	3
	3000	1000	1.5×10^{-7}	.36	1.2
	4800	500	1.9×10^{-7}	.48	7.5
	4500	500	1.9×10^{-7}	.54	12.0
	4000	500	1.5×10^{-7}	.53	9.0
	3000	500	1.2×10^{-7}	.51	6.0
	2000	500	1.0×10^{-7}	.55	6.0
	1000	500	2.5×10^{-8}	nd.	.6

In Figure 21 an attempt has been made to estimate the
variation of the light intensity as a function of the radial
position. There appears to be a rapid decrease in intensity
at about half the radial distance to the anode. Increased
anode voltage resulted in higher intensities but this
increase was greatest at the cathode. At 5000 and 6000
volts, the intensity appeared to be relatively constant
for a considerable fraction of the distance out from the
cathode. The results obtained on varying the magnetic
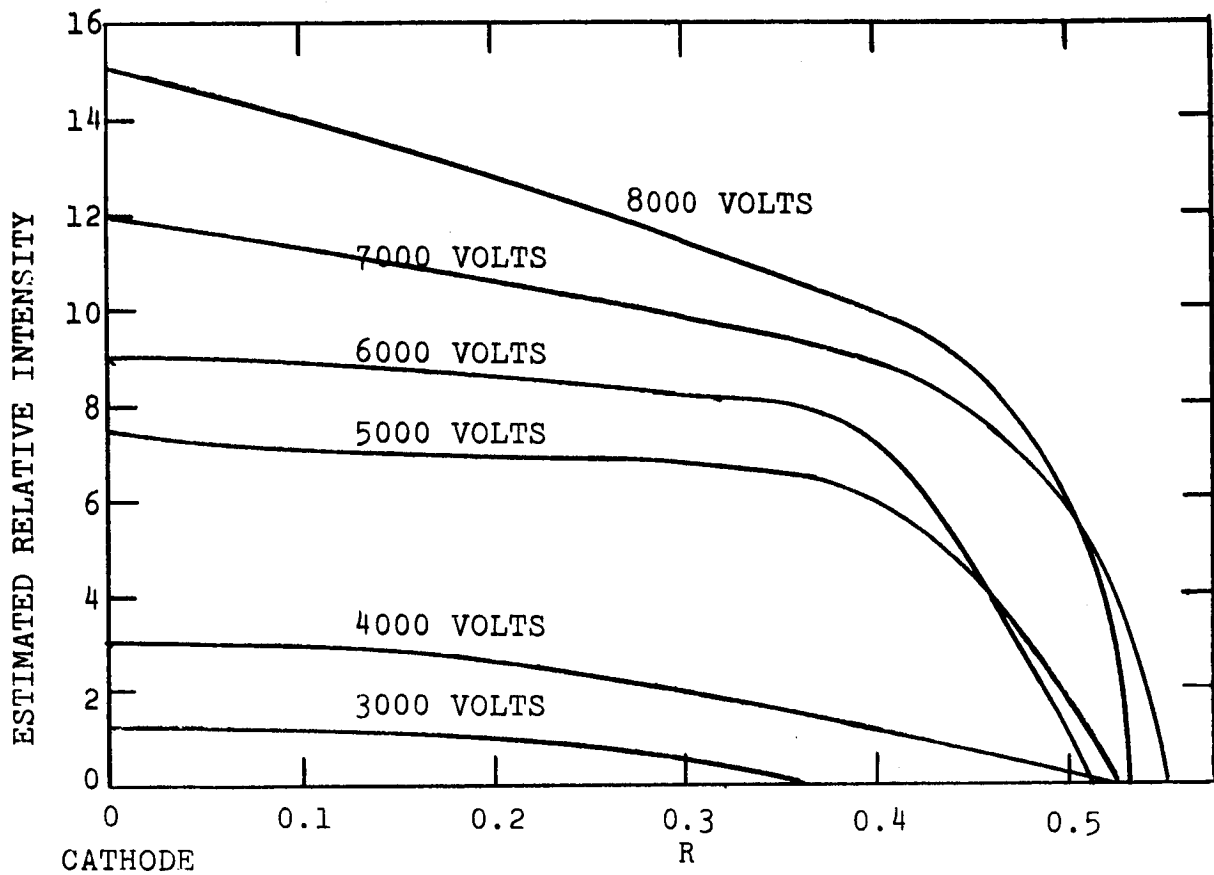field from 600 to 2400 gauss are summarized in Table VI.

TABLE VI

EFFECT OF MAGNETIC FIELD VARIATIONS (B)
ON INTENSITY OF DISCHARGE ON ARGON

| Pressure (Torr N_2)	V_A (Volts)	B (Gauss)	i^+ Exp. (Amps)	R	Relative Max. Intensity
4.5×10^{-8} Torr	4800	600	2.0×10^{-7}	.52	5
	4800	800	2.9×10^{-7}	.58	7.5
	4800	1000	2.2×10^{-7}	.56	7.0
	4800	1200	2.5×10^{-7}	.59	8.0
	4800	1400	1.4×10^{-7}	.51	6.3
	4800	1600	1.4×10^{-7}	.58	6.5
	4800	1800	1.2×10^{-7}	.58	6.1
	4800	2000	1.15×10^{-7}	.56	6.0
	4800	2400	1.15×10^{-7}	.56	6.0

In Figure 22 an attempt has again been made to estimate
the variation in the radial light intensity as a function of
the magnetic field intensity. It is noteworthy that the
gauge has the highest sensitivity at 1200 gauss - a condition
where the intensity was the highest and constant for a
considerable fraction of the radial distance. At both higher
and lower magnetic fields the intensity was lower, and
appeared to decrease continually from the maximum value at
the cathode. In general, the areas under the curve
correlated with the gauge sensitivity - except at
extreme values. For instance, the sensitivity of the gauge at

FIG. 21

EFFECT OF ANODE VOLTAGE ON RADIAL
DISTRIBUTION OF LIGHT

ARGON   4.5 x 10^{-8} Torr

B = 1000 GAUSS

R = FRACTION OF CATHODE TO ANODE DISTANCE

FIG. 22
EFFECT OF MAGNETIC FIELD INTENSITY
ON RADIAL DISTRIBUTION OF LIGHT

ARGON 4.5 x 10^{-8} Torr N_2
4800 VOLTS

R = FRACTION OF CATHODE TO ANODE DISTANCE
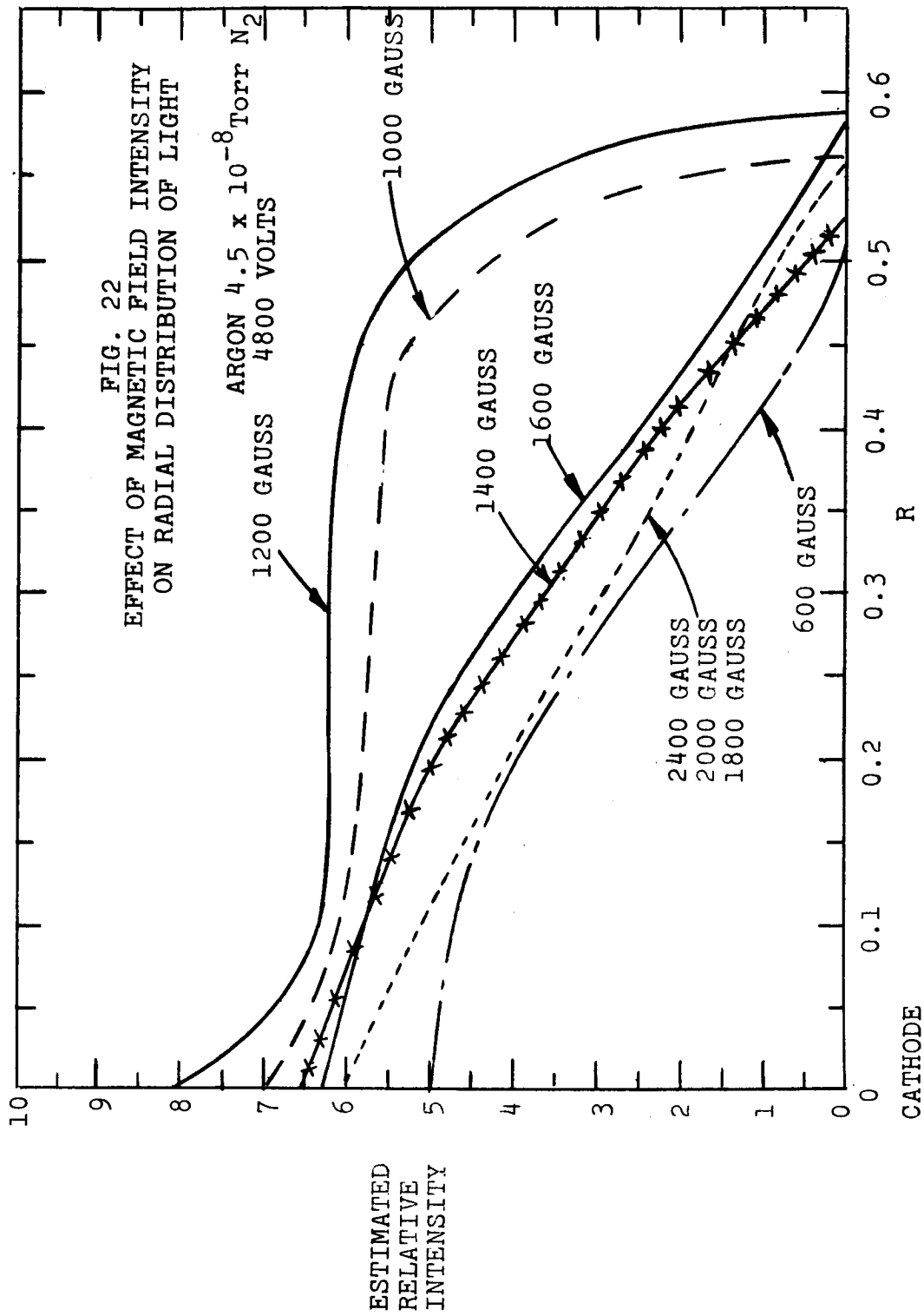
600 gauss was 74% higher than at 2400 gauss. However, the data suggest that increased sensitivity of the gause is associated with higher intensities of the discharge at larger distances from the cathode.

In all of the work reported above, argon was used. Photographs were also taken for helium and hydrogen. These gases were chosen because they have spectra which are very significantly different from each other and argon. When the gauges were operated at the same cathode current levels, there was no significant difference in the shape of the discharge. However, the intensity of argon was greater than that of helium which in turn was greater than hydrogen. The relative intensities at 4800 volts, 1000 gauss in 4.5×10^{-8} Torr N_2 were estimated as follows: argon 7, helium 3, and hydrogen 2.

The main results of the photographic studies may be summarized as follows:

i) In the linear region of the gauge, the glow is located around the cathode rod. It extends about half way to the anode but not to the cathode end plates. It is roughly doughnut shaped.
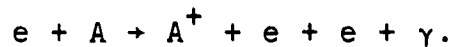
ii) The intensity is approximately constant within the major part of glow region. The intensity appeared to be more nearly constant at those V_A - B conditions which gave highest gauge sensitivity, e.g., 4800 volts, 1000 gauss.

iii) The intensity is a strong function of pressure. It appeared directly proportional to the cathode current.

iv) The location and intensity of the discharge appeared to be essentially independent of anode voltage and magnetic field. Any change in intensity observed on varying either the anode voltage or magnetic field could be attributed to the change in the cathode current.

127

v) It was not possible to obtain photographs of the discharge below the linear region of the gauge.

The fact that the intensity of the emitted light is directly proportional to the cathode current suggests that the glow is in fact directly associated with the ionization process. While a number of possible processes may be suggested to account for the generation of light, the simplest overall explanation is probably as follows. Within the glow regions, electrons have the required energies to cause ionization. Some of the excess energy of the electrons then appears as photons after the impact

$$e + A \rightarrow A^+ + e + e + \gamma.$$

The fact that the intensity appears relatively constant within the discharge at the optimum operating parameters of the gauge suggests that the volumetric ionization rate is constant and therefore the electron density is approximately constant in its glow region. It also suggests that the magnitudes of the radial electric fields within the glow region are relatively small, and most likely constant. This is consistent with the fact that the volume of the discharge was essentially independent of the anode voltage. This would result in constant values of the cycloidal diameter, $d = \frac{2Em}{B^2 \ell}$ for the electrons in the glow region. It is interesting to note that the glow appears to extend out to slightly beyond the radius value $(0.45(r_a - r_c))$ at which the radial electric field is a minimum for the space charge free case. (The space charge free potential distribution has been measured by Redhead[12] using electric analogue techniques.)

The above interpretations are largely dependent on the assumption that the region of ionization is essentially confined to the region emitting the light as evidenced by the

photographic techniques. However, the apparent limitation of
the useful discharge to within about half the cathode-anode
distances may have other explanations. For instance, it was
not unlikely that significant radiation was emitted beyond
half the cathode-anode distance, but that it was absorbed in
either the camera lens or the film. Tests with a pinhole
camera did not resolve the problem because the film gelatin
starts to absorb at 3200Å and reaches a maximum at 3000Å.
What is required is a high speed film with special sensitivity
down to at least 1800Å. It is not unlikely that such a
film will shortly be available commercially.

In one overexposed photograph of the radial distribution
taken at 5×10^{-7} Torr, a dark space was observed between
0.73 and 0.82 of the cathode-anode distance. However, beyond
0.82, a faint glow was evident. The intensity of the light
in the anode region was at least an order of magnitude
lower than measured closer to the cathode. However, it
does raise the question as to whether the dark space was
attributable to gelatin absorption and that anode glow was
perhaps associated with light with a wavelength of less
than 3000Å where the gelatin has a higher transmissivity.
If this is the case, it would appear that there are con-
sistent radial variations of the spectral distribution.
However, the use of filters with cut-offs above 3200A did
not indicate that the above was in fact the case. Because
of the nature of the ionization process, it is unlikely
that the emitted light would be a single function of the
radial position. Further work with a film of such
spectral sensitivity would be warranted to resolve this
question.

1.7 ANOMOLOUS CURRENT STUDIES

Pressure measurements in the XHV range are made difficult by the problems associated with reliable low current measurements. The highest sensitivity pressure sensor at present available in this region is the cold cathode magnetron gauge. At pressures below 10^{-13} torr, a readout current of less than 10^{-14} amp must be measured.

A number of possible sources of erroneous current can effect the reliability of low pressure measurements. These are related to four fundamental electrical properties of glass and ceramic insulators used as vacuum feedthroughs.[13] They are:

Volume Electrical Resistivity - The volume resistivity of a dielectric has two components.[14] The first is the usual conduction term similar to that for metallic conductors which obey Ohm's law. The second term is associated with a transient current which may be many times greater than the conduction term. The net result is that dielectrics exhibit a conduction current which not only depends on the applied voltage and temperature, but also on the elapsed time after the initial application of the voltage. This time dependence is also effected by the electrical and thermal history of the dielectric.

Surface Electrical Resistivity - The adsorption of a film of extraneous impurities on a dielectric surface will generally result in a decrease of its electrical resistivity. The adsorption effect can be significantly reduced by chemical cleaning and bakeout prior to pressure measurement. In addition, when charged particles come into contact with a dielectric surface a similar effect can take place.[15,16] Results of experimentally induced surface charging of a borosilicate glass by Muray show that millisecond time constants for resistance changes were obtained in a 10^{-8} torr background vacuum. These measurements were carried out at stress levels in the dielectric of up

to 600 volts. The effect of surface charging in the 10^{-14} amp range and at XHV pressure has not yet been investigated.

Dielectric Constant - The dielectric constant is effected by dielectric absorption in a way similar to the effects described for volume electrical resistance. The dielectric absorption current, as will be shown, is caused by the finite time required for dielectric dipole moments to accommodate their orientation to the applied field.[17]

Dielectric Strength - In normal operation of the Redhead Gauge, the pressure dependent ion current is measured between the main cathode and ground. The auxiliary cathode is held at ground potential. The potential difference between measuring electrodes and ground is approximately 1 mV in the lowest pressure range when conventional electrometers are used. Hence, induced current in a dielectric due to high voltage breakdown is not of interest in XHV pressure measurement due to the low value of applied voltage.

This section of the report deals with influence of the dielectric absorption current in the insulation region separating the main cathode and auxiliary cathode electrode on electrometer currents in the 10^{-14} amp region. Surface resistivity effects were not investigated although a complete evaluation of this effect is suggested.

Dielectric polarization phenomena result when charges are displaced interior to a dielectric. Two types of dipoles may result:

i   Permanent dipoles interior to the dielectric material, which are randomly oriented without the field, but which may be selectively oriented when the field is applied.

ii   Induced dipoles created by the application of the external field.

For the purposes of this report, gases and liquids will not be considered. In solids, if molecules with permanent dipole moments are allowed to rotate, however small, they can contribute to the total polarization by increasing the number and degree of alignment with the increased external field.

Induced dipole moments occur only in the presence of the applied field. The value of the dipole moment induced in the dielectric depends, among other things, on the magnitude of the applied field. The induced dipole may be caused by three types of interaction of charge particles with the applied field. The first of these is the distortion of ionic bonding by the applied field. This is often referred to as atomic polarizability, and is caused by the relative motion of ions in the solid material. The second source is caused by the deformation of the electron cloud at individual atom sites. In this type, the center of charge of the electron cloud is displaced from the nucleus. This type of polarization is often referred to as the electronic polarizability of the solid. The third type of induced dipole moment is cause- by the movement of free electronic and/or ionic charges in the applied field. If the movement of the free charge is restricted at crystalline boundaries, a dipole moment will result, but if the charges move freely to the electrode then a component of the dc conduction results.

The total effect of both permanent dipoles and induced dipoles in the dielectric is to create an average dipole moment associated with the dielectric which depends on the applied field. This dipole moment is given by:

$$\bar{\mu} = \alpha\, E$$

where $\bar{\mu}$ = the average dipole moment per molecule
α = the total polarizability
E = the local electric field.

132

The total polarizability is given by:

$$\alpha = \alpha_d + \alpha_a + d_e + \alpha_f$$

where:

α_d = the polarizability for permanent dipoles

α_a = the polarizability for induced ionic dipoles

α_e = the polarizability for induced electronic dipoles

α_f = the polarizability for induced free dipoles.

The total polarization is given by:

$$P = N \alpha E$$

where:

N = the total number of dipoles in the solid dielectric.

From macroscopic theory, it can be shown that

$$\frac{K^* - 1}{K^* + 2} = \frac{4\pi}{3} N \alpha$$

where

K* = the complex dielectric constant

E = the externally applied field.

This equation defines the relationship between the polarizability and the complex dielectric constant K*.

When a constant electric field is applied to a set of condenser plates which have a dielectric placed between them, the resulting electronic dipoles induced in the dielectric material are oriented almost immediately. This polarization is often referred to as P_∞ (the initial polarization or the polarization at very high frequencies).

The polarization will increase gradually as the orientation of the dipoles or the displacement of the ions takes

place. This increase will continue until equilibrium is established
and the dielectric approaches the static polarization condition,[18,19]
P_O. The equation describing the change in polarization in the
dielectric with time is given by:

$$P_a = [P_O - P_\infty][1 - \exp.(- \frac{t-to}{\tau})]$$

where τ is the well known relaxation time for this process (see
Figure 23). The polarization process is analogous to a
diffusion process where the relaxation time τ is given by:

$$\tau = \tau_o \ e^{q/KT}$$

where q is the activation energy and τ_o is determined by
calculating the vibrational frequency of particles in a potential
well and is of the order of 10^{-13} sec.

To determine if volume polarization effects substantially
influence the current readings in Redhead Gauges at low current
levels($<10^{-14}$ amps) the experiment shown in Figure 24 was per-
formed. In this experiment low voltage pulses were applied
between the auxiliary cathode and the main cathode of a model
552 Redhead Gauge. Typical charging and discharging procedure
was as follows: 1) open S_2, 2) close S_1, 3) short input of
the electrometer, 4) allow a charging period of 1 - 40 minutes,
5) open the input to the electrometer, 6) short S_2, 7) open
S_1, 8) observe the decay of current recorded by the electro-
meter.

This procedure assured that the full battery voltage would
not appear across the input terminal of the electrometer. The
potential divider network of the supply was designed to allow
its output terminal to be grounded without significantly reducing
the battery emf. The voltage pulses applied were between 0.1
and 0.5 volts in amplitude for periods of time not less than
1 minute. The gauge was not operative for long periods of
time (e.g. one week) prior to application of the voltage pulse.
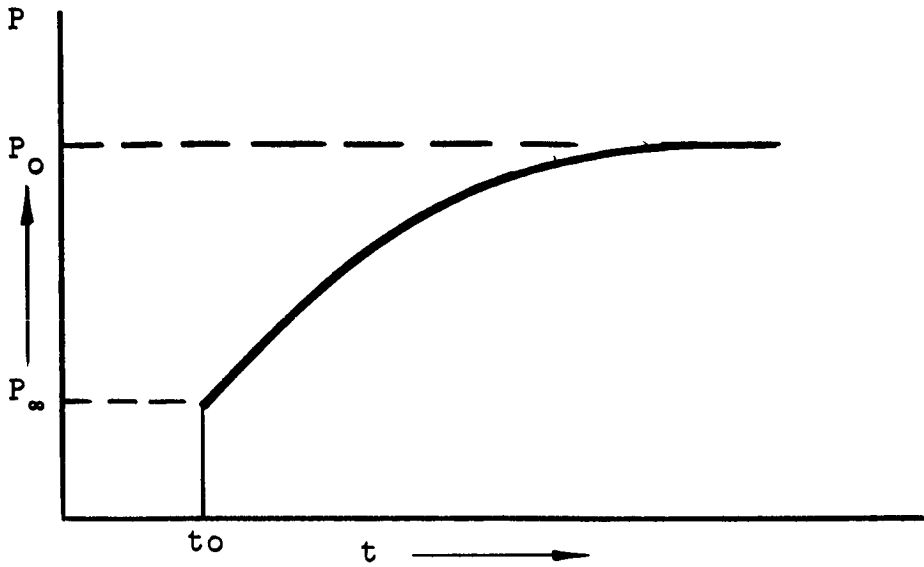
POLARIZATION P   AS A FUNCTION OF TIME t AFTER A
CONSTANT ELECTRIC FIELD IS APPLIED TO THE DIELECTRIC

FIG. 23
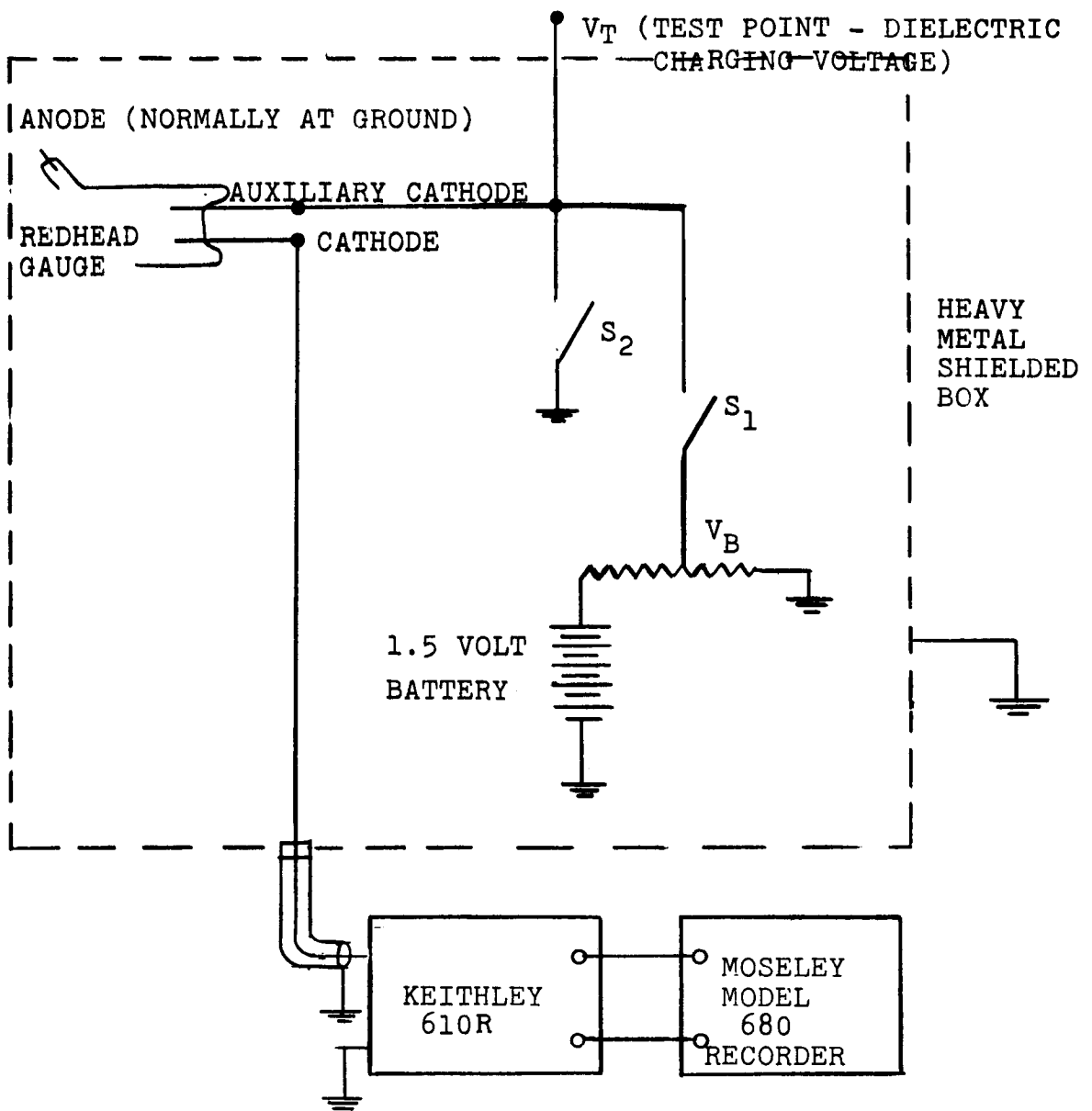
DIELECTRIC POLARIZATION EXPERIMENTAL TEST ARRANGEMENT

FIG. 24

This assured that no surface charge was present on the interior dielectric surface of the gauge surrounding the electrode feedthrough. The gauge was inoperative during the measurement, i.e., no magnetic field or anode voltage was applied. This test was used to determine if the normal voltage stress level in the dielectric was sufficient to create long term anomolous charging currents which could be seen by the external instrumentation.

It is important to note that this stress level far exceeds (>100 times) those levels found in normal operation of the gauge. A characteristic response curve is shown in Fig. 25. This curve shows that the current to the electrometer was in the noise level in less than one minute after the removal of applied voltage stress. This strongly suggests that anomolous charging current in the dielectric separating the auxiliary cathode from the main cathode cannot be considered the major difficulty in making XHV pressure measurement.

Figure 26 shows the effect of high voltage disturbances at the anode on the electrometer current measurements at the metering terminal. This graph shows that large voltage changes resulting from high voltage turn off and local disturbances in the vicinity of the anode, i.e., removal of the anode lead, give rise to measurement current perturbations which persist with time constants of approximately 40 minutes.

Instrument time constants associated with the Keithley electrometer and Moseley recorder were evaluated during the measurement cycle. Periodically the electrodes of the auxiliary cathode and main cathode were shorted at the input to the electrometer thus assuring that the free charge on the surface of the dielectric under investigation would be neutralized. When the monitoring instruments were reconnected, the decay curve was retraced thus indicating that the decay was due to an internal relaxation phenomena.
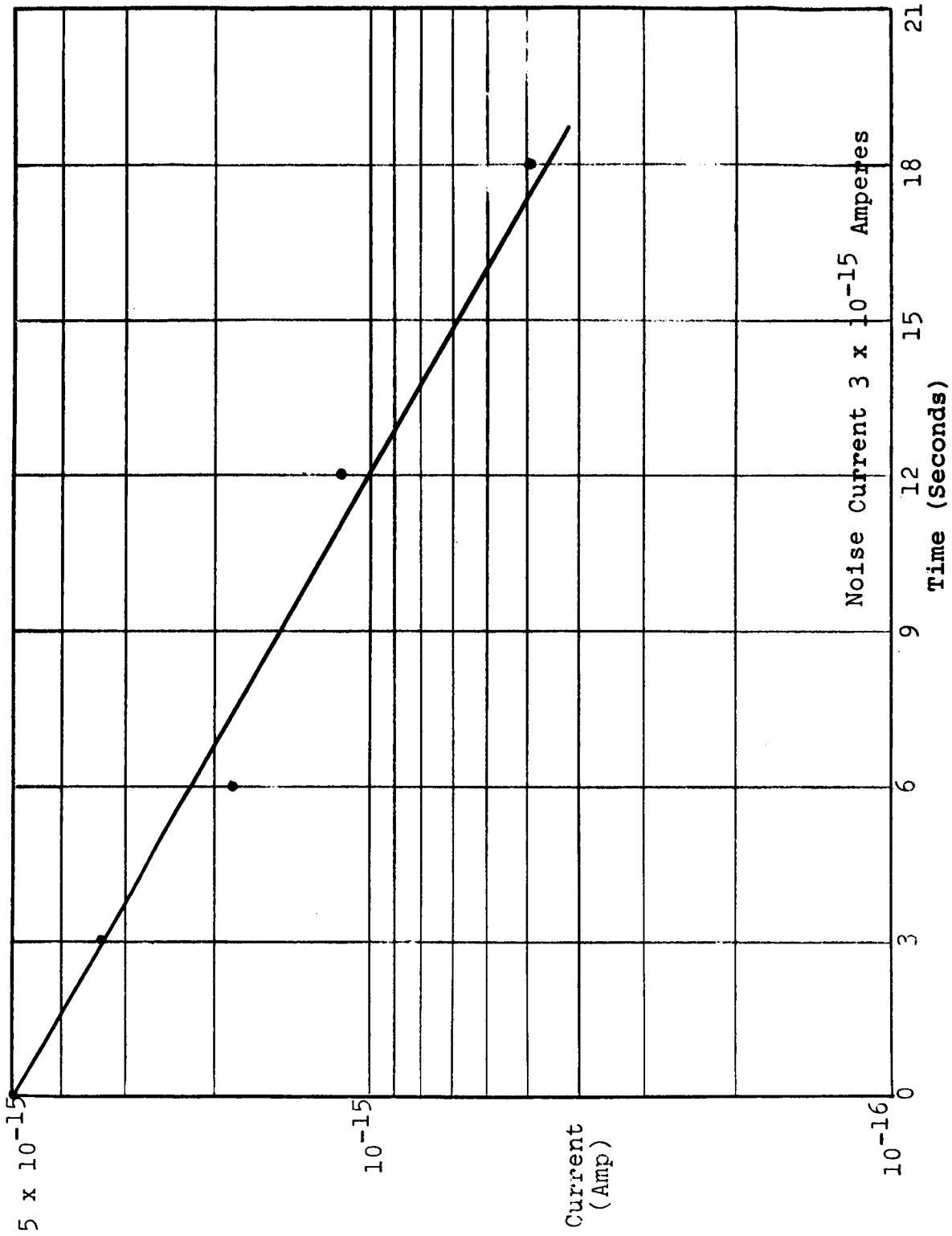
FIG. 25 Cathode to Auxiliary Cathode Leaking Current Versus Time After
a .170 Volt Stress Was Removed. (This Stress Was Applied for
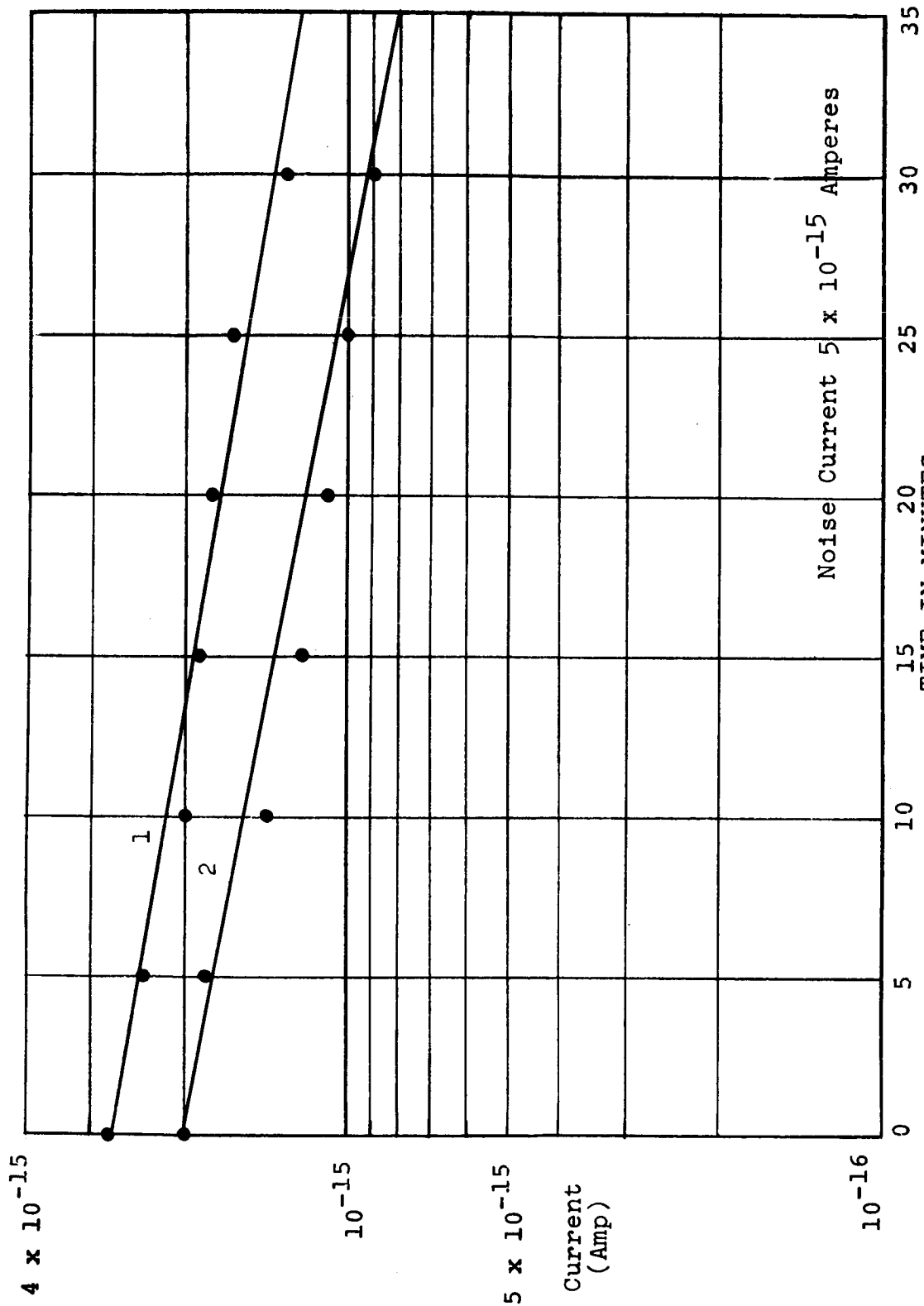32 Minutes)

FIG. 26 Cathode to Auxiliary Cathode Leakage Current Versus Time after an Anode Disturbance. (1 - High Voltage Power Supply Turned Off, 2 - Anode Head Disconnected)

139

The results of this preliminary investigation into the influence of polarization currents on vacuum measurement in the XHV region indicate that:

i   Low voltage stress of the auxiliary cathode to main cathode dielectric does not result in long term polarization current in the 10^{-14} to 10^{-15} amp level measurement region.

ii   High voltage stress transients at the anode have pronounced long term effects on the current measurements.

The results of this investigation do not preclude the effects of surface polarization currents induced on the interior dielectric surface when the gauge is in operation as the existence of dielectric adsorption at current levels below 10^{-15} amp. A complete analysis of this problem should be carried out utilizing:

i   A modulated anode supply. The use of such a supply will allow the potential of the electron space charge to be varied and hence any electron charge arriving at the dielectric surface will have an ac component.

ii   The use of temperature control of the gauge envelope.

iii   The removal of the magnetron field while the gauge is in operation. This should cause the scattering of the electron space charge over the gauge envelope thus creating the ultimate charging condition on the interior dielectric surface.

REFERENCES

1. R.G. Herb, T. Pauly and K.J. Fisher, Bull. Am. Phys. Soc. <u>8</u>, 336 (1963).

   W.G. Mourad, T. Pauly and R.G. Herb, Bull. Am. Phys. Soc. <u>8</u>, 336 (1963).

2. W.E. Waters, Diamond Ordnance Fuze Laboratory, DOFL Proj. 52050, TR-525 "Motion of Electrons Between Concentric Cylinders," 1 November 1957.

3. R.H. Hooverman, J. Appl. Phys. <u>34</u>, 3505 (1963).

4. L.D. Landau and E.M. Lifshitz, <u>Mechanics</u>. Trans. from Russian by J.B. Sykes and J.S. Bell. Addision-Wesley Pub. Co., Reading, Mass. 1960.

5. L.D. Landau and E.M. Lifshitz, <u>Quantum Mechanics</u>, Ch. VII. Trans. from Russian by J.B. Sykes and J.S. Bell. Addison-Wesley Pub. Co., Reading, Mass. 1958.

6. P.A. Redhead, Can. J. Phys. <u>37</u>, 1260 (1959).

7. F.L. Torney and F. Feakes, Rev. Sci. Instr. <u>34</u>, 1041, (1963).

8. F. Feakes and F.L. Torney, Jr. Trans. 10th Nat'l. Vac. Symp., 257 (1963), The Macmillan Company, New York.

9. P.J. Bryant, C.M. Yosselin, W.W. Langley Jr., NASA CR-324 (Nov. 1965).

10. F. Feakes, F.L. Torney, Jr. and F.J. Brock "Gauge Calibration Study in Extreme High Vacuum" NASA CR-167 (Feb. 1965).

11. P.A. Redhead, Can. J. Phys. <u>43</u>, 1001 (1965).

12. P.A. Redhead, "Private Communication; Potential Distribution in Gauge".

13. E.M. Guyer, Proc. IRE <u>32</u>, 443 (1944).

14. Julius J. Muray, J. Appl. Phys. <u>33</u>, 1517, (1962).

15. Julius J. Muray, J. Appl. Phys. <u>33</u>, 1525, (1967).

16. R.G. Fowler and M. Sakuntala, J. Chem. Phys. <u>27</u>, 824, (1957).

17. "Imperfections in Nearly Perfect Crystals", W. Shockley, John Wiley and Sons, New York, 1952, pp. 219-245.

18. M.M. Penlman and J. Meunier, J. Appl. Phys. <u>36</u>, 420, (1965).

19. D.W. Davidson, R.P. Autz, and R.H. Cole, Rev. Sci. Inst. <u>22</u>, 678, (1951).